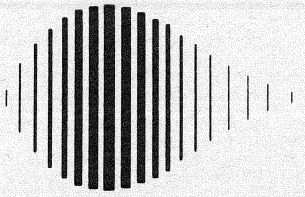

**NATIONAL CENTER FOR EARTHQUAKE ENGINEERING RESEARCH**

State University of New York at Buffalo

# Shape Memory Structural Dampers: Material Properties, Design and Seismic Testing

by

P. R. Witting and F. A. Cozzarelli

State University of New York at Buffalo
Department of Civil Engineering
Buffalo, New York 14260

Technical Report NCEER-92-0013

May 26, 1992

This research was conducted at the State University of New York at Buffalo and was partially supported by the National Science Foundation under Grant No. BCS 90-25010 and the New York State Science and Technology Foundation under Grant No. NEC-91029.

# NOTICE

This report was prepared by the State University of New York at Buffalo as a result of research sponsored by the National Center for Earthquake Engineering Research (NCEER) through grants from the National Science Foundation, the New York State Science and Technology Foundation, and other sponsors. Neither NCEER, associates of NCEER, its sponsors, the State University of New York at Buffalo, nor any person acting on their behalf:

a. makes any warranty, express or implied, with respect to the use of any information, apparatus, method, or process disclosed in this report or that such use may not infringe upon privately owned rights; or

b. assumes any liabilities of whatsoever kind with respect to the use of, or the damage resulting from the use of, any information, apparatus, method or process disclosed in this report.

Any opinions, findings, and conclusions or recommendations expressed in this publication are those of the author(s) and do not necessarily reflect the views of NCEER, the National Science Foundation, the New York State Science and Technology Foundation, or other sponsors.

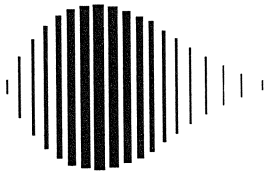

# Shape Memory Structural Dampers: Material Properties, Design and Seismic Testing

by

P.R. Witting[1] and F.A. Cozzarelli[2]

May 26, 1992

Technical Report NCEER-92-0013

NCEER Project Number 90-2103

NSF Master Contract Number BCS 90-25010
and
NYSSTF Grant Number NEC-91029

1 Graduate Student, Department of Mechanical and Aerospace Engineering, State University of New York at Buffalo
2 Professor, Department of Mechanical and Aerospace Engineering, State University of New York at Buffalo

NATIONAL CENTER FOR EARTHQUAKE ENGINEERING RESEARCH
State University of New York at Buffalo
Red Jacket Quadrangle, Buffalo, NY 14261

## PREFACE

The National Center for Earthquake Engineering Research (NCEER) was established to expand and disseminate knowledge about earthquakes, improve earthquake-resistant design, and implement seismic hazard mitigation procedures to minimize loss of lives and property. The emphasis is on structures in the eastern and central United States and lifelines throughout the country that are found in zones of low, moderate, and high seismicity.

NCEER's research and implementation plan in years six through ten (1991-1996) comprises four interlocked elements, as shown in the figure below. Element I, Basic Research, is carried out to support projects in the Applied Research area. Element II, Applied Research, is the major focus of work for years six through ten. Element III, Demonstration Projects, have been planned to support Applied Research projects, and will be either case studies or regional studies. Element IV, Implementation, will result from activity in the four Applied Research projects, and from Demonstration Projects.

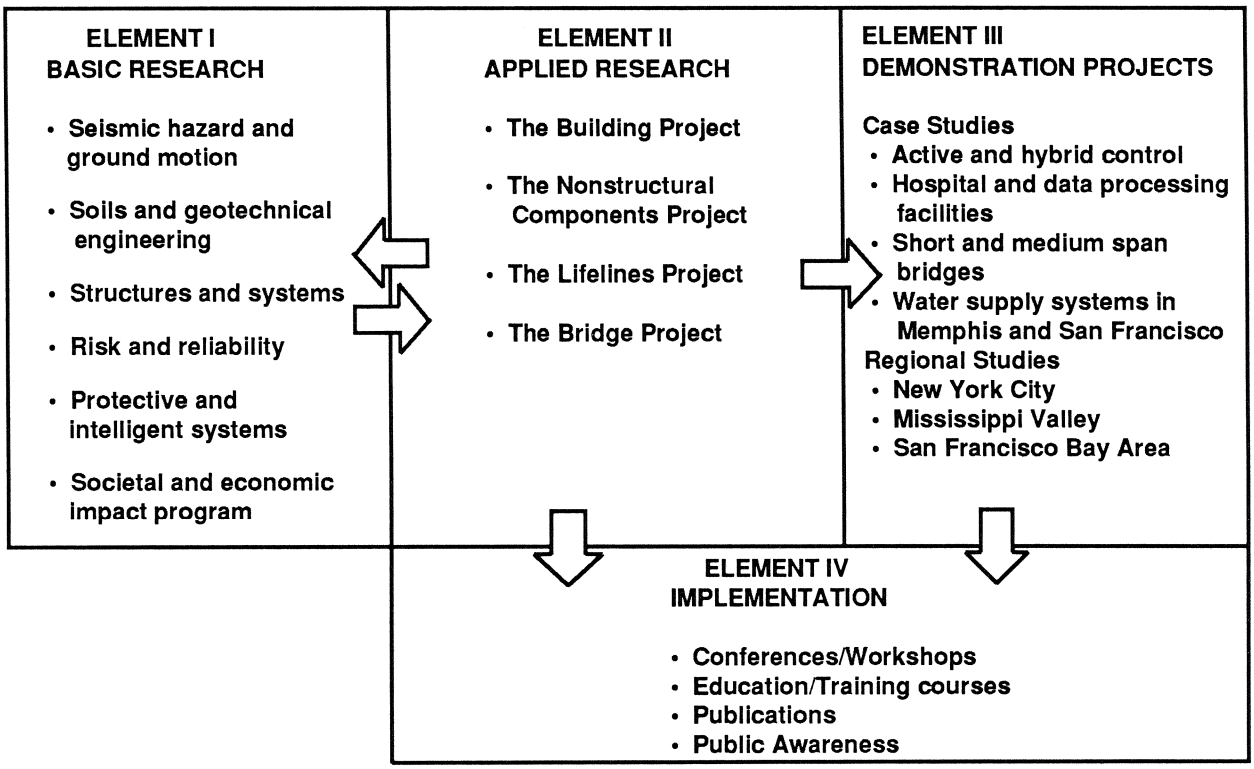


Research in the **Building Project** focuses on the evaluation and retrofit of buildings in regions of moderate seismicity. Emphasis is on lightly reinforced concrete buildings, steel semi-rigid frames, and masonry walls or infills. The research involves small- and medium-scale shake table tests and full-scale component tests at several institutions. In a parallel effort, analytical models and computer programs are being developed to aid in the prediction of the response of these buildings to various types of ground motion.

Two of the short-term products of the **Building Project** will be a monograph on the evaluation of lightly reinforced concrete buildings and a state-of-the-art report on unreinforced masonry.

The **protective and intelligent systems program** constitutes one of the important areas of research in the **Building Project**. Current tasks include the following:

1. Evaluate the performance of full-scale active bracing and active mass dampers already in place in terms of performance, power requirements, maintenance, reliability and cost.
2. Compare passive and active control strategies in terms of structural type, degree of effectiveness, cost and long-term reliability.
3. Perform fundamental studies of hybrid control.
4. Develop and test hybrid control systems.

*One of the passive energy dissipation devices studied at NCEER is made of shape memory alloys. The basic idea behind the use of shape memory structural dampers in a structure is to take advantage of the superelastic material properties of shape memory alloys so that significant damping effect can be achieved, while a centering force can be generated to restore the structure to its original position after an earthquake.*

*This report describes the design, fabrication, and laboratory testing of a class of shape memory structural dampers. Their performance, when added to a 2/5-scale model structure, is compared with that achieved by using traditional viscoelastic dampers.*

**ABSTRACT**

The results of material tests on the shape memory alloy Cu-Zn-Al are presented and discussed. The results of the material tests are then applied in the design of a structural damper, with Cu-Zn-Al providing the dominant damping force. Different damping designs are examined to determine the best design. The finalized design was then mechanically tested.

Seismic response characteristics of a 2/5 model five story building, with and without added Cu-Zn-Al shape memory dampers are studied experimentally. These results are then compared with the studies of viscoelastic dampers tested on the same model five story building.

**ACKNOWLEDGEMENT**

The funding support granted to the authors by the NCEER is gratefully acknowledged. The authors also gratefully acknowledge the help of Dr. L. McDonald Schetky and Dr. Wu of Memry Metals Inc. Both have provided valuable recommendations on the development of the material experimental program. Also, the authors wish to thank Dr. K.C. Chang for his help with the seismic experimental testing.

TABLE OF CONTENTS

## LIST OF ILLUSTRATIONS

## LIST OF TABLES

# SECTION 1

## INTRODUCTION

The use of structural dampers and base isolators have been shown to greatly reduce the damage to a structure due to an earthquake [5,9,11,12]. The study of these devices is somewhat limited, in terms of the material used in the structural dampers and base isolator devices. Viscoelastic structural dampers have been studied in [5,9], and frictional structural dampers were studied in [10,11]. Rubber bearing base isolation devices have also been studied. These are, however, only a few of the many materials which may be used to create the vibration control desired during an earthquake. The emphasis in this study is to research the possible benefits, to passive structural vibration control techniques, of the relatively new class of materials, the shape memory alloy.

Constitutive relation for the shape memory alloy (SMA) have been developed in [13]. In addition, the material properties of a few different shape memory alloys are explored in [7,12]. The objectives of this study were to design, build and test a structural damper which uses a shape memory alloy. The testing of the SMA damper included a study of the dynamic response of a 2/5 scale five-story steel frame structure with added SMA dampers. These results were then compared to viscoelastic dampers, which were tested on the same structure.

# SECTION 2

# MATERIAL CONSIDERATIONS

## 2.1 Pseudoelasticity

A shape memory alloy (SMA) undergoes a reversible phase transformation or phase reorientation when deformed. In addition, the SMA can undergo a reversible change in geometry with a change in temperature, which is due to a phase transformation. Pseudoelasticity is the constitutive behavior which describes the above mentioned phenomena. In this study, however, we will only be concerned with stress induced pseudoelastic behavior.

There are two different classes of stress induced pseudoelastic behavior: large area hysteretic behavior and superelasticity. The difference between the two is due to differing $A_f$ and $M_f$ temperatures. The $M_f$ temperature is the temperature below which the alloy has a body centered tetragonal (BCT) martensitic crystal structure. Conversely, above the $A_f$ temperature the alloy has a body centered cubic (BCC) austenitic crystal structure. It should be pointed out that $A_f > M_f$. In addition, if the material temperature falls between $A_f$ and $M_f$ the material will have a mixture of both BCC and BCT crystal structures.

If a SMA at a temperature below its $M_f$ temperature is cyclicly loaded, a large area hysteresis loop is formed. This hysteresis loop, however, is not formed by the dislocation glide mechanism typical of a plastically deforming metal. This loop is due to the growth, shrinkage and rotation of the martensitic crystals. This

allows the SMA to undergo many more large strain high damping cycles than a typical plastically deforming metal. In addition to resistance to large strain fatigue, the material reverts back to the original crystal orientation and therefore to its original shape, if the temperature is raised above the $A_f$ temperature. Thus the material exhibits a shape memory effect.

The superelastic constitutive model describes the stress-strain relation of a SMA at a temperature above the $A_f$ temperature. At low stress levels, a material with superelastic properties will behave elastically. However, at some higher stress level, which depends on the material and its heat treatment, a phase transformation from BCC to BCT begins. This transformation will reduce the modulus of the material as seen in Fig. 2.1. Upon unloading, the material undergoes a reverse transformation at a lower stress level. The difference in the transformation stress level between loading and unloading is due to internal friction in the diffusionless phase transformation. Once the reverse phase transformation is complete, the material behaves elastically, and with complete unloading of the material, a complete recovery is ideally seen. The complete cycle is shown in Fig. 2.1.

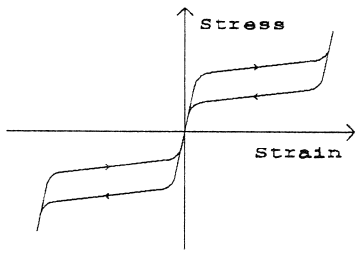


**Fig. 2-1 Superelastic Stress Strain Relationship**

## 2.2 Material Selection

Initially this project began by using the SMA nitinal to verify the proposed superelastic constitutive law in [6,16]. While nitinal has very good SMA material properties, it is extremely difficult to machine. Because nitinal is hard and highly abrasive, it requires special tools for machining and thus some machining operations are impractical [6,16]. In addition, nitinal's high cost inhibits its use. Therefore a considerably less expensive shape memory alloy (Cu-Zn-Al) was selected. In addition to its attractive low cost, the machining of this alloy required no special tools and could be completed relatively quickly.

## 2.3 Cu-Zn-Al Phases and Heat Treatment

The composition of Cu-Zn-Al by weight percent used in this study was 69.1% Cu, 26.9% Zn, 3.75% Al, and 0.1% Zr. This composition of Cu-Zn-Al, in equilibrium at room temperature, has two phases $\alpha$ and $\gamma$. The $\alpha$ phase is the copper FCC structure, and the $\gamma$ phase is an intermediate compound with the composition of $Cu_5Zn_8$. Above 725°C, the Cu-Zn-Al is in the $\beta$ phase which has a BBC structure. Just below 725°C, the equilibrium phases are $\beta$ and $\alpha$. The $\gamma$ phase appears below 300°C and has much slower kinetics [14]. Even with a moderately slow cool to room temperature, only the $\alpha$ and $\beta$ phases would be present.

Since the tensile bars were machined from a 3 inch diameter bar of Cu-Zn-Al, considerable machining was necessary. This machining heats up the material significantly. To prevent the

problem of the machining process annealing the heat treatment, the Cu-Zn-Al SMA was heat treated after the machining process was complete.

The heat treatment began by heating the Cu-Zn-Al SMA in an argon bath at 800°C for 30 minutes, which is then followed by a water quench. At 800°C the microstructure of Cu-Zn-Al is the single phase β. Immediately after the water quench, the Cu-Zn-Al is aged at 80°C for 24 hours. The argon bath was used to prevent nitrogen embrittlement, and reduce dezincification during the high temperature part of the heat treatment [15]. Since the second part of the heat treatment is at a much lower temperature, it was performed without an argon bath. The water quench from 800°C prevents the Cu-Zn-Al from transforming from the β phase, however the martensitic transformation temperature of this as-quenched single β phase is unstable. The aging at 80°C allows the short range order of the β phase to reorient to a more stable form [7]. Despite the use of the argon gas to prevent extensive damage to the surface of the specimen during heat treatment, the surface still needed hand sanding to remove some damaged surface without heating up the material.

## 2.4 Material Testing

Tensile and differential scanning calorimeter (DSC) tests were performed to verify the $A_f$ and $M_f$ temperatures as well as the superelastic properties. The DSC tests were performed at Memry Technologies Inc. by Dr. Wu.

A Mechanical Testing System (MTS) machine was used to perform the mechanical tests. This MTS machine was configured to use feedback control of strain to produce a ramp strain loading on the sample. The strain was measured with a model 11B-20 MTS extensometer. This extensometer measures the average strain over an one inch region. An OPTILOG data acquisition system, which was connected to a PC, was used to convert the voltage signals from the MTS load cell, displacement transducer and extensometer to mechanical measurements, which could be stored on computer disk.

The tensile bars used in the mechanical testing were designed to undergo both tensile and compressive loads without bucking. Appendix B contains drawings of both the tensile bar and the grip design. Sample bar D was heat treated then tested under strain controlled conditions to a maximum strain of .1% strain to determine the elastic modulus. The elastic modulus was found to be $7.2 \times 10^6$ Psi. Sample bar A was heat treated then tested under strain controlled conditions to a maximum strain of 2.2%. Six tension compression cycles were performed. The resulting stress-strain curve is presented in Fig. 2.2. The initial elastic modulus of the first cycle of the stress strain curve was $7.6 \times 10^6$ Psi. At .25% strain the modulus begins to drop and at 1.00% strain it has leveled out at $5.8 \times 10^5$ Psi. The maximum tensile strain was 2.22% under a load of 34.8 Ksi. A plastic constitutive law would predict that the remaining strain after unloading would be 1.76%. The remaining strain was .26% which indicates a 1.50% strain springback.

The first cycle of the stress strain curve has a much more pronounced superelastic characteristic than the subsequent cycles. Notice in Fig. 2.2 that the loading of the first compressive load show a pronounced softening of modulus at -.25% strain. The second compressive cycle has a less pronounced softening of modulus at -.7% strain. This softening of modulus all but disappears after the 3rd cycle. The overall appearance of the 3rd and subsequent cycles is of a slightly hour-glass-shaped hysteresis loop. The local modulus of the Cu-Zn-Al after several cycles is $3.3 \times 10^6$ on initial unloading of the stress. This is much less then the elastic modulus measured. In addition, the modulus reduces during the unloading to $2.2 \times 10^6$ Psi. If the Cu-Zn-Al were deforming though dislocation slip/glide mechanisms, then these moduli would be equal to the elastic modulus.

The test was repeated on sample bar C with the same heat treatment and the results were similar. These results are presented in Fig. 2.3.

Heat Treatment: 800°C 30 min (Argon) W.Q.

: 80°C 24 hours (Air)

ε Limits: -0.022/0.022 (Rate=.000077/sec)

Test Section Diameter D = 0.496 in

Extensometer Gage Length: L = 1.0 in

6 Cycles

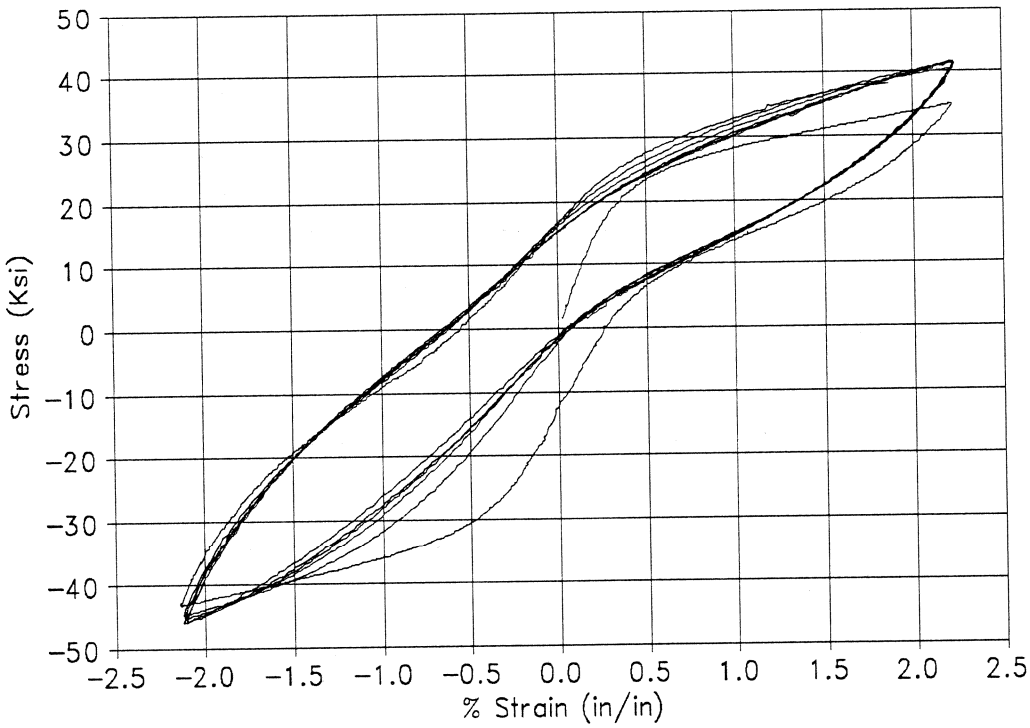


**Fig. 2-2 Six Cycle test of heat treated Cu-Zn-Al, Bar A**

Heat Treatment: 800°C 30 min (Argon) W.Q.

: 80°C 24 hours (Air)

ε Limits: -0.020/0.020 (Rate=.000382/sec)

Test Section Diameter D = 0.485 in

Extensometer Gage Length: L = 1.0 in

6 Cycles

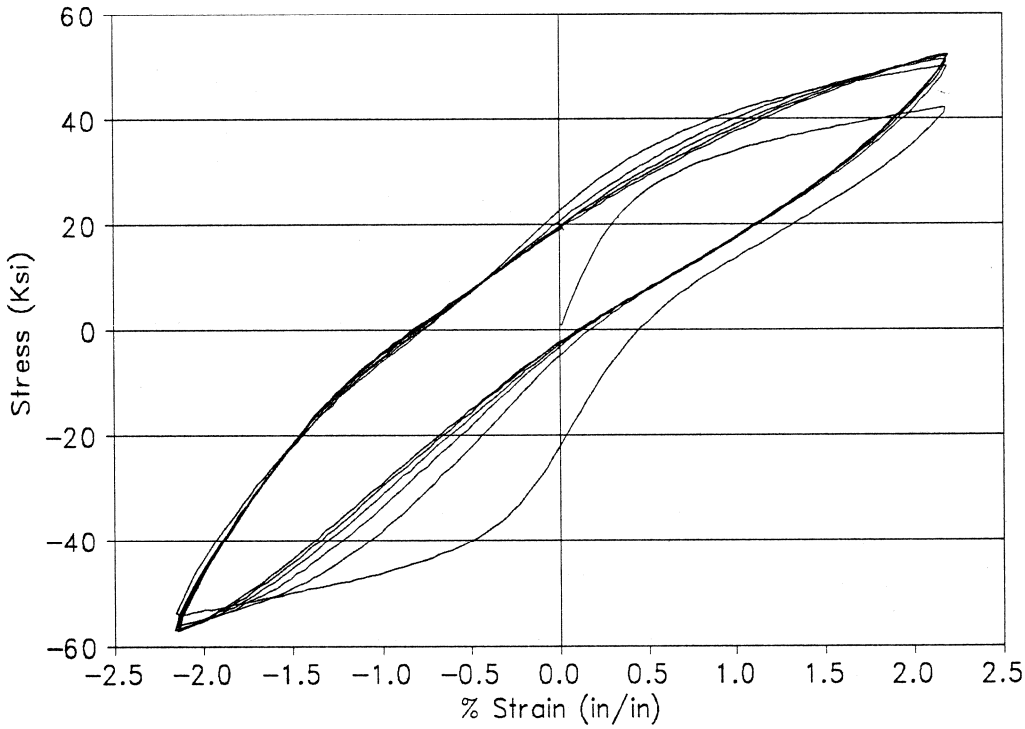


**Fig. 2-3 Six Cycle test of heat treated Cu-Zn-Al, Bar C**

A DSC test was performed on a sample of the strained section of bar A. A DSC was also performed on a unstrained heat treated sample of the Cu-Zn-Al for comparison. Table 2.1 presents the results of these tests.

| DSC Test Results | Heat treated Unstrained | Heat treated Strained Bar A |
|---|---|---|
| $\Delta h$ for BCC to BCT phase transformation | -0.86 cal/gram | -0.34 cal/gram |
| $\Delta h$ for BCT to BCC phase transformation | 1.21 cal/gram | 0.87 cal/gram |
| Onset temperature of BCC to BCT phase transformation | -8°C | -15°C |
| Completion temperature of BCC to BCT phase transformation | -30°C | -52°C |
| Onset temperature of BCT to BCC phase transformation | -12°C | -23°C |
| Completion temperature of BCT to BCC phase transformation | 8°C | 1°C |

**Table 2-I DSC Results of Strained and Unstrained Cu-Zn-Al**

The onset and completion temperatures are lower for the strained bar, and the total temperature range in which the phase transformation takes place is wider for the strained sample. In addition, the magnitude of the enthalpy change ($\Delta h$) for both phase transformations is smaller in the strained sample.

It should be noted that the magnitude of the enthalpy change for the BCC to BCT phase transformation is smaller than the magnitude for the BCT to BCC transformation. If the transformations were thermodynamically reversible, the magnitudes

of the enthalpy changes would be identical. However this is not the case with Cu-Zn-Al. Frictional energy is lost during a martensitic transformation. This frictional energy will always contribute a positive term to the enthalpy change. The BCC to BCT transformation is endothermic, and will produce a negative enthalpy change. The BCT to BCC phase transformation is exothermic, and will produce a positive enthalpy change. The frictional term is added to both of these reactions, which decreases the magnitude of the BCT to BCC enthalpy change and increases the BCC to BCT enthalpy change. If we assume that the frictional energies produced by both the forward and reverse martensitic transformations are the same, then the average of the magnitudes of the enthalpies is the enthalpy associated with phase transformation. With the same assumption, one half the difference of the magnitudes is the enthalpy change due to friction. Thus

$$\Delta h_{pt} = \frac{|\Delta h_{BCT\text{-}BCC}| + |\Delta h_{BCC\text{-}BCT}|}{2}$$
$$\Delta h_{f} = \frac{|\Delta h_{BCT\text{-}BCC}| - |\Delta h_{BCC\text{-}BCT}|}{2} \qquad (2.1)$$

where subscripts pt and f refer to phase transformation and friction respectively.

The $\Delta h_{pt}$ of the unstrained sample is 1.05 cal/gram, while the $\Delta h_{pt}$ of the strained sample is 0.61 cal/gram. This indicates that less of the strained sample is transformed. The frictional enthalpy change was calculated as 0.16 cal/gram for the unstrained

sample and 0.26 cal/gram for the strained sample, using Eq. 2.1. Thus the strained sample had a smaller amount of material transformed and a greater amount of friction associated with this transformation.

With the above knowledge of the increased friction of transformation and the decrease in the amount of Cu-Zn-Al transforming, the Stress vs Strain curves of Fig. 2.2 can be explained. The first cycle is the expected superelastic relationship. During this cycle, the dislocations are formed from the phase transformation [17] and the internal friction increases. The increased friction has the effect of widening the interval between the loading and unloading stress strain paths. In Cu-Zn-Al, this widening is large enough to cause a stress strain curve to look like a simple hysteresis loop.

# SECTION 3

# DAMPER DESIGN

## 3.1 Requirements of SMA Damper

The essential idea behind the damper design was to create a structural damper that would take advantage of the Cu-Zn-Al superelastic material properties, discussed in Sec. 2, to damp the building's motion and generate a centering force on the building. The purpose of this form of a damper is to minimize the motion of the building during the earthquake, and to restore the building to its original position after the earthquake is over.

A model five story building, built by the joint U.S.-China Cooperative Research Program, was used to test the SMA dampers. The building was designed to allow different dampers to be installed in the cross bracing. The cross bracing is at a 45° angle to the floor as shown in Fig. 3.1.

The dampers had to be designed to satisfy the requirements of the model five story building, on which the earthquake tests were performed. Because the building is used for many tests, the tests must of course not damage the building. To prevent such damage, the maximum inter-story drift was limited to .25 inches. Furthermore, since we did not want to drastically change the natural frequency of the building, the maximum additional inter-story stiffness, due to the presence of the dampers, was set at 9000 lbs/inch maximum.

Along with constraints imposed by the building there were also some material constraints to be considered in the design. The

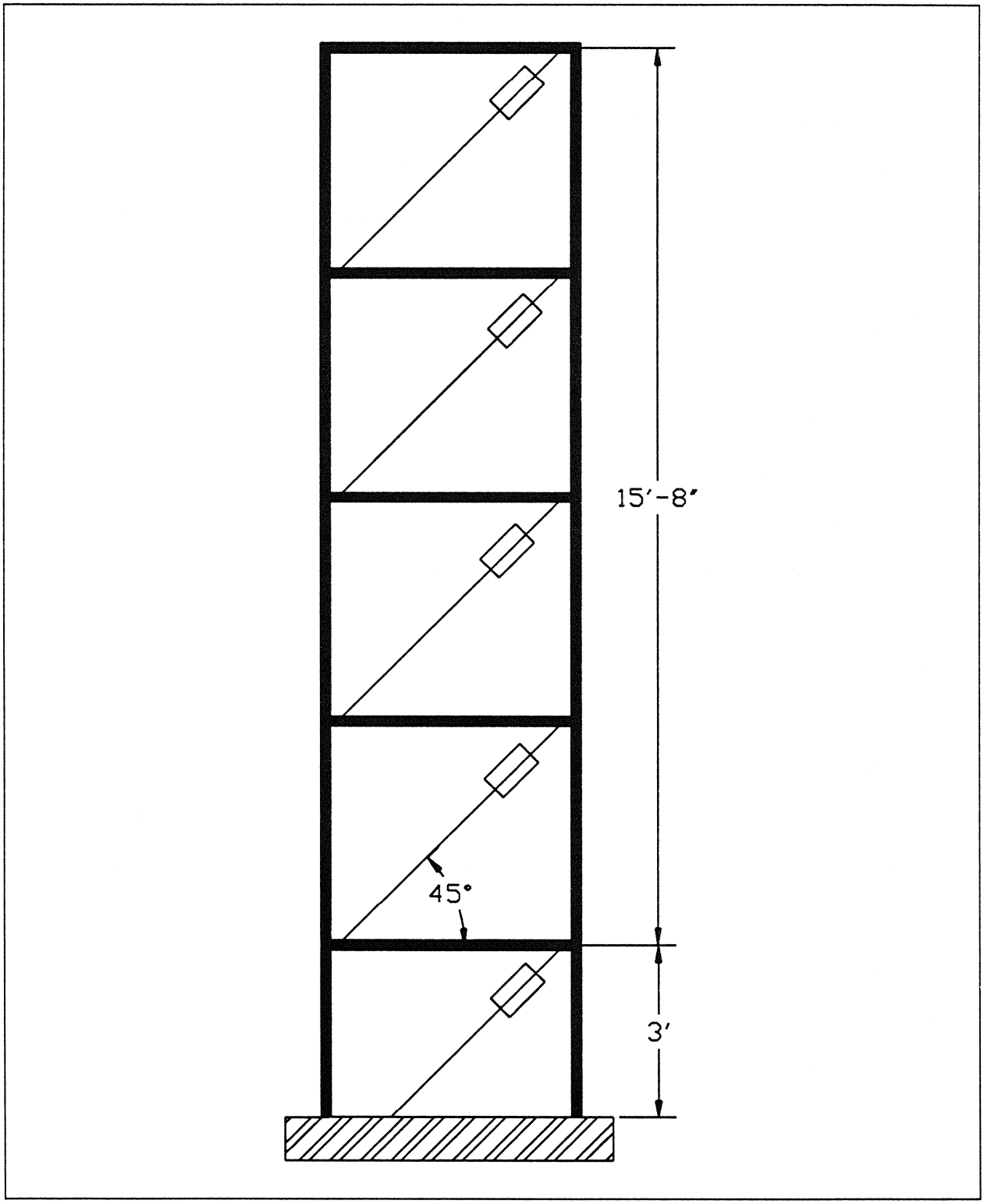


**Figure 3-1 Five Story Model building**

maximum strain in the Cu-Zn-Al was set at 2% to guarantee that the material would not yield plastically. However the design had to ensure that strains up to this 2% maximum would be induced, because larger energy absorbing shape memory hysteresis loops occur at the high strain levels.

## 3.2 Selecting Damper Design

Four designs for producing such a damping device using Cu-Zn-Al were investigated. The designs' principal mechanisms were the bar in torsion, beam in bending, axially loaded beam and the clamped plate loaded in the center. In the comparison of these different types of devices, a linear constitutive law was used although it is quite clear from Sec. 2 that a nonlinear model would more accurately predict the behavior. However, it became clear, from the linear analysis to follow, which design would work the best. A nonlinear model was then used to more accurately determine the exact dimensions of the design.

In the following analysis, the shear and Young's moduli were estimated from the tensile tests on Cu-Zn-Al (Sec. 2.4). Young's modulus was taken to be the stress divided by the strain at 2.4% strain. The shear modulus was then taken to be half the Young's modulus. The values gave a rough estimate on the performance of the damper, and was all that was needed to determine which design to use.

The first design considered was the Cu-Zn-Al annular plate clamped at the inside edge and at the outside edge (Fig. 3.2).

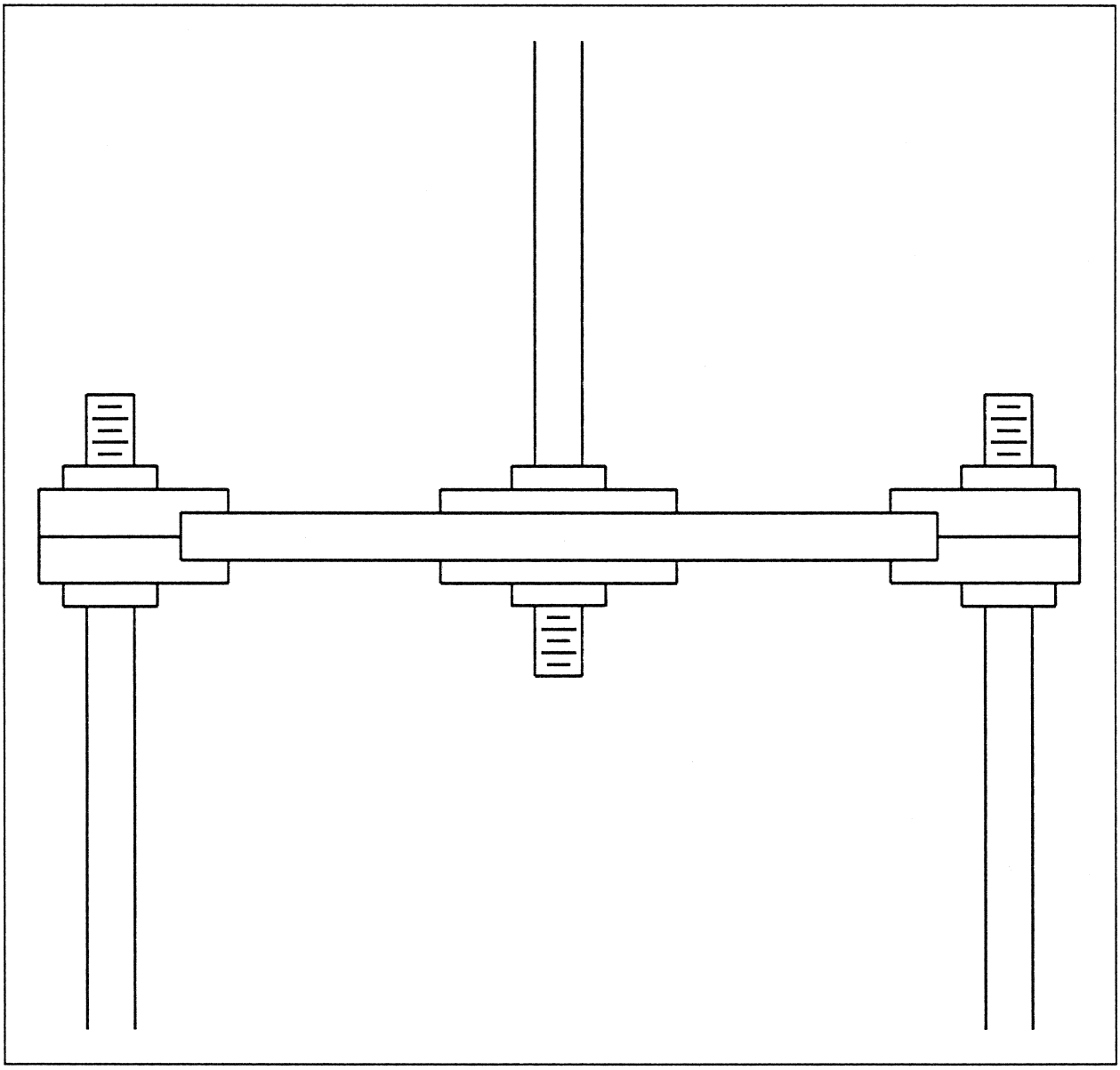

**Fig 3-2 Annular Plate**

After an examination at the force deflection equation [1], with thicknesses and radii of Cu-Zn-Al washers that were practical to machine, it was found that the idea was much too stiff and resulted in very small strains. The axially loaded beam was also found to be unsuitable, because the constraints of stiffness and strain would cause a beam, made from Cu-Zn-Al with these properties, to buckle.

The torsional bar and bending beam designs both could be made with the suitable stiffness and the desirable strains. Therefore an analysis comparing the two energy absorbing capabilities of the two designs was completed in order to determine which design is best. Since larger strains clearly result in more energy absorbed during cyclic loading (Sec 2), the strain ranges $\varepsilon_{low}$ to $\varepsilon_{max}$ that contain 90% of the strain energy was compared between the two designs. Below is the development of the analysis for both the bending beam and torsional bar designs.

The bending beam design (Fig. 3.3) is clamped in the middle and at the outside edges. Note that the direction of the deflection of the damper ($\delta$) is in the same direction as the applied force F. The force (F) deflection ($\delta$) equation in terms of the length of the beam (L), width of beam (B), height of beam (H), and modulus of Cu-Zn-Al (E) becomes [1]

$$F=\frac{2EBH^3}{L^3}\delta \qquad (3.1)$$

Due to the constraint of stiffness (S) imposed by the building, we

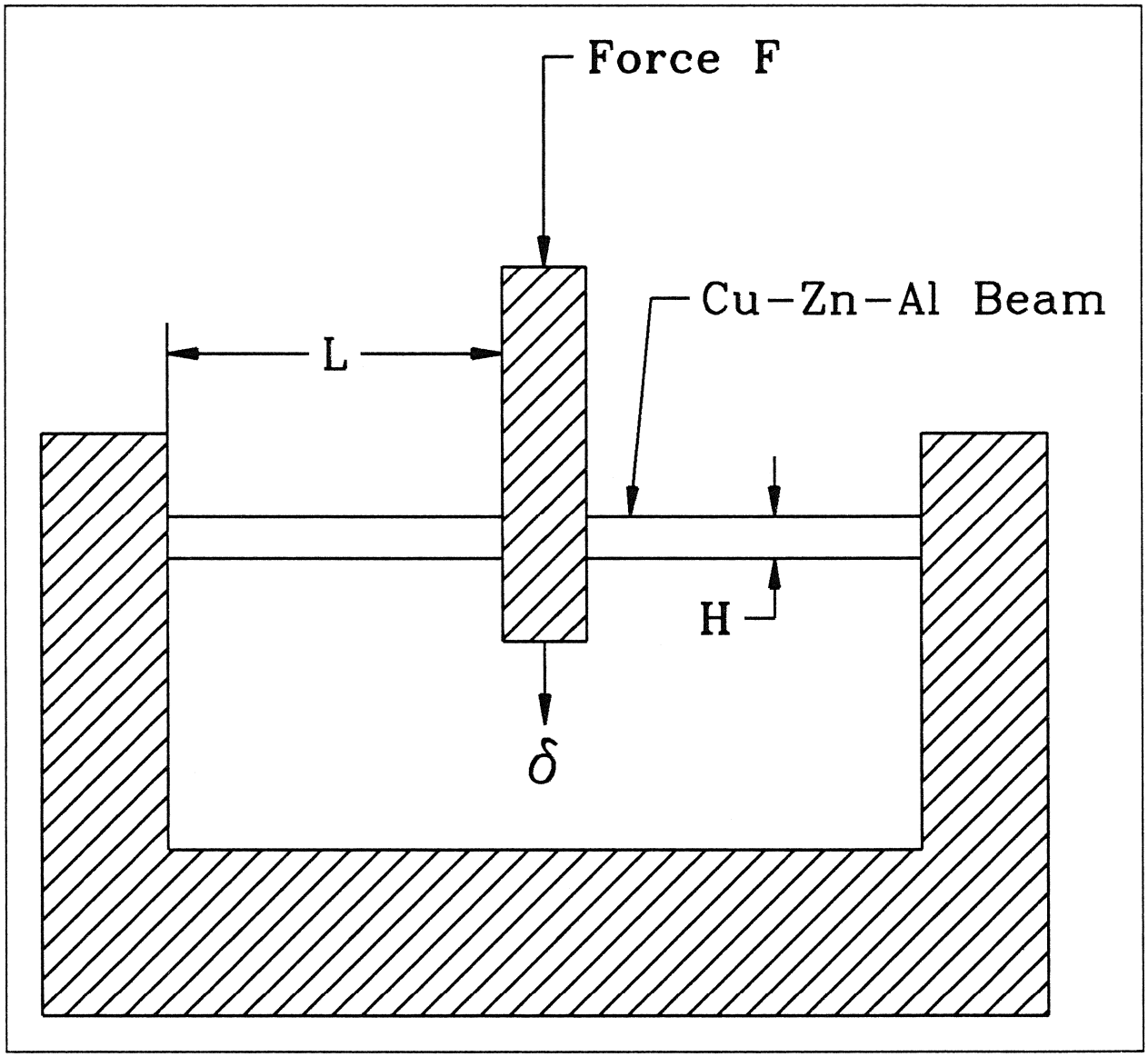


**Fig. 3-3 Bending Beam Design**

shall ensure the proper stiffness S by setting it to the expression

$$S=\frac{2EBH^3}{L^3} \tag{3.2}$$

Therefore the force deflection equation reduces to $F=S\delta$. The bending moment equation along the length of the beam [2] is

$$M(X)=\frac{F}{4}[2X-L] \tag{3.3}$$

Combining the linear elastic constitutive law $\tau=E\varepsilon_{xx}$, the strength of materials flexure formula, and the bending moment equation above, and then solving for the strain yields

$$\epsilon_{xx}=\frac{3Fy}{EBH^3}[2X-L] \tag{3.4}$$

The maximum strain $\varepsilon_{max}$ occurs at x=L, y=H/2, and the maximum force $F=S\Delta$, where $\Delta$ is the maximum expected displacement of the damper. Substituting these values in Eq. (3.4) yields

$$\epsilon_{max}=\frac{3LS\Delta}{2EBH^2} \tag{3.5}$$

Solving Eq. (3.2) and (3.5) for B and H then yields

$$B=\frac{27S\Delta^3}{2E\epsilon_{max}^3L^3} \qquad H=\frac{\epsilon_{max}L^2}{3\Delta} \tag{3.6}$$

Substituting Eq. (3.6) back into Eq. (3.4) yields

$$\epsilon_{xx}=\frac{6\Delta(2x-L)y}{L^3} \tag{7}$$

Eq. (3.6) and Eq. (3.7) allow the constraints of stiffness (S), maximum strain ($\varepsilon_{xx}$), and maximum deflection ($\Delta$) to be prescribed, so that the height (H) and thickness (B) of the beam becomes a function of L only.

The strain energy density is given by $U_o=\frac{1}{2}E\varepsilon^2_{xx}$. The strain energy function is symmetric in both the horizontal and vertical directions. Therefore, it is necessary to integrate over only one quarter of the beam. However, if only one quarter of the beam is used for integration, the total strain function must be multiplied by eight, since there are two symmetric beams (Fig 3.3) of length L with four sections of symmetry. The integral of the strain energy is thus

$$U=8\int_{x_{min}}^{x_{max}}\int_{y_{min}}^{y_{max}}\int_{z_{min}}^{z_{max}}\frac{1}{2}E\epsilon^2_{xx}dzdydx \tag{8}$$

In order to integrate over the region of high strain, the limits of integration must be found. The region of high strain shall be defined as the region with strains between $\varepsilon_{low}$ and $\varepsilon_{max}$. Since the strain is not a function of the z direction, the limits become $Z_{min}=0$ and $z_{max}=B$. Clearly the end of the beam is the high limit of integration in the x direction thus $x_{max}=L$. The lower limit can be found by substituting into Eq. (3.7) the values $\varepsilon_{xx}=\varepsilon_{low}$ and y=H/2, and solving for x. Substituting Eq. (3.6) into the resulting expression yields

$$x_{min}=\frac{L}{4}\left[\frac{\epsilon_{low}}{\epsilon_{max}}+1\right] \tag{3.9}$$

The top of the beam is clearly the max limit in the y direction $y_{max}=H/2$. The lower limit can be found as a function of x by setting $\varepsilon_{xx}=\varepsilon_{low}$ and solving for y. This limit becomes

$$y_{min}=\frac{L^3\epsilon_{low}}{6\Delta(2x-L)} \tag{3.10}$$

The integral over the area of high strain, with appropriate limits, now becomes

$$U=8\int_{\frac{L}{2}\left[\frac{\epsilon_{low}}{\epsilon_{max}}+1\right]}^{L}\int_{\frac{L^3\epsilon_{low}}{6\Delta(2x-L)}}^{\frac{H}{2}}\int_0^B\frac{18\Delta^2E(2x-L)y^2}{L^6}dzdydx \tag{3.11}$$

Integrating and substituting $\beta=\varepsilon_{low}/\varepsilon_{max}$ yields

$$U=\frac{S\Delta^2}{2}\left[1-\beta^3+3\beta^3\ln(\beta)\right] \tag{3.12}$$

If $\varepsilon_{low}=0$ then $\beta=0$ and Eq. (3.12) simplifies to $U=\Delta^2S/2$ which is the total energy of the system.

The strain energy of the torsional bar will now be investigated. The basic dimensions of the damper used in the design are the torsion arm length D, radius of torsion bar R, and length of torsion bar L (Fig. 3.4). Note that the torsion bar length L is defined as the distance between the torsion arm and the side grips as shown in the drawing of the torsional bar design (Fig. 3.4) The torsion arm length is measured from the center of

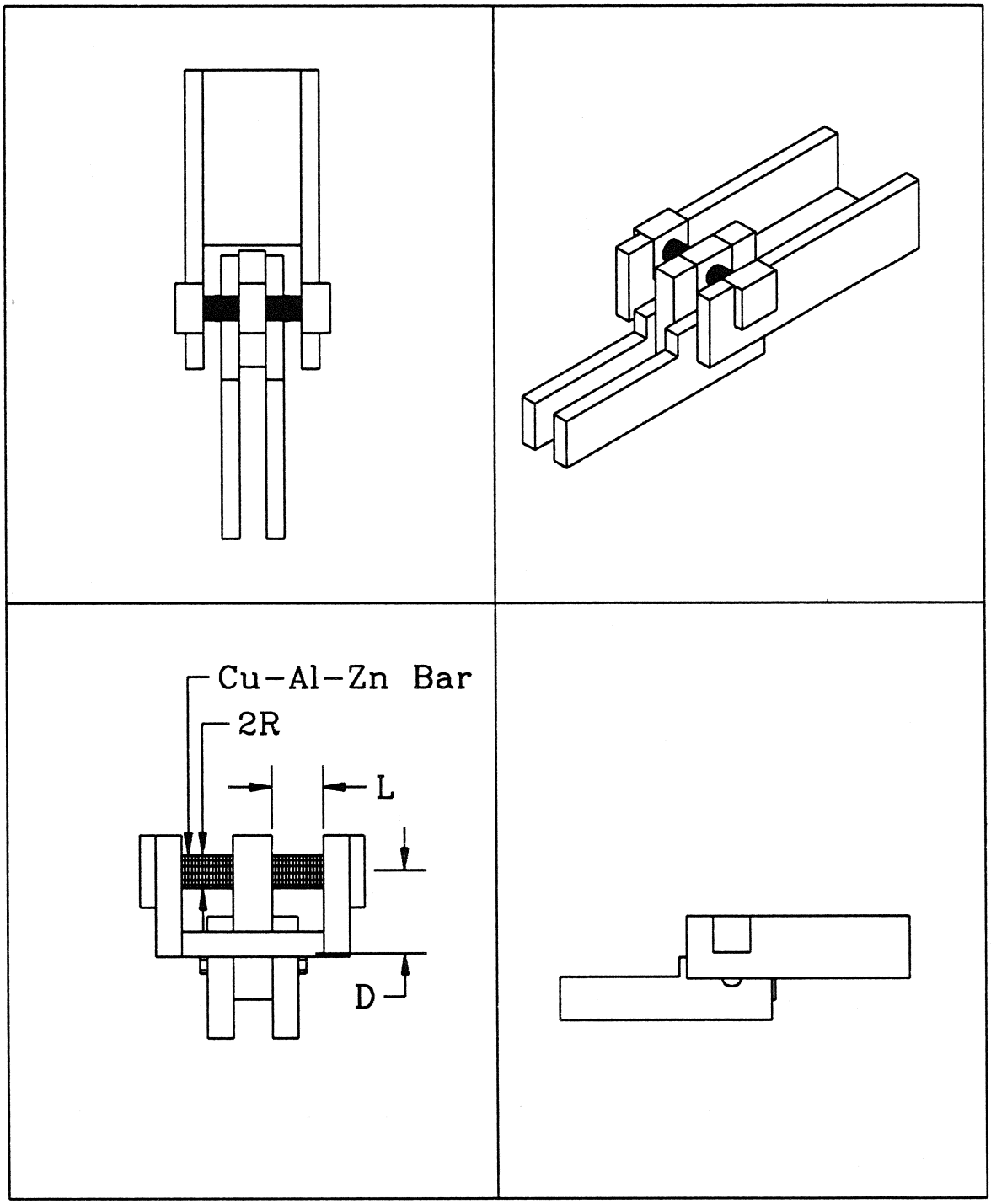


**Fig. 3-4 Torsional Bar Design**

the torsion arm to the center of the pivot. The displacement $\delta$ is again in the same direction as the force F (Fig. 3.4).

From solid mechanics, the angle of twist $\theta$ of a solid round bar of radius R and length L with a torque T applied at the end of the bar is

$$\theta = \frac{2TL}{GR^4} \tag{3.13}$$

The angle of twist $\theta$ due to the displacement $\delta$ is expected to be small, therefore

$$\frac{\delta}{D} = \sin(\theta) \approx \theta \tag{3.14}$$

The equation for shear strain $\varepsilon_{xy}$, in terms of the L,D,$\delta$ and the radial distance from the center of the Cu-Zn-Al bar r, is

$$\epsilon_{xy} = \frac{\theta r}{2L} = \frac{\delta r}{2LD} \tag{3.15}$$

Also, the equation for the force F on the damper in terms of L,D,$\delta$ and r is given by

$$F = \frac{\pi G R^4 \delta}{LD^2} \tag{3.16}$$

As before, the stiffness S is defined so that $F = S\delta$, giving

$$S = \frac{\pi G R^4}{LD^2} \tag{3.17}$$

The maximum shear strain occurs at r=R when $\delta$ is equal to the maximum deflection allowed ($\Delta$). Substitution into Eq. (3.15) yields

$$\epsilon_{max}=\frac{\Delta R}{2LD} \tag{3.18}$$

Solving Eq. (3.17) and Eq. (3.18) for L and D yields

$$L=\frac{\Delta^2 S}{4\pi GR^2\epsilon_{max}^2}, \qquad D=\frac{2\pi GR^3\epsilon_{max}}{\Delta S} \tag{3.19}$$

Upon substitution of Eq. (3.19) into Eq. (3.15) the following simple expression for shear strain results

$$\epsilon_{xy}=\frac{\epsilon_{max}r}{R} \tag{3.20}$$

The equation for strain energy density is $U_o=2G\varepsilon^2_{xy}$. This equation must be integrated over the high strain region in a manner similar to the procedure used for the bending beam design. The strain is independent of the y and $\theta$ directions, so those limits become $y_{min}=0$, $y_{max}=L$, $\theta_{min}=0$ and $\theta_{max}=2\pi$. The maximum limit in the r direction is $r_{max}=R$. The minimum value of r can be found by substituting $\varepsilon_{low}$ for $\varepsilon_{xx}$ in Eq. (3.20); this limit then becomes $r_{low}=R\varepsilon_{low}/\varepsilon_{max}$. The total strain energy function, after using Eq. (3.19) to eliminate L, finally becomes

$$U=2\int_0^{2\pi}\int_0^{\frac{\Delta^2 S}{4\pi GR^2\epsilon_{max}^2}}\int_{\frac{R\epsilon_{low}}{\epsilon_{max}}}^{R}\frac{2G\epsilon_{low}^2}{R^2}r^3\,dr\,dy\,d\theta \qquad (3.21)$$

Integrating and substituting $\beta=\varepsilon_{low}/\varepsilon_{max}$ yields

$$U=\frac{\Delta^2 S}{2}[1-\beta^4] \qquad (3.22)$$

If $\varepsilon_{low}=0$ then $\beta=0$, and Eq. (3.20) simplifies to $U=\Delta^2 S/2$ which is the total energy put into the system.

The strain energy equations Eq. (3.12) and Eq. (3.22) can be divided by $\Delta^2 S/2$ to yield the percent of the total strain energy $\Delta^2 S/2$ as a function of the strain range $\beta$ integrated over. Fig. 3-5 is a comparative plot of the percent total strain energy vs the strain range $\beta$ for the torsional bar and the bending beam designs. It can be seen from Fig. 3-5 that for any given $\beta$ between 0 and 1 the percent of total strain energy contained within that region is higher for the torsional bar damper design. This means that more of the energy is put into higher strain regions in the torsional bar design than the bending beam design. The larger strain results in a greater amount of energy absorbed, and therefore the torsional bar design apparently results in a more effective damper.

### 3.3 Final Damper Design

The finalized damper design was determined though analytical and experimental methods. The first damper was designed by employing available analytical tools and material data. This

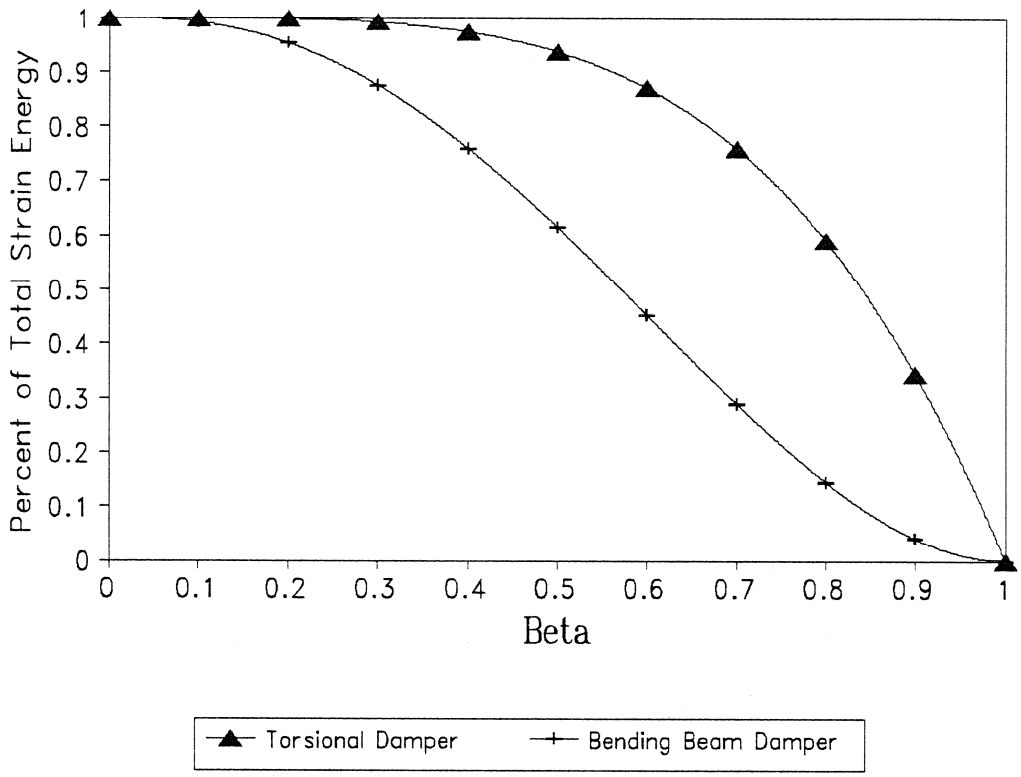


**Fig. 3-5 Percent Strain Energy vs Strain Range β**

design was then built and tested on the MTS tensile tester. The results were then used to modify the estimated material properties and determine a new design.

After the torsional bar design was chosen, a more accurate nonlinear model for design was developed. The constitutive law used in the analysis was bilinear, i.e.

$$\tau_{xy}=2G_1\epsilon_{xy}+[2(G_1-G_2)(\epsilon_t-\epsilon_{xy})]U(\epsilon_{xy}-\epsilon_t) \qquad (3.23)$$

Notice there are two shear moduli: $G_1$ which is the elastic shear modulus and $G_2$ the inelastic shear modulus (see Fig 3.6). Also

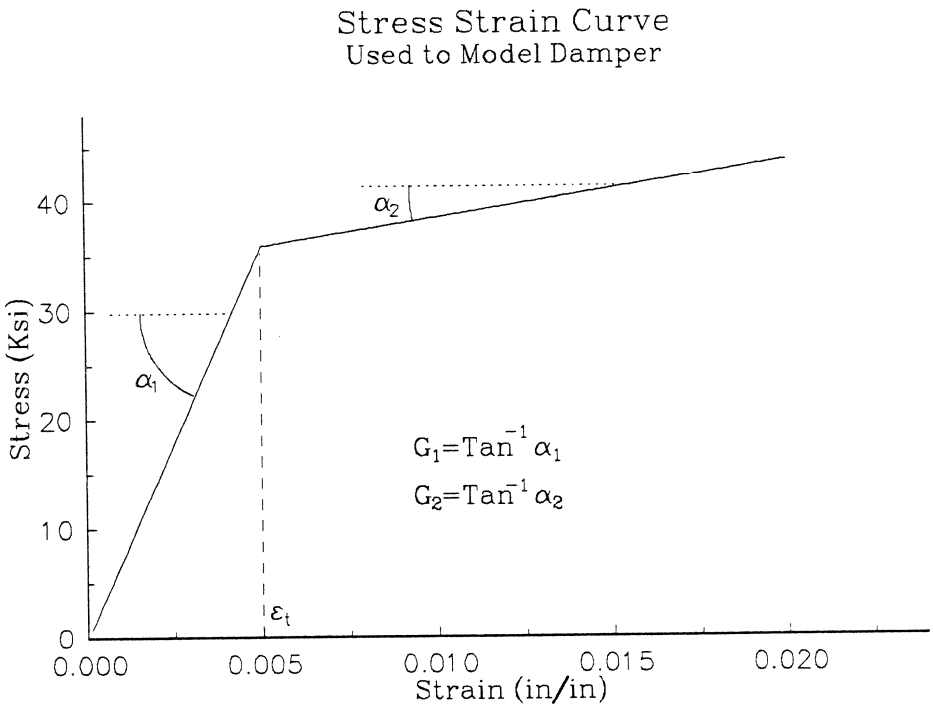


**Fig. 3-6 Stress Strain Curve Used to Model Damper.**

note from the figure that $\varepsilon_t$ is the value of the strain at which the stress strain diagram changes slope. The term $U(\varepsilon_{xy}-\varepsilon_t)$ is a step function and is defined as follows:

$$U(x)=\begin{cases}0 & \text{if } x\le 0\\ 1 & \text{if } x>0\end{cases} \qquad (3.24)$$

The stress strain curve for Eq. (3.23) is given in Fig 3.6.

The torque produced from the two torsional bars in the damper design (Fig. 3.4) is

$$T=FD=2\int_0^{2\pi}\int_0^{R}(\tau_{xy}r)\,r\,dr\,d\theta \qquad (3.25)$$

Substituting in the constitutive law, Eq. (3.23), and Eq. (3.15) for the shear strain, and solving for the force F gives the following:

$$F=\frac{4}{D}\int_0^{2\pi}\int_0^{R}\left\{\frac{G_2\delta}{2LD^2}r+[(G_1-G_2)(\epsilon_t-\frac{\delta}{2LD}r)]U(\epsilon_{xy}-\epsilon_t)\right\}r^2\,dr\,d\theta \qquad (3.26)$$

Assuming that $R>2LD\varepsilon_t/\delta$, the integration of Eq. (3.26) simplifies after some manipulation to

$$F=\frac{\pi G_2R^4}{LD^2}\delta+\frac{8\pi\epsilon_t}{3D}(G_1-G_2)\left[R^3-\frac{2(LD\epsilon_t)^3}{\delta^3}\right] \qquad (3.27)$$

The above equation gives the force deflection curve for different values of L,D and R. For design, however, we must control the

maximum strain $\varepsilon_{max}$ and the stiffness S. The stiffness will now be redefined as the force needed to produce the maximum deflection $\Delta$, divided by $\Delta$. With $\delta$ equal to $\Delta$ and with S as defined above, Eq. (3.18) and Eq. (3.27) are solved for D and R in terms of L. The results are as follows:

$$D=\left(\frac{3S\Delta^4}{2^4\pi L^3\epsilon_{max}[3G_2\epsilon_{max}^4+\epsilon_t(G_1-G_2)(4\epsilon_{max}^3-\epsilon_t^3)]}\right)^{\frac{1}{2}}$$

$$R=\left(\frac{3S\Delta^2\epsilon_{max}}{2^2\pi L[3G_2\epsilon_{max}^4+\epsilon_t(G_1-G_2)(4\epsilon_{max}^3-\epsilon_t^3)]}\right)^{\frac{1}{2}} \qquad (3.28)$$

The original damper was designed to err on the stiff side, because the radius of the torsional bar could be turned down on the lathe and then retested until the correct stiffness was achieved. After the first damper was built and tested at different radii, the shear modulus was modified to fit the results of the testing and the final design was determined. A schematic drawing of the damper and the bracing is presented in Appendix A.

It should be noted that in the torsion bar design, the Cu-Zn-Al bar acts as a beam in bending in addition to the desired mechanism of a bar in torsion. Since the Cu-Zn-Al bar is clamped on both ends, the deflection of the Cu-Zn-Al bar due to bending can be modeled as a beam clamped at the ends and loaded at midspan. Using a linear constitutive relationship, the stiffness K of the torsion bar in bending is

The stiffness due to torsion for the same bar is given in Eq. 3.17.

$$K = \frac{6\pi E R^4}{L^3} \tag{3.29}$$

Dividing Eq. 3.17 by Eq. 3.29 and replacing G with E/(1+ν) gives with a little rearrangement

$$\frac{S}{K} = \frac{1}{6(1+\nu)}\left(\frac{L}{D}\right)^2 \tag{3.30}$$

To ensure that the deflection of the Cu-Zn-Al bar in bending is insignificant in comparison to the deflection due to the torsion, we set $S/K<0.1$. Assuming $\nu=0.3$, $D>1.13L$ would satisfy the above conditions.

### 3.4 Cu-Zn-Al Damper Testing

After the damper had been constructed and the Cu-Zn-Al heat treated, the damper was tested on the MTS machine. Fig. 3.6 shows the force deflection relationship of the Cu-Zn-Al torsional bar structural damper. The shape of the force deflection curve changes in a similar fashion to the Cu-Zn-Al stress strain curves in Sec. 2.4. The first cycle of the force deflection curve has a much more pronounced superelastic characteristic than the subsequent cycles.

A comparison between the stiffness and energy loss between the SMA damper and the viscoelastic damper can now be made. The stiffness of the SMA damper was 8813 lb/inch, which was the target stiffness. In addition, the energy loss per cycle was calculated to be 68.1 lb-in. The fourth cycle was used for this calculation since the force deflection curve has stabilized at that cycle. The

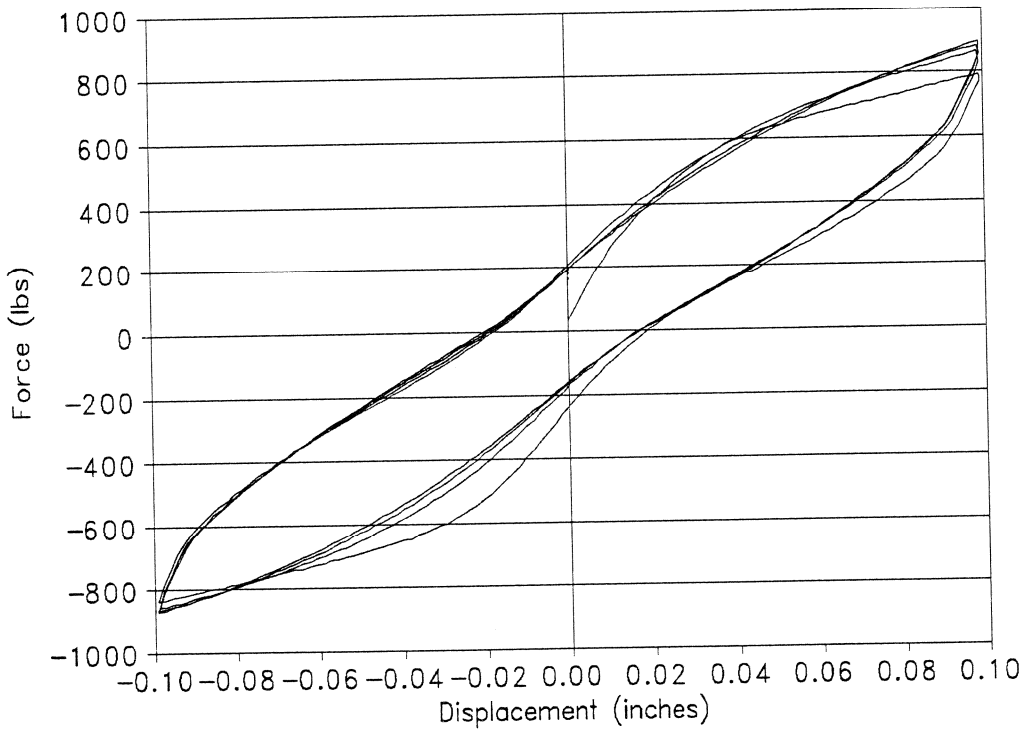


**Fig. 3-7 Force vs Disp. of Cu-Zn-Al Damper.**

viscoelastic damper's stiffness and energy loss per cycle varied with frequency, temperature and percent strain [5]. At 0.1 Hz, 5% strain and 40°C, the viscoelastic damper had a energy loss per cycle of 69 lb-in and a stiffness of 322 lb/inch. However at 4 Hz, and 20% strain and 21°C, the same viscoelastic damper had a energy loss per cycle of 28431 lb-in and a stiffness of 5311 lb/inch. These results would indicate that the viscoelastic damper would provide greater damping than the SMA damper.

It should be pointed out that while the SMA damper does not provide as much damping as a viscoelastic damper, it can be used in applications where the viscoelastic damper cannot. The three fundamental advantages of a damper designed with SMA material over viscoelastic material are: SMA are much stronger, relatively insensitive to temperature, and it can provide a restoring force. These three factors make SMA materials suitable for a base isolation system. A base isolation system must be strong enough to support the building and should restore the building back to its original position after an earthquake. The viscoelastic damper could not be used for this purpose since the material is much to soft to support this type of load.

# SECTION 4

# EARTHQUAKE SIMULATOR TESTS

## 4.1 Test Set-Up

As noted in Sec. 3, the test structure used was a five-story model building (refer back to Fig. 3.1). The model building is 224.0" in height and 52.0" on each side. Diagonal braces with SMA dampers were bolted to the gusset plates welded to the girders (Fig. 4.1). The acceleration and absolute displacement in the horizontal direction were measured on the east and west sides of the concrete base and on each floor of the building. In addition, the displacement $\delta$, across the damper between the second and third floors on both sides of the building, was also measured. The placement of the displacement and acceleration measurement devices is shown in Fig. 4.2. Temposonic displacement transducer's and Endevco accelerometer's were used for the displacement and acceleration measurements. Strain was also measured using strain gauges on the top and bottom of the girders of the second and third floors, where the strain was expected to be the largest.

A banded white noise test was run to determine the frequency response function of the structure. This frequency response function was then used to construct simulated ground motions of the Hachinohe, Olympia, El Centro and Quebec earthquake records. To prevent damage to the structure, each ground motion was initially run with a conservatively small peak acceleration of 0.06g's. The magnitudes of the ground motions were then increased until it was determined that the structure would be damaged by any further

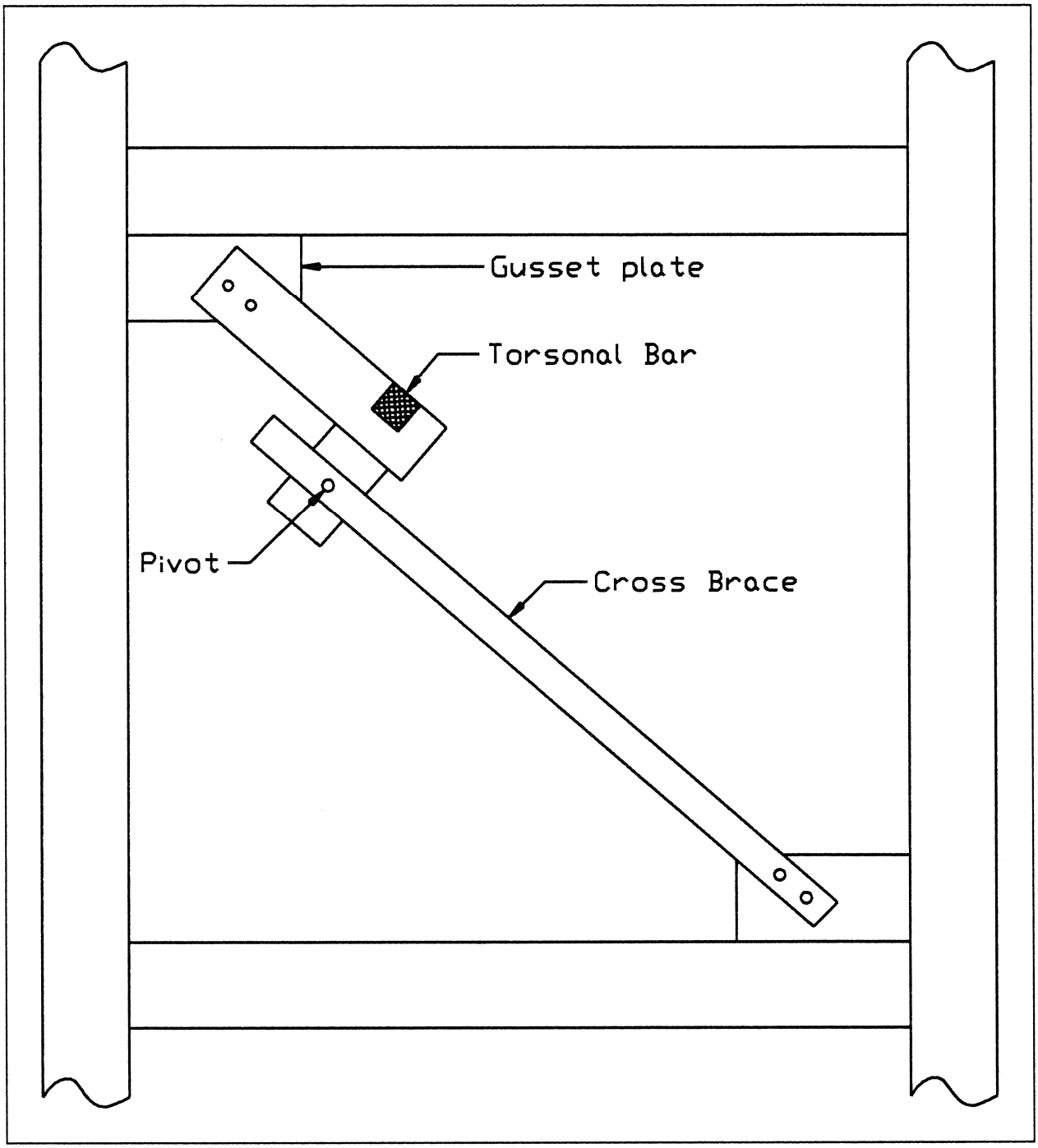


**Fig. 4-1 Placement of SMA Dampers Between Floors**

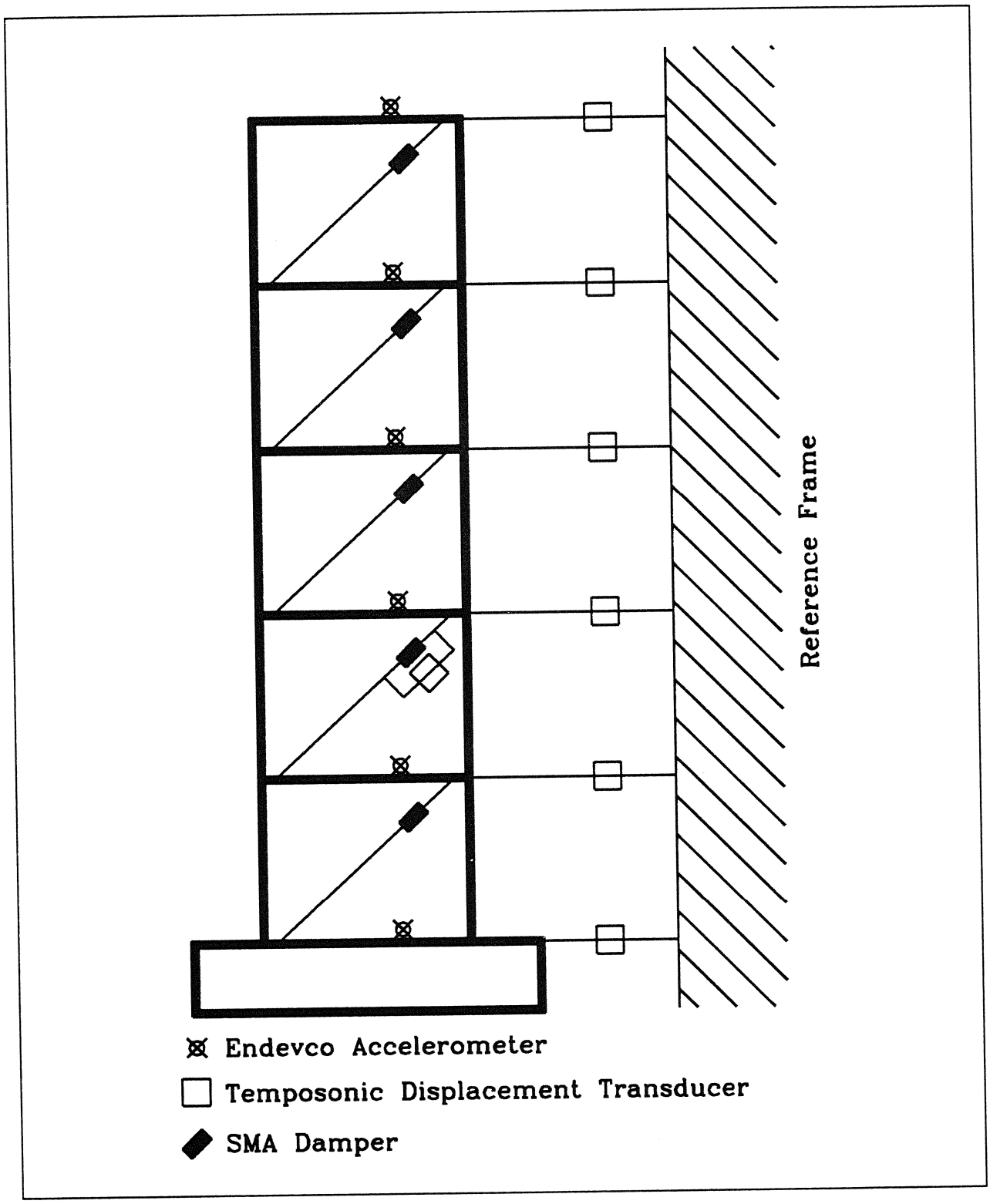


Fig. 4-2 Instrumentation of Model Structure

increase. The maximum inter-story drift and maximum strain measured during the tests determined whether or not an earthquake of greater magnitude would be run. All four earthquakes and banded white noise were run with peak accelerations of 0.06g, 0.12g, 0.24g and 0.36g. In addition, the structure was subjected to banded white noise and the four ground motions at 0.06g's with no dampers.

## 4.2 Test Results

Bar graphs, which compare the damped to undamped building responses for the four earthquake records, are given in Figs. 4.3-4.15. Figs. 4.3-4.6 present the maximum relative floor displacements, with and without dampers, for the four earthquake records. Figs. 4.7-4.10 present the maximum floor accelerations for the same cases. Finally, Figs. 4.11-4.15 present the maximum inter-story drift for these same cases. Table 4.1 summarizes the results of Figs. 4.3-4.15 by listing the maximum responses of the undamped structure and the percent reduction of responses of the damped structure, for all the above mentioned cases.

In Sec. 3.3, we noted that larger damper displacements resulted in larger energy absorbing hysteresis loops. It was also noted that the damper stiffness decreases with increasing deflections. This change in stiffness and energy absorbing hysteresis loops with deflection, was expected to cause a change in the natural frequency and damping ratio of the building as the magnitudes of the ground motions increased. Since the damper stiffness decreases with larger deformation (Sec. 3.3), the natural

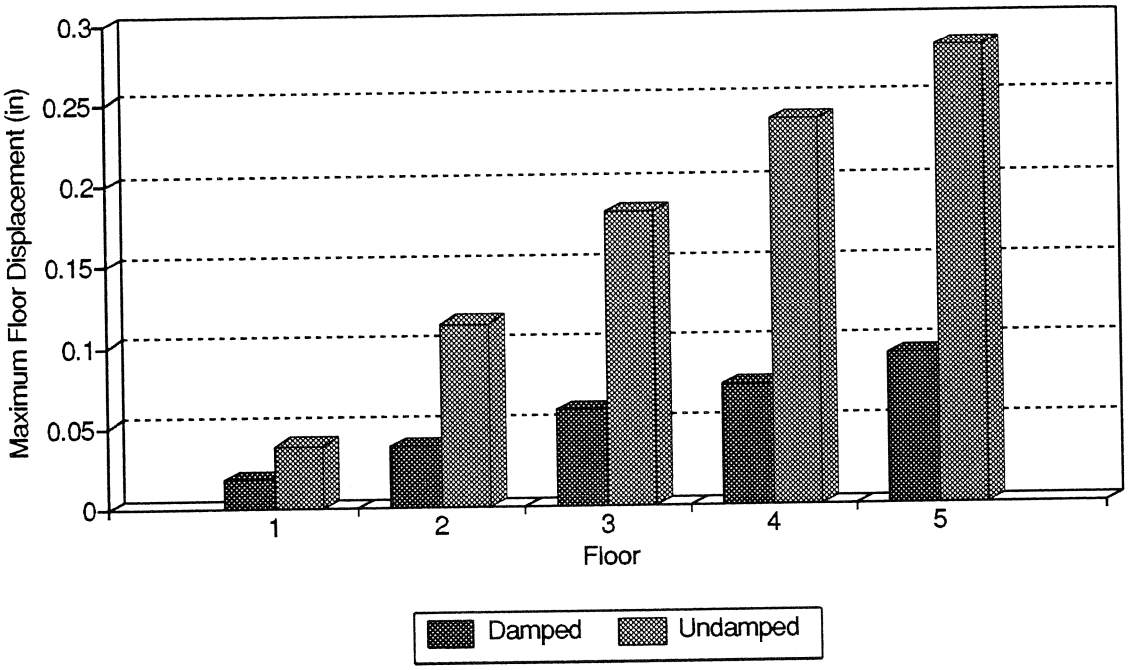


**Fig 4-3 Max Floor Disp. (0.06 El Centro)**

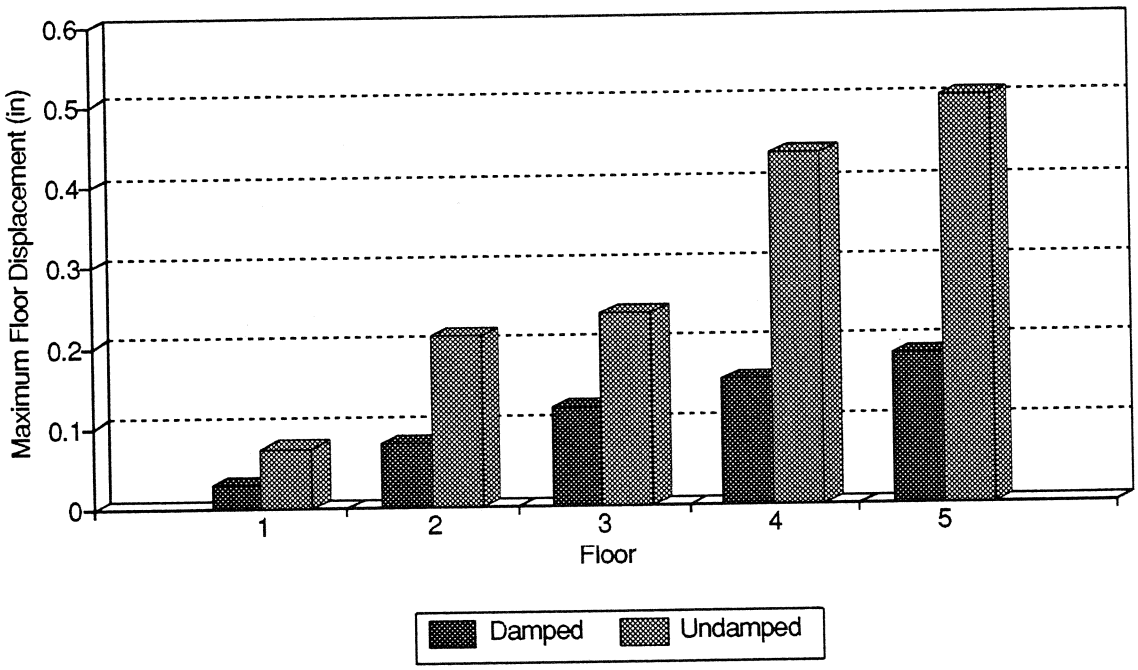


**Fig 4-4 Max Floor Disp. (0.06 Hachinohe)**

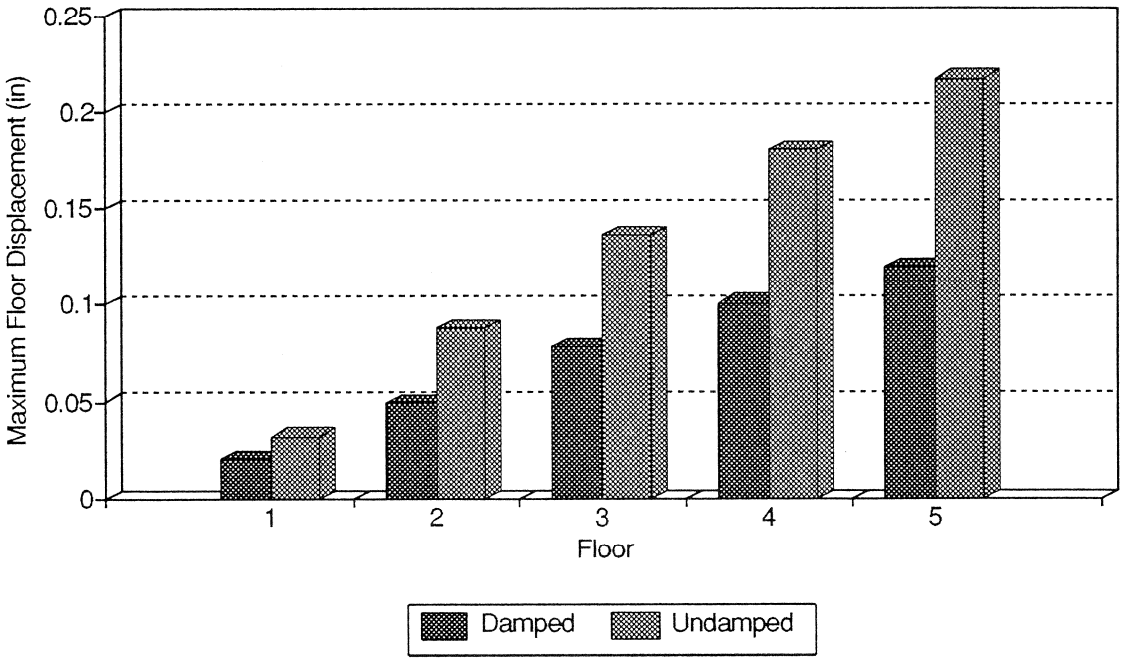


**Fig 4-5 Max Floor Disp. (0.06 Olypia)**

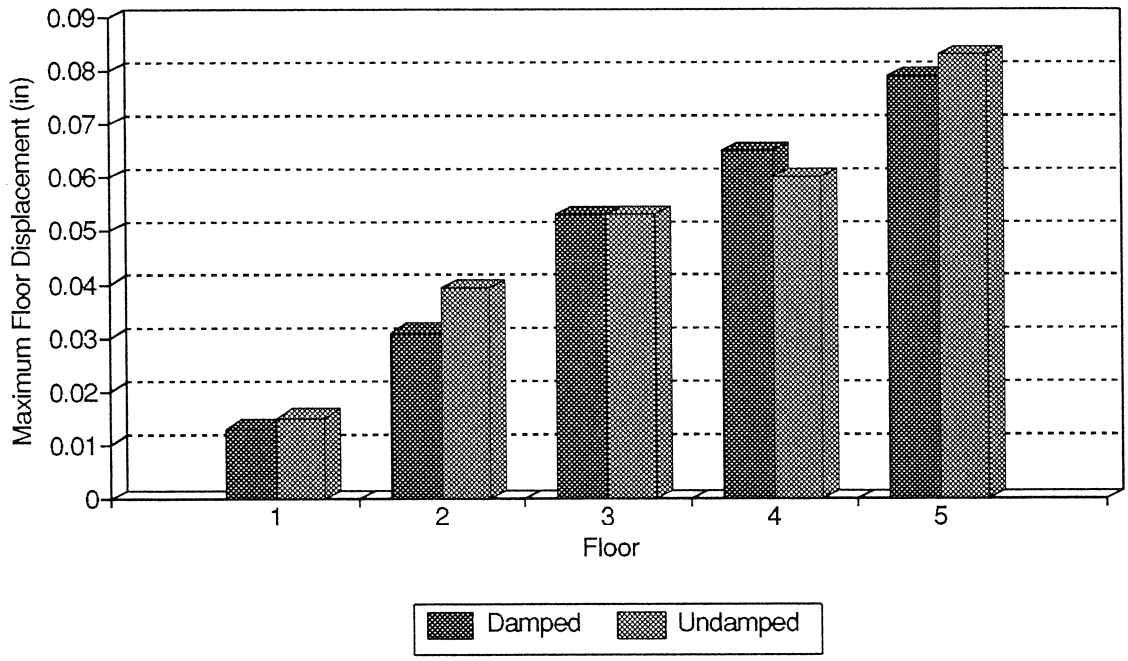


**Fig 4-6 Max Floor Disp. (0.06 Quebec)**

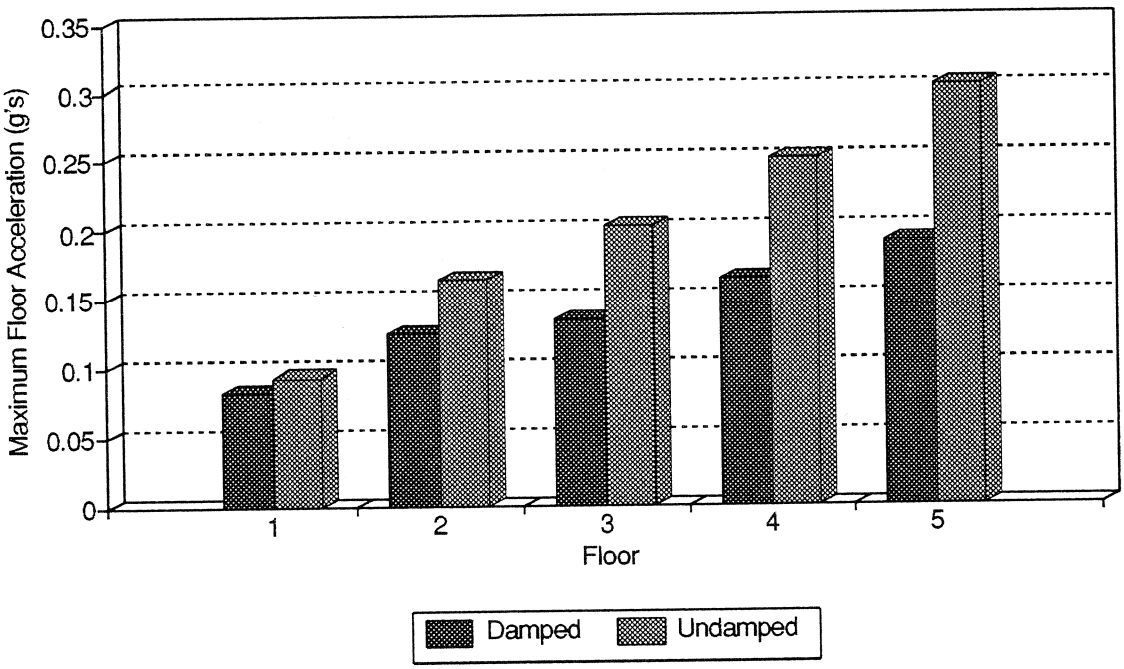


**Fig 4-7 Max Floor Acceleration (0.06 El Centro)**

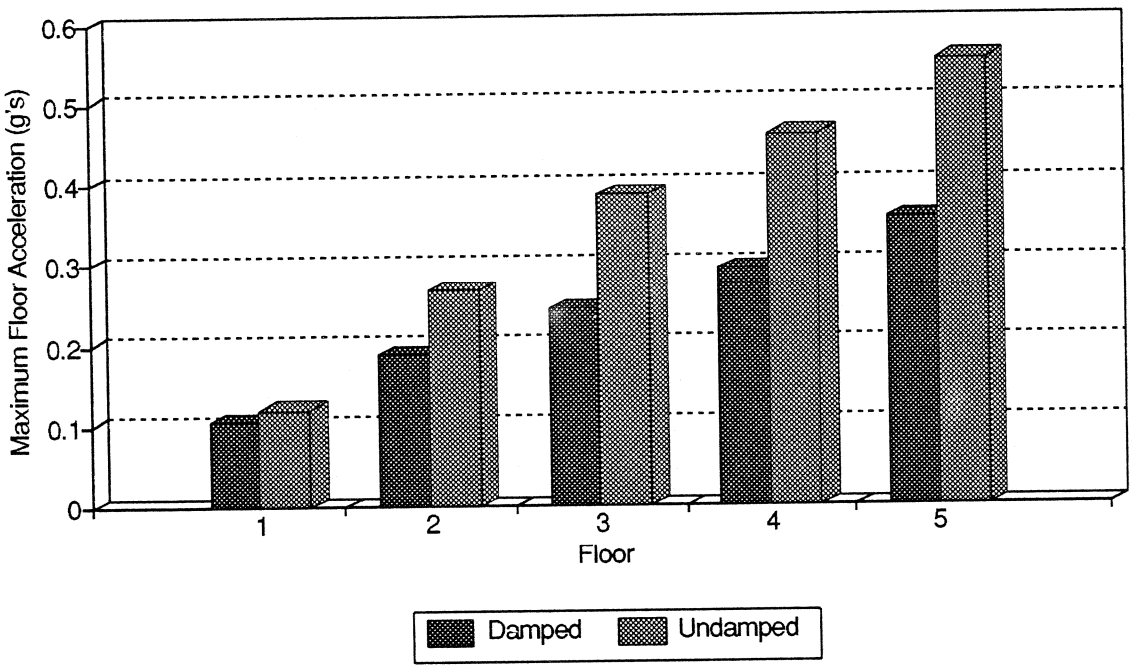


**Fig 4-8 Max Floor Acceleration (0.06 Hachinohe)**

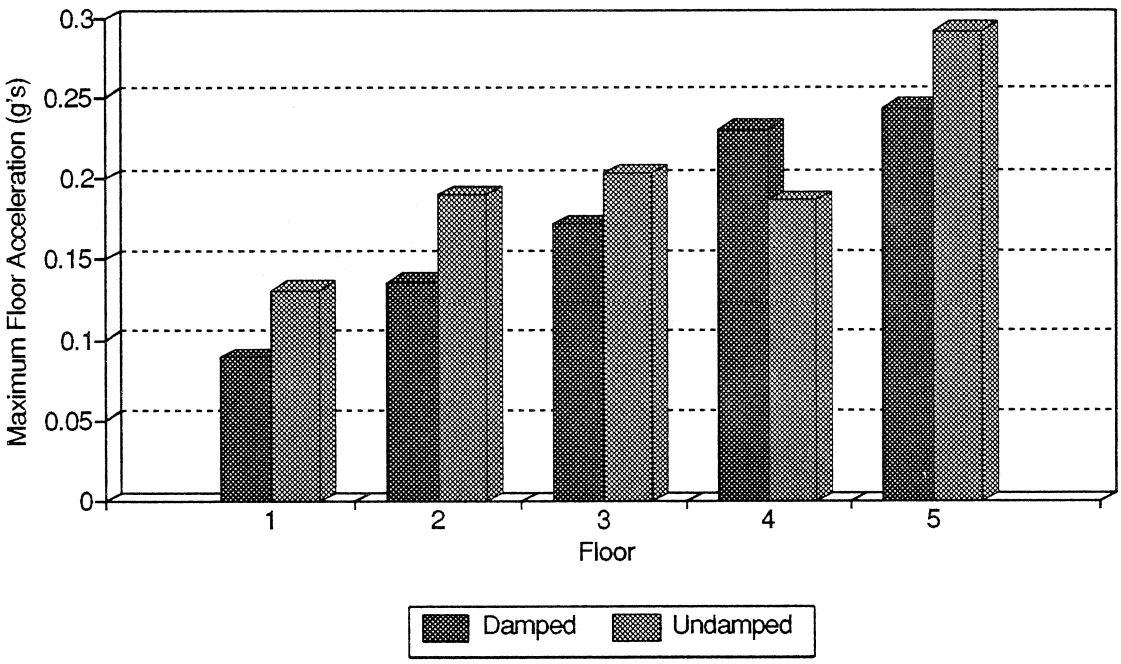


**Fig 4-9 Max Floor Acceleration (0.06 Olypia)**

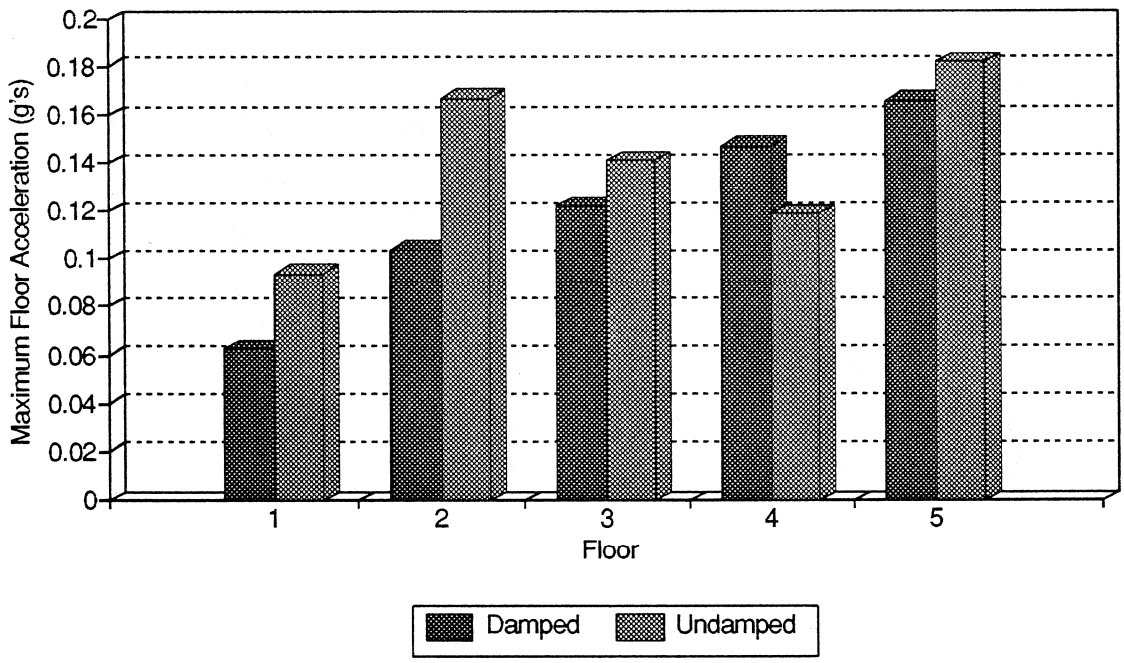


**Fig 4-10 Max Floor Acceleration (0.06 Quebec)**

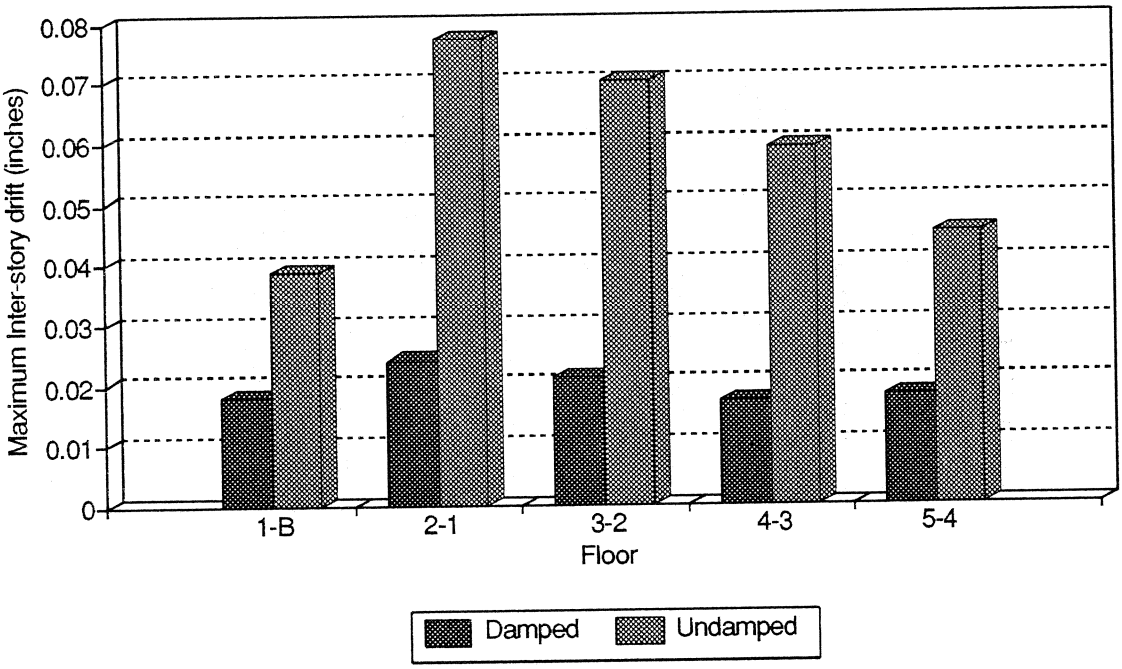


**Fig 4-11 Max Inter-Story Drift (0.06 El Centro)**

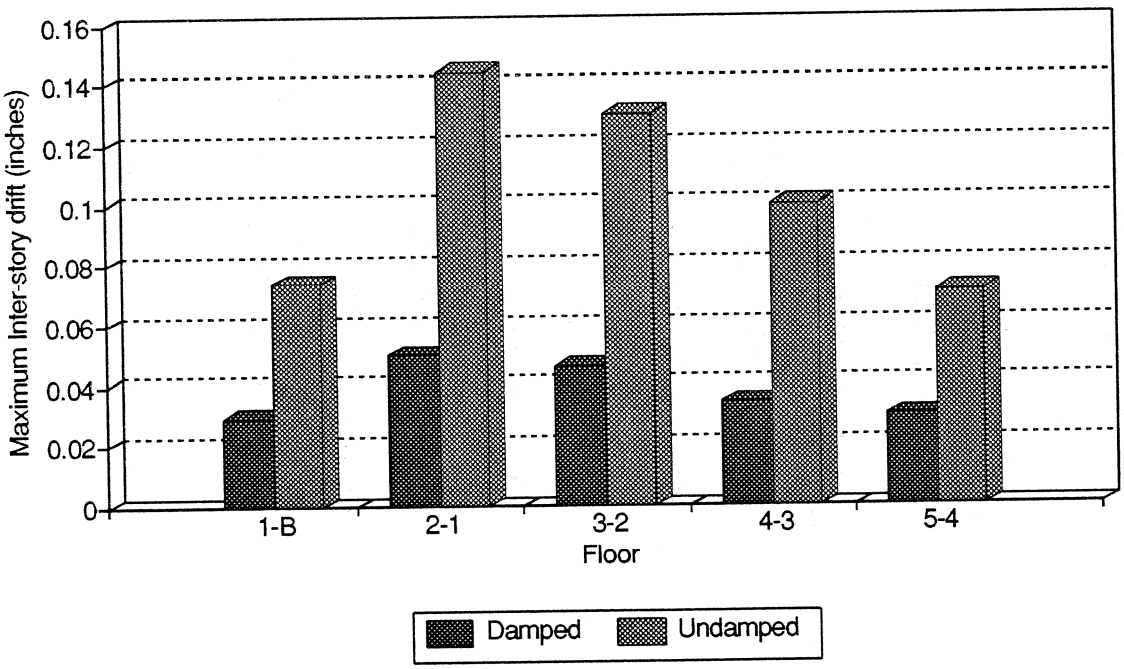


**Fig 4-12 Max Inter-Story Drift (0.06 Hachinohe)**

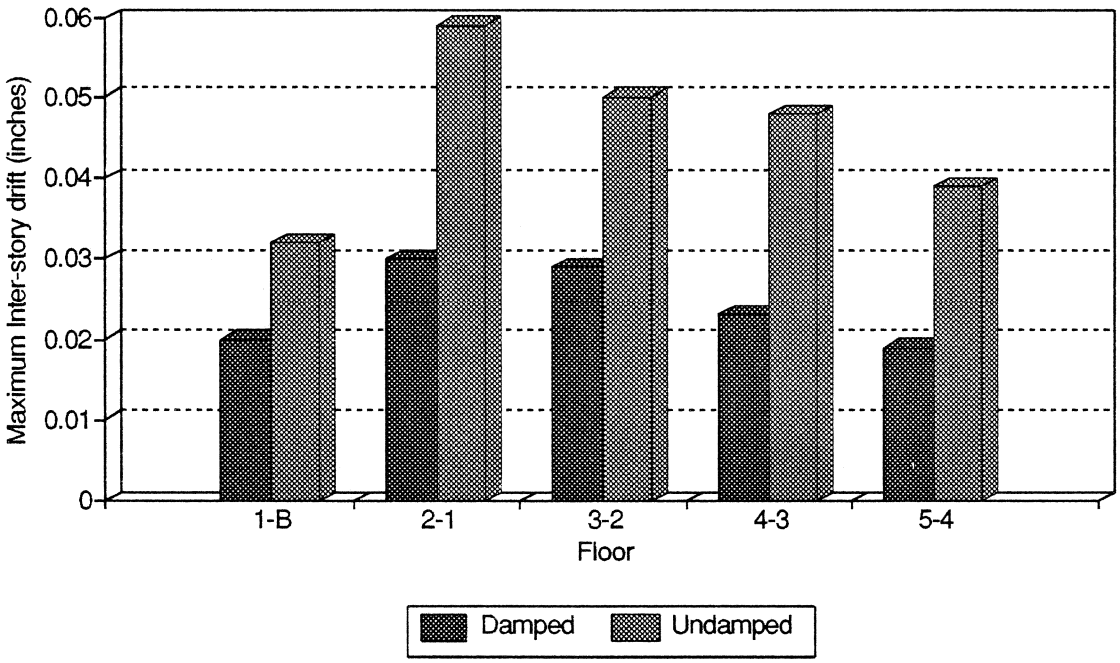


**Fig 4-13 Max Inter-Story Drift (0.06 Olypia)**

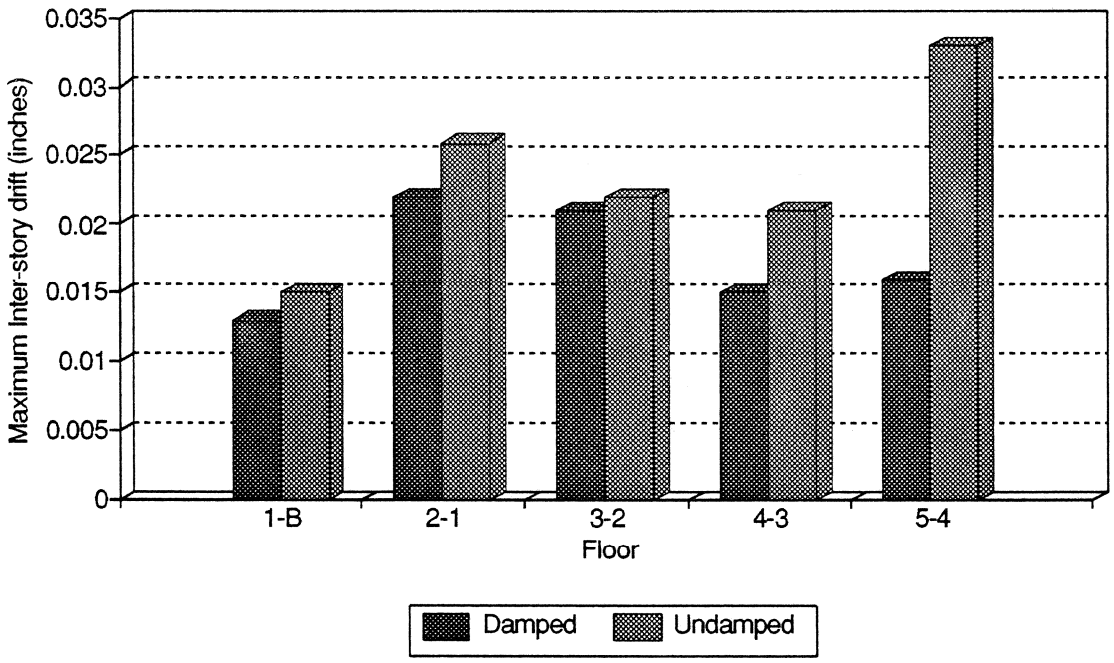


**Fig 4-14 Max Inter-Story Drift (0.06 Quebec)**

| Maximum Response | Floor Level | Earthquake's with 0.06g max acceleration | | | |
|---|---|---|---|---|---|
| | | Hachinohe | | El Centro | |
| | | Undamped | % Reduction | Undamped | % Reduction |
| Relative Floor Disp. (inch) | 1 | 0.074 | 60.4% | 0.039 | 53.4% |
| | 2 | 0.211 | 62.7% | 0.113 | 66.4% |
| | 3 | 0.237 | 48.9% | 0.182 | 67.6% |
| | 4 | 0.436 | 64.4% | 0.238 | 68.9% |
| | 5 | 0.507 | 63.5% | 0.283 | 67.5% |
| Maximum Floor Acc. (g's) | 1 | 0.119 | 12.6% | 0.093 | 11.8% |
| | 2 | 0.267 | 29.2% | 0.163 | 23.3% |
| | 3 | 0.387 | 36.7% | 0.203 | 33.5% |
| | 4 | 0.461 | 36.2% | 0.251 | 34.7% |
| | 5 | 0.554 | 35.6% | 0.303 | 37.3% |
| Inter-Story Drift (inch) | 1-B | 0.074 | 60.4% | 0.039 | 53.4% |
| | 2-1 | 0.144 | 65.3% | 0.077 | 68.8% |
| | 3-2 | 0.130 | 64.6% | 0.070 | 70.0% |
| | 4-3 | 0.100 | 66.0% | 0.059 | 71.2% |
| | 5-4 | 0.071 | 57.7% | 0.045 | 60.0% |
| | | Quebec | | Olympia | |
| | | Undamped | % Reduction | Undamped | % Reduction |
| Relative Floor Disp. (inch) | 1 | 0.015 | 13.3% | 0.032 | 37.5% |
| | 2 | 0.039 | 20.5% | 0.088 | 44.3% |
| | 3 | 0.053 | 0.0% | 0.136 | 42.6% |
| | 4 | 0.060 | -8.3% | 0.181 | 44.2% |
| | 5 | 0.083 | 4.8% | 0.217 | 44.7% |
| Maximum Floor Acc. (g's) | 1 | 0.094 | 33.0% | 0.131 | 32.1% |
| | 2 | 0.167 | 37.7% | 0.190 | 28.4% |
| | 3 | 0.141 | 13.5% | 0.203 | 15.3% |
| | 4 | 0.119 | -23.5% | 0.187 | -23.5% |
| | 5 | 0.182 | 8.8% | 0.292 | 16.4% |
| Inter-Story Drift (inch) | B-1 | 0.015 | 13.3% | 0.032 | 37.5% |
| | 2-1 | 0.026 | 15.4% | 0.059 | 49.2% |
| | 3-2 | 0.022 | 4.5% | 0.050 | 42.0% |
| | 4-3 | 0.021 | 28.6% | 0.048 | 52.1% |
| | 5-4 | 0.033 | 51.5% | 0.039 | 51.3% |

**Table 4-I Summary of Dynamic Response of Model Building**

frequency of the building was also expected to decrease under the larger earthquakes. Fig. 4.15a shows the expected decrease in the natural frequency with increase of the base excitation. Under larger deformation, larger energy absorbing force deflection cycles are experienced which causes an increase in the damping ratio. Fig. 4.15b shows such an increase in damping with larger earthquakes.

It should be noted that the above mentioned damping ratios were calculated by the half-power method [5] for the first mode of vibration only. Since the damping ratio is less the 15%, the half-power method can be considered accurate. A plot of a typical third floor acceleration frequency transfer function with SMA dampers (Fig. 4.16), reveals the first and second modes of vibration clearly. However, the frequency response of the second mode of vibration is less then half that of the first mode. Therefore, the discussion of results will be limited to the first mode of vibration, since it dominates the dynamic response of the structure. In addition to the damped third floor transfer function the undamped the bare frame transfer function the undamped third floor acceleration frequency transfer function (Fig. 4.17) is shown for comparison. The bare frame transfer function is characterized by a tall and narrow spike at 3.2 Hz. This indicates little damping. The frequency response of the SMA damped building is wider and shorter which shows an increased damping from the undamped case.

Fig. 4-15a
Natural Frequency vs Base Excitation

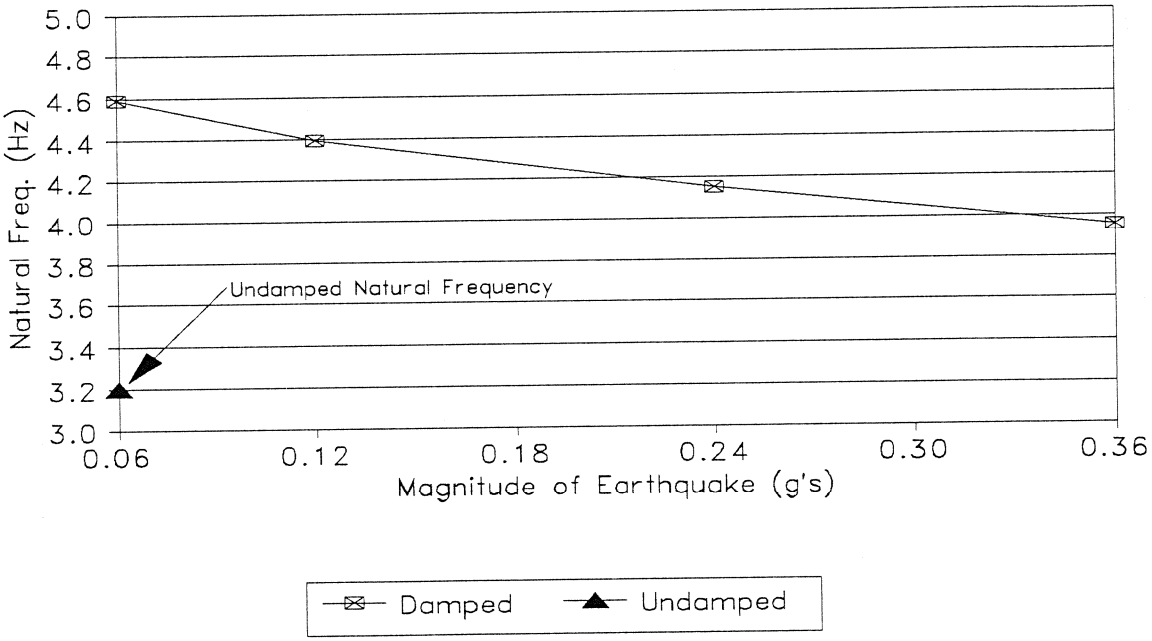


Fig. 4-15b
Damping Ratio vs Base Excitation

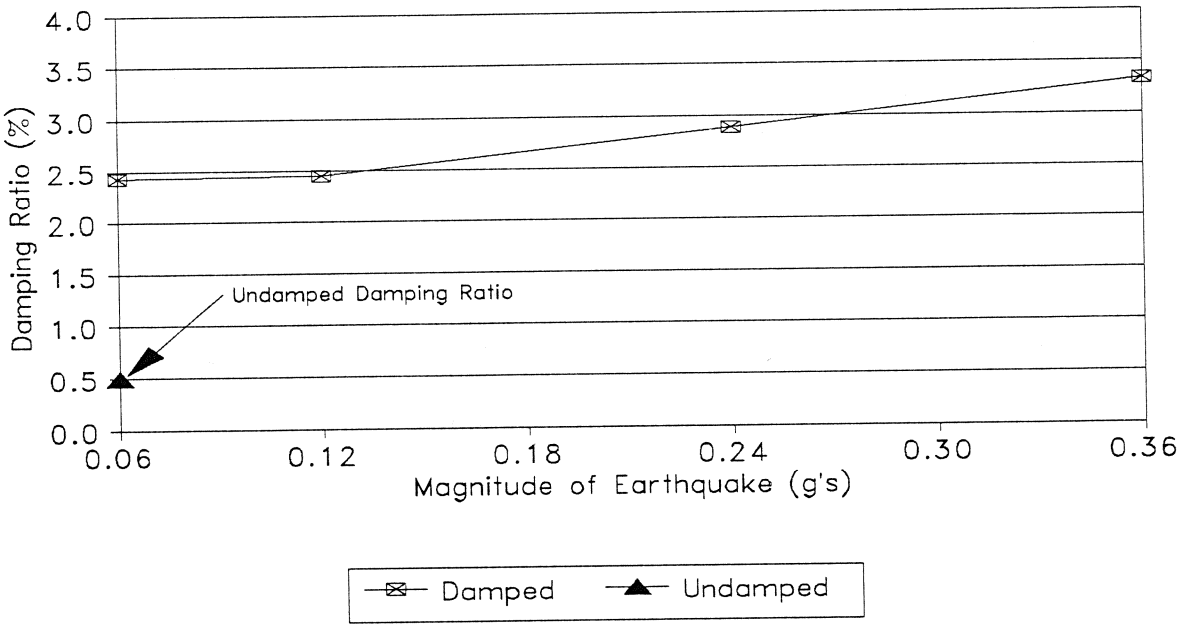


**Fig 4-15 Natural Frequency and Damping Ratio**

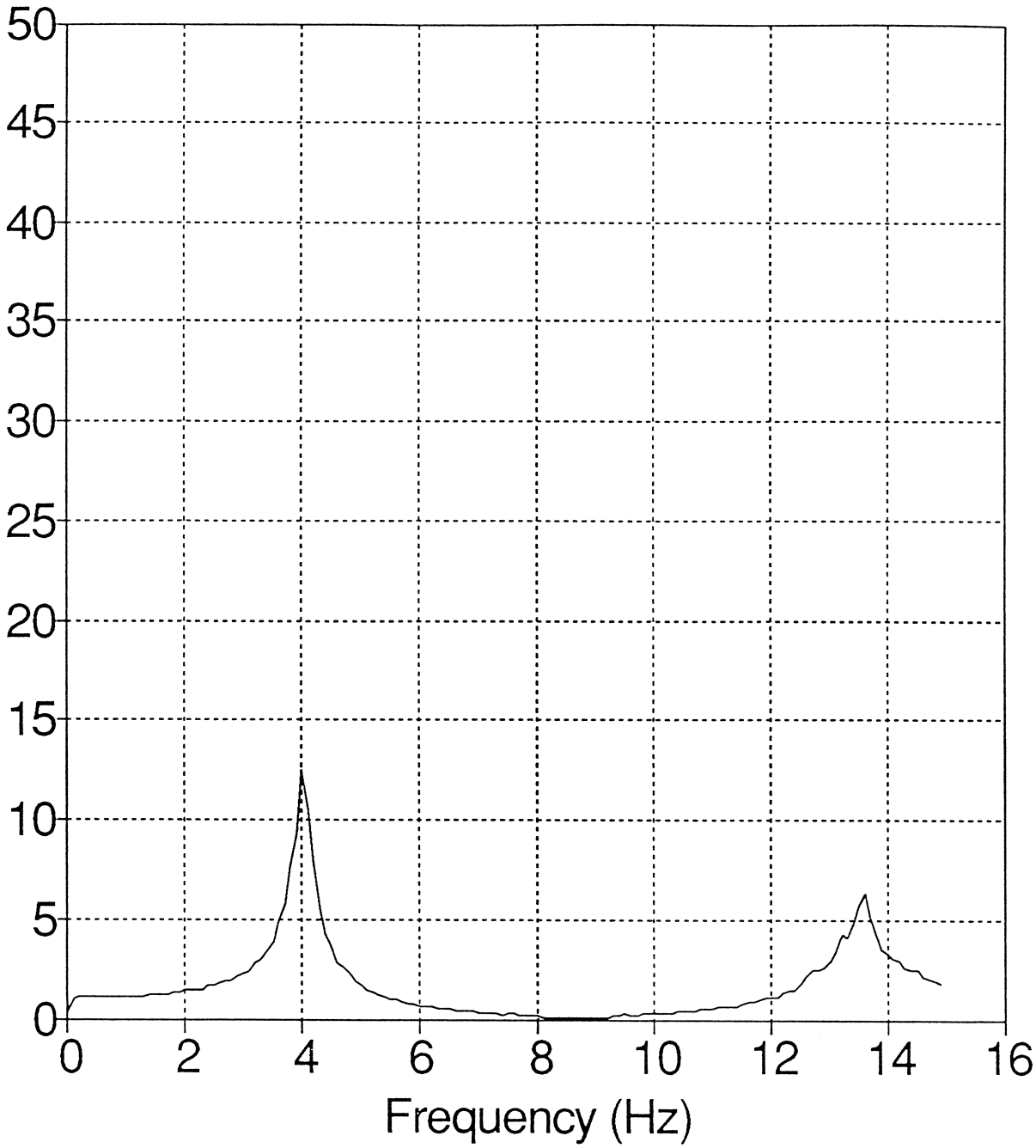


**Fig 4-16 Frequency Response of Damped Building**

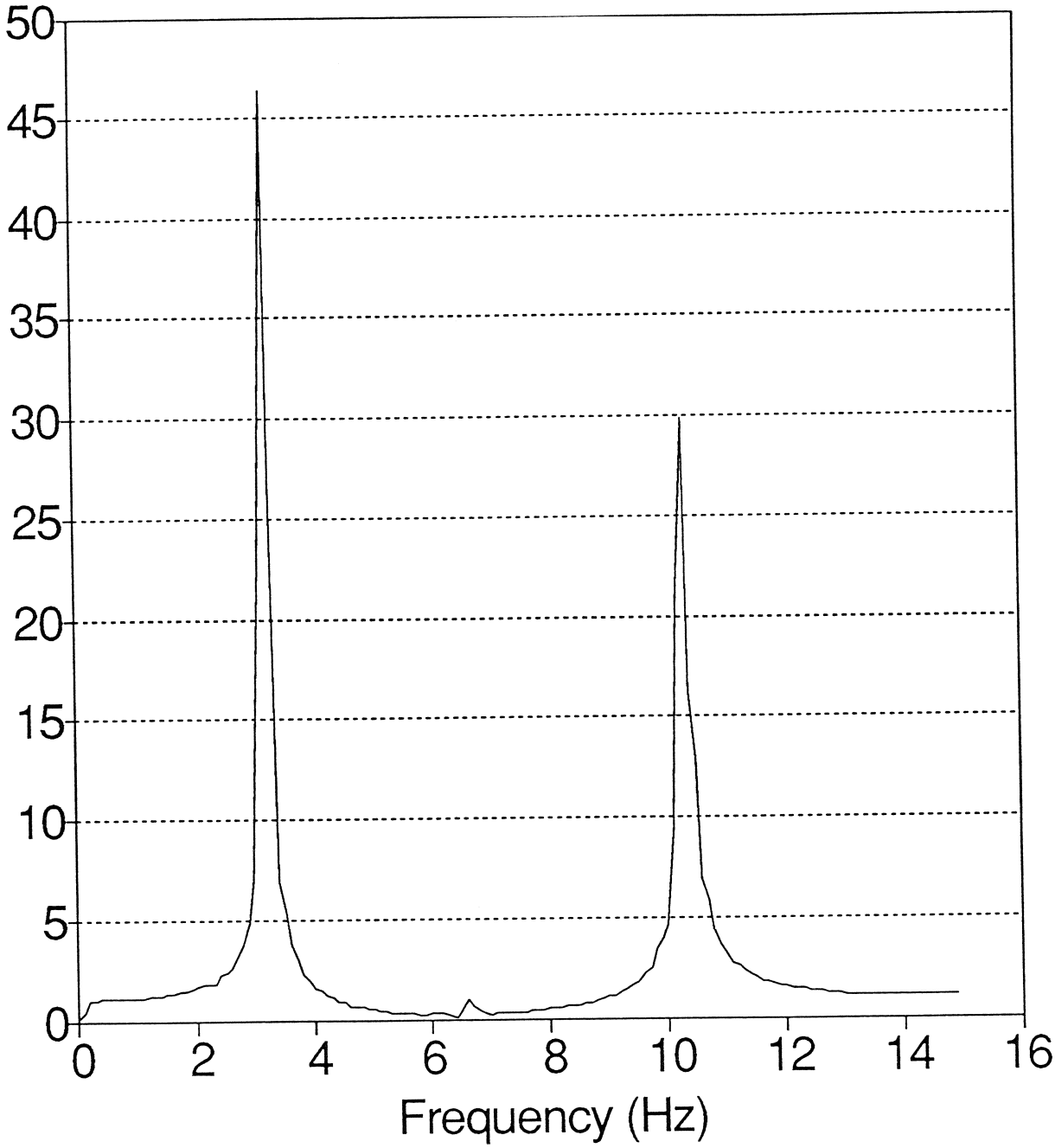


**Fig 4-17 Frequency Response of Undamped Building**

## 4.3 Discussion of Results

It seems apparent from an examination of Table 4.1 that the effectiveness of the damper varies with the earthquake. For instance, the percent reduction of the maximum relative floor displacement due to the Hachinohe ground motion averaged over the five floors is 60.0%, while same averaged percent reduction for the Quebec earthquake case is only 6.1%. In fact, the forth floor maximum relative floor displacement and maximum acceleration of the damped building was greater then the response of the undamped building in the Quebec earthquake case. The other floors maximum responses as well as the inter-story drift response for all floors, however, were smaller in the damped case then the undamped case. These sizable differences can be accounted for by noting that the frequency contents of the four ground motions are different. The Quebec earthquake has a larger content of higher frequencies then the Hachinohe earthquake. Since the SMA dampers increase the natural frequencies of the building (Fig. 4.15a), the SMA dampers will be more effective against earthquakes with lower frequencies.

The calculated damping ratios are less dependent upon the frequency content of the earthquake record. Fig. 4.15b shows an increase of damping over the undamped case. However, the damping for SMA dampers is not as great as for viscoelastic dampers. Viscoelastic dampers have been shown [5] to yield a damping ratio between 5% and 14%, depending on the temperature of the viscoelastic material, for the same five story model building. Whereas the SMA damper properties are not highly temperature

dependent, the damping measured was less than for the viscoelastic dampers at their least favorable temperature. Since the SMA damper was designed to maximize the benefits of the Shape Memory Material properties of Cu-Zn-Al (Sec. 3.3), there is no evidence to indicate that a redesign of the damper would result in improved damping.

In spite of the above drawbacks, the potential for effective SMA damping is apparent. The dampers did mitigate the building's motion and the building was safely tested with the SMA dampers at levels where the building would have been severely damaged without the dampers. In addition, the test results indicate that the SMA damper is probably best suited for base isolation applications. One of the features of the SMA damper is the self centering hysteresis loop. It became evident that this feature is not effectively utilized in structural damping, because the building's inherent stiffness creates a self centering force that is much greater than the damper's. However, in base isolation this self centering property would be of great benefit, since the base isolation device acting alone must restore the building to its original position.

Another indication that the SMA damper would be useful in base isolation is the change in natural frequency of the building with increased levels of base excitation (Fig. 4.15a). A base isolation device should be stiff for small deflection, so that wind loading and small tremors will not cause the building to move excessively. In the event of a large earthquake, the stiffness should reduce and allow the building greater mobility to isolate itself from the

ground motion. The decrease in natural frequency of the damped building (Fig. 4.15a) with increased base excitation indicates a corresponding decrease of damper stiffness with increased damper deflection. This same change in damper stiffness was also noted in Sec. 3.3.

# SECTION 5

## SUMMARY AND CONCLUSION

The results of experimental studies on the material properties of the shape memory material (SMA) Cu-Zn-Al have been presented and analyzed. Experimental results on the seismic behavior of a Cu-Zn-Al SMA damped steel-frame 2/5 scale model structure have also been presented. In addition, a discussion of the advantages of the torsion bar SMA damper over other SMA damper designs was included.

The material test results show that this composition of Cu-Zn-Al has a superelastic stress strain relation for a very limited number of cycles. After a few cycles, the internal friction will increase and cause a hysteretic material behavior with a very small amount of spring back. The final hysteretic stress strain behavior was found to be caused by martensitic transformation rather than by slip/glide dislocation motion.

The seismic test results demonstrated that Cu-Zn-Al dampers are effective at mitigating the 2/5 model five story building's response to various ground motions. The results were compared to results of tests done with viscoelastic dampers, and it was concluded that the Cu-Zn-Al dampers were not as effective as the viscoelastic dampers. The test results of the structural dampers indicated that the SMA dampers are better suited for base isolation.

## SECTION 6
## REFERENCES


1. Roark, Raymond J., and Young, Warren C., "Formulas for Stress and Strain fifth edition," McGraw-Hill Inc., 1975.

2. Shigley, Joseph E., and Mitchell, Larry D., "Mechanical Engineering Design-Fifth Edition," McGraw-Hill Inc., 1983.

3. Ugural, A. C., and Fenster, S. K., "Advanced Strength and Applied Elasticity-Second SI Edition," Elsevier, 1987.

4. Shames, Irving H., "Introduction to Solid Mechanics," Prentice-Hall Inc., 1974.

5. Chang, K.C., Soong, T.T., Oh, S-T., and Lai, M.L., "Seismic Response of a 2/5 Scale Steel Structure with Added Viscoelastic Dampers," Technical Report NCEER-91-0012, 1991.

5. Clough, Ray W., and Penzien, Joseph, "Dynamics of Structures," McGraw-Hill Inc., 1975.

6. Graesser, Edward J., "Multi-Dimensional Modeling of Hysteretic Materials Including Shape Memory Alloys: Theory and Experiment," Ph.D. Dissertation, SUNY Buffalo, Buffalo, NY, January, 1990.

7. Duerig, T. W., Melton, K. N., Stöckel, D., Mayman, C. M., "Engineering Aspects of Shape Memory Alloys," Butterworth-Heinemann Ltd., 1990.

8. Filiatrault, A., Cherry, S., "Comparative Performance of Friction Damped Systems and Base Isolation Systems for Earthquake Retrofit and Aseismic Design," Earthquake Engineering and structural Dynamics, 1988, Vol. 16, pp. 389-416.

9. Zhang, Ri-Hui., Soong, T.T. Mahmood, P., "Seismic Response of steel Frame Structures with Added Viscoelastic Dampers," Earthquake Engineering and structural Dynamics, 1989, Vol 18, pp. 389-396.

10. Roik, K., Dorka, U., Dechent, P., "Vibration Control of Structures Under Earthquake Loading By Three-Stage Friction-Grip Elements," Earthquake Engineering and structural Dynamics, 1988, Vol. 16, pp. 501-521.

11 Malushte, S.R., Singh, M.P., "A Study Of Seismic Response Characteristics Of Structures With Friction Damping," Earthquake Engineering and structural Dynamics, Vol. 18, pp. 767-783.

12 Hna, Yon S., Kim, Young G., "The Effects of Boron and Aging on Mechanical Properties and Martensitic Temperatures in Cu-Zn-Al Shape-Memory Alloys," Scripta Metallurgica, 1987, Vol. 21, pp 947-952.

13 Graesser, E. J., Cozzarelli, F. A., "A multidimensional Hysteretic Model for Plastically Deforming Metals in Energy Absorbing Devices," Technical Report NCEER-91-0006, 1991.

14 Fletcher, A. J., Thomas, D. L., "Solid-State Transformations in Certain Copper-Aluminum-Zinc Alloys." Journal of the Institute of Metals, 1970, Vol 98, pp 188-192.

15 Itoh, I., Hikage, T., "Dezincification Mechanism of Brass in Vacuum at High Temperature," Transactions of the Japan Institute of Metals, 1976, Vol. 17, pp 165-169.

16 Graesser, E. J., Cozzarelli, F. A., "Shape Memory Alloys as New Materials for Aseismic Isolation," Journal of Engineering Mechanics Vol. 117, No. 11, pp 2590-2688, Nov., 1991.

17 Kajiwara, S., Kikuchi, T., "Dislocation Structures Produced by Reverse Martensitic Transformation in a Cu-Zn Alloy," Acta Metall., 1982, Vol. 30, pp 589-598.

## APPENDIX A

## DAMPER ASSEMBLY

All parts of the damper are made from steel, except the torsion bar which is made from Cu-Zn-Al SMA (Fig. A-1). After the Cu-Zn-Al has been machined into the torsion bar, whose dimensions are given in Fig. A-1, it is heat treated by the heat treatment given in Sec. 2. After the heat treatment, the Cu-Zn-Al bar must be hand sanded to remove the damaged surface.

Assembly

1. Slide the center square section of the torsion bar (Fig. A-1) in the grove of the torsion arm (Fig. A-2)
2. Take the large clamp (Fig. A-5) and align its holes with the tapped screw holes of the torsion arm. Screw the large clamp in tightly. This should prevent the torsion bar from sliding out of the grove in the torsion arm.
3. Place a small amount of oil on the pin (Fig. A-5), and then slide the pin through the reamed hole in the torsion arm.
4. Slide a connector (Fig. A-3) over the pin to each side of the torsion arm.
5. Next fit the torsion arm into the groves of the holder (Fig. A-4).
6. Screw the small clamps to the holder to clamp the torsion bar in place.
7. Bolt with 1/4 inch bolts the holes labeled A in brace A (Fig.

A-6) to the holes labeled A in the holder. Bolt with 1/4 inch bolts the holes labeled B (Fig. A-7) in brace B to the holes labeled B in the holder.

8. Arrange brace D and brace E so that the two holes near the center of the bar are aligned. Place a spacer between the bars and bolt brace D to brace E with a spacer in between.

9. Place a double spacer between brace D and brace E aligned with the 1.25" space holes. Align the connectors with the 1.25" spaced holes of brace D and Brace E and bolt in place. Note that these bolts should pass through these components in the following order: connector, brace, double spacer, brace, connector.

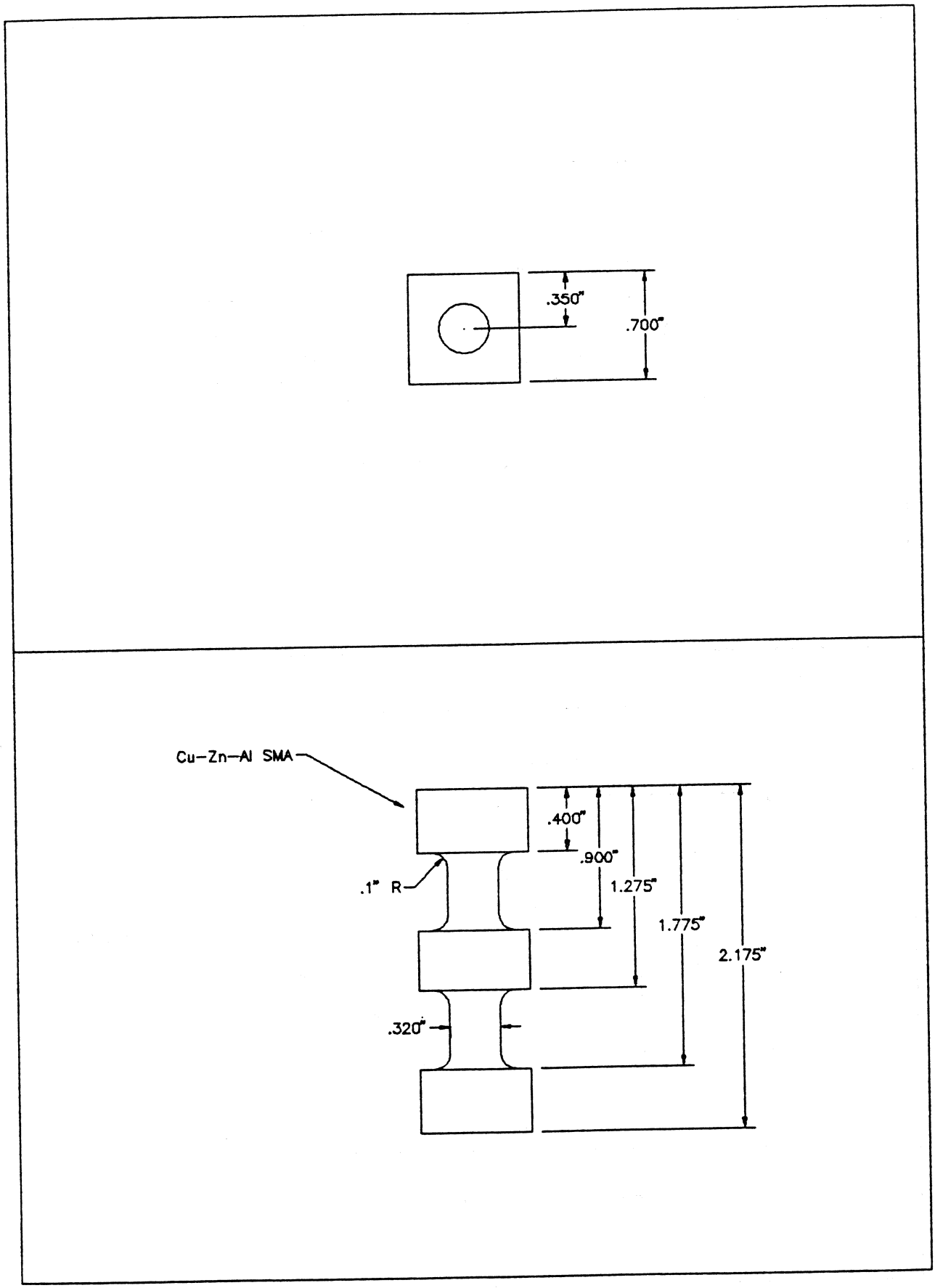


Fig. A-1 Torsion Bar

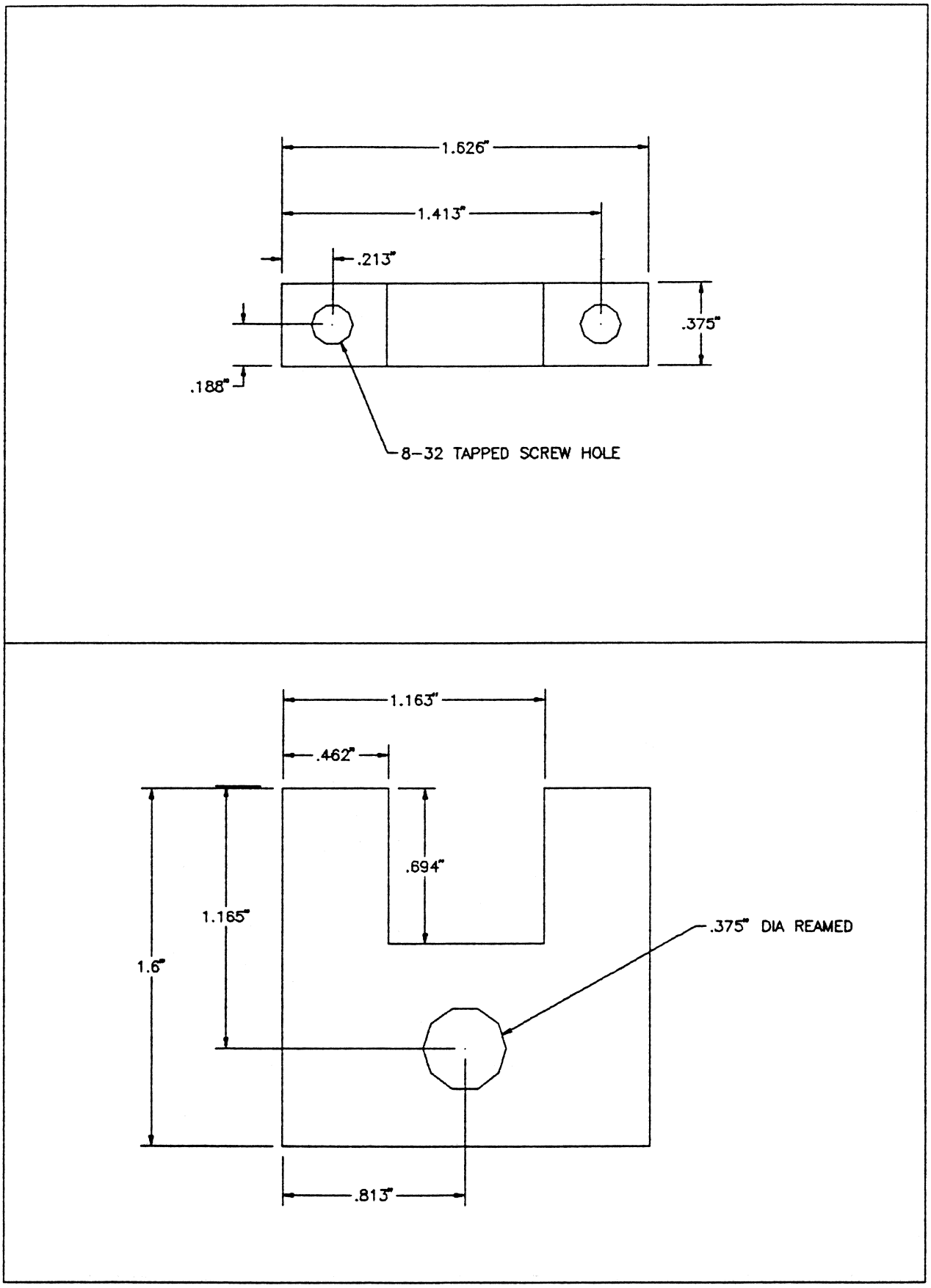


Fig. A-2 Torsion Arm

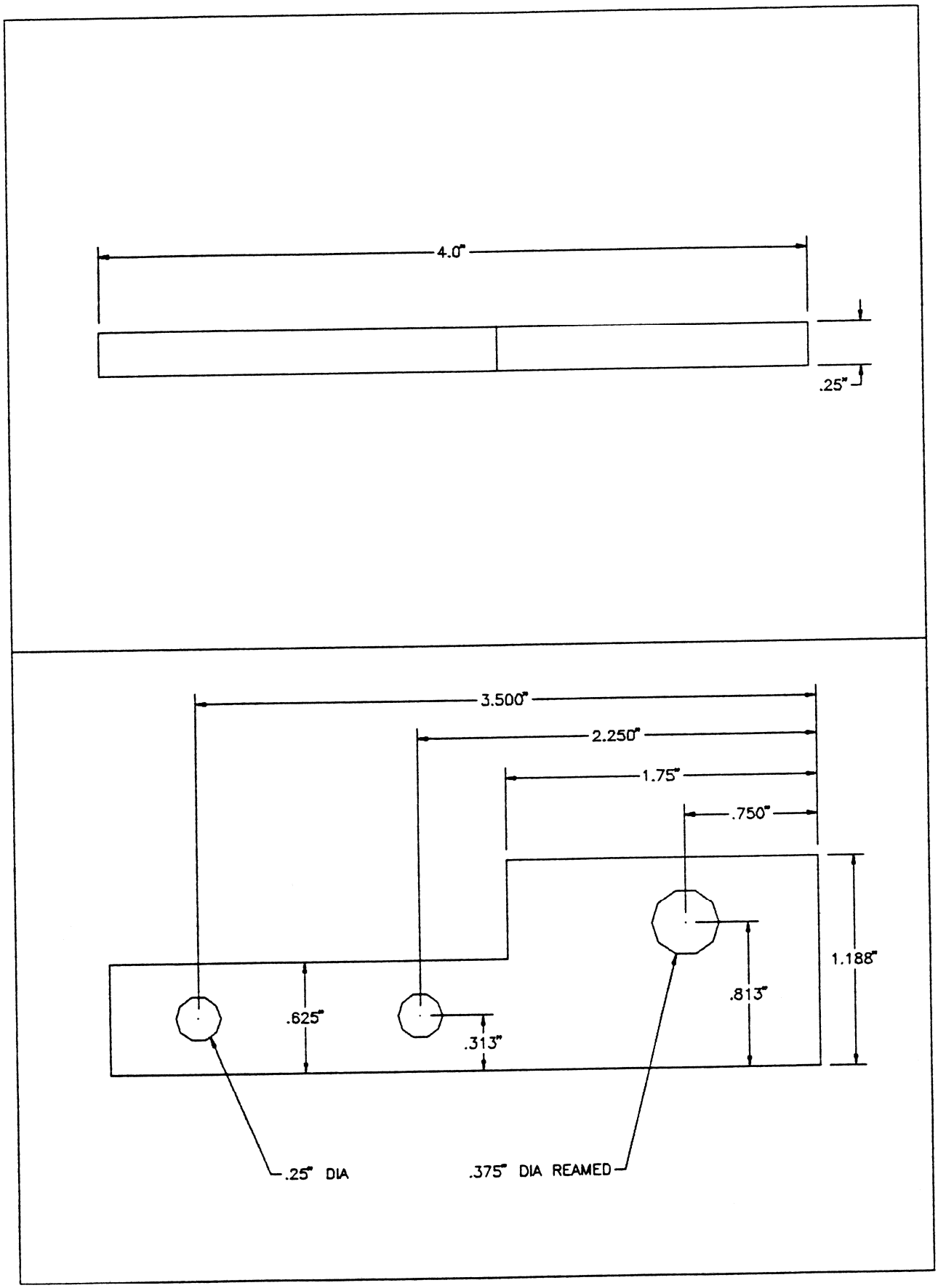


Fig. A-3 Connector

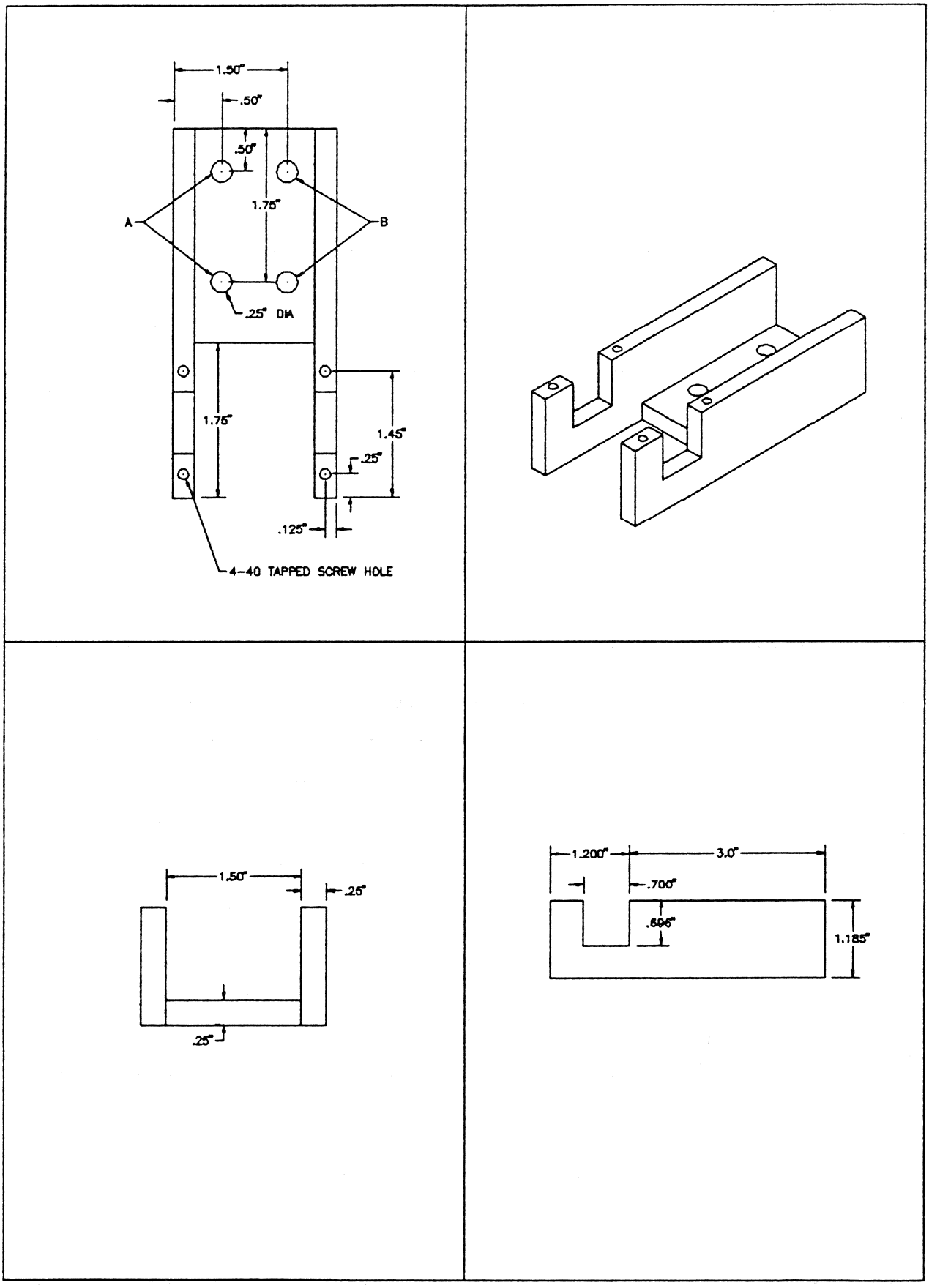


Fig. A-4 Holder

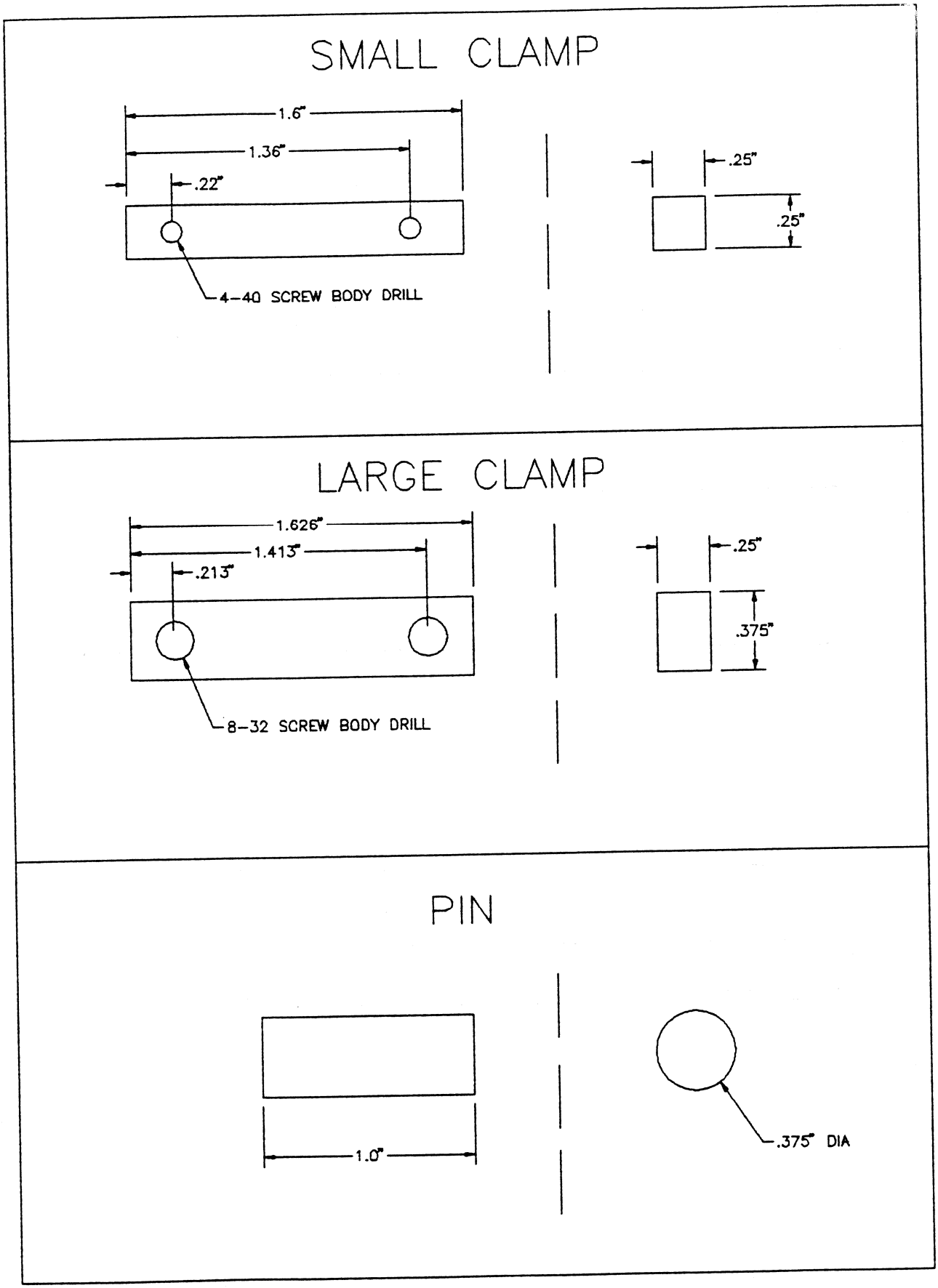


Fig. A-5 Large Clamp, Small Clamp and Pin

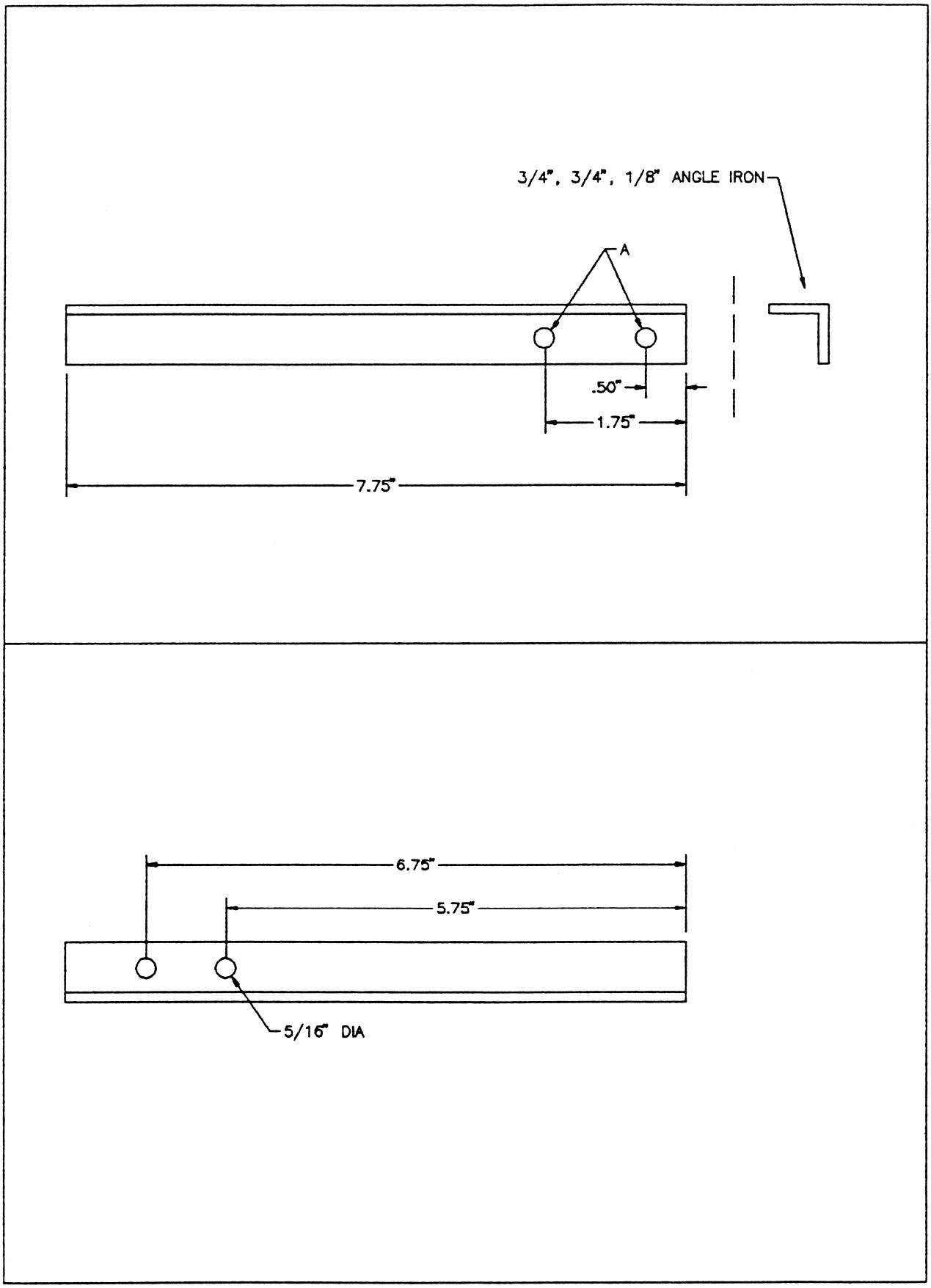


Fig. A-6 Brace A

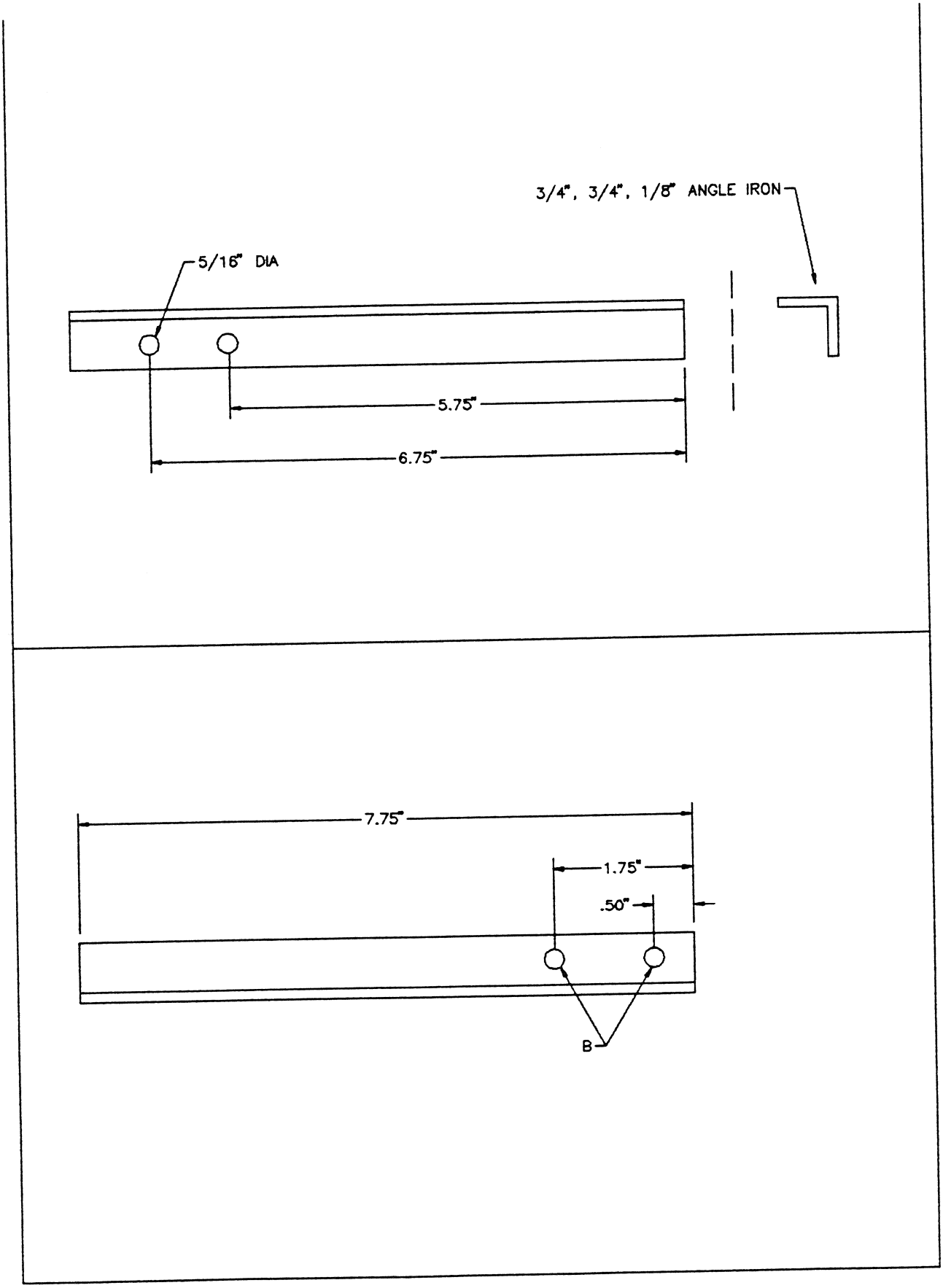


Fig. A-7 Brace B

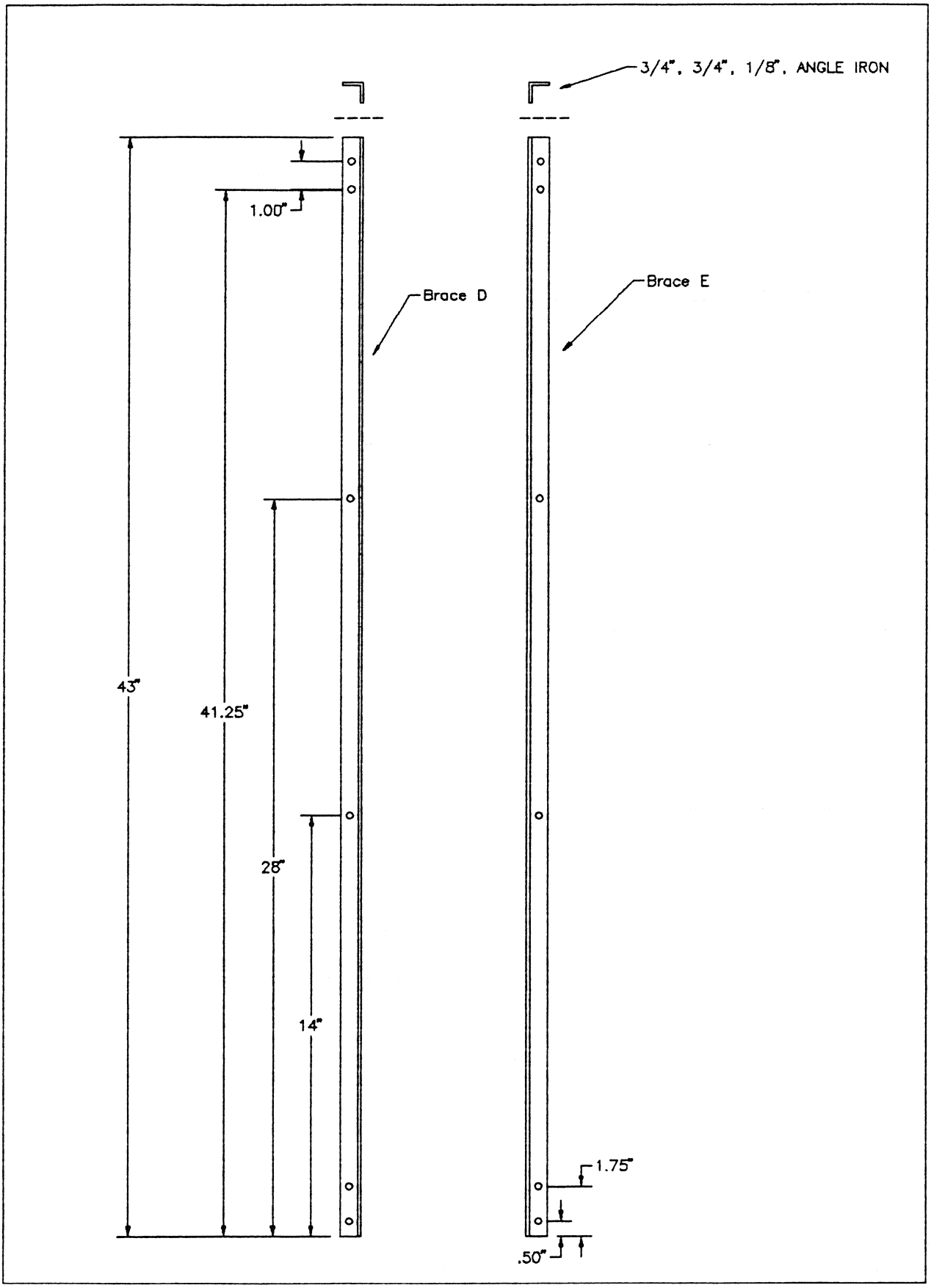


Fig. A-8 Brace D and Brace E

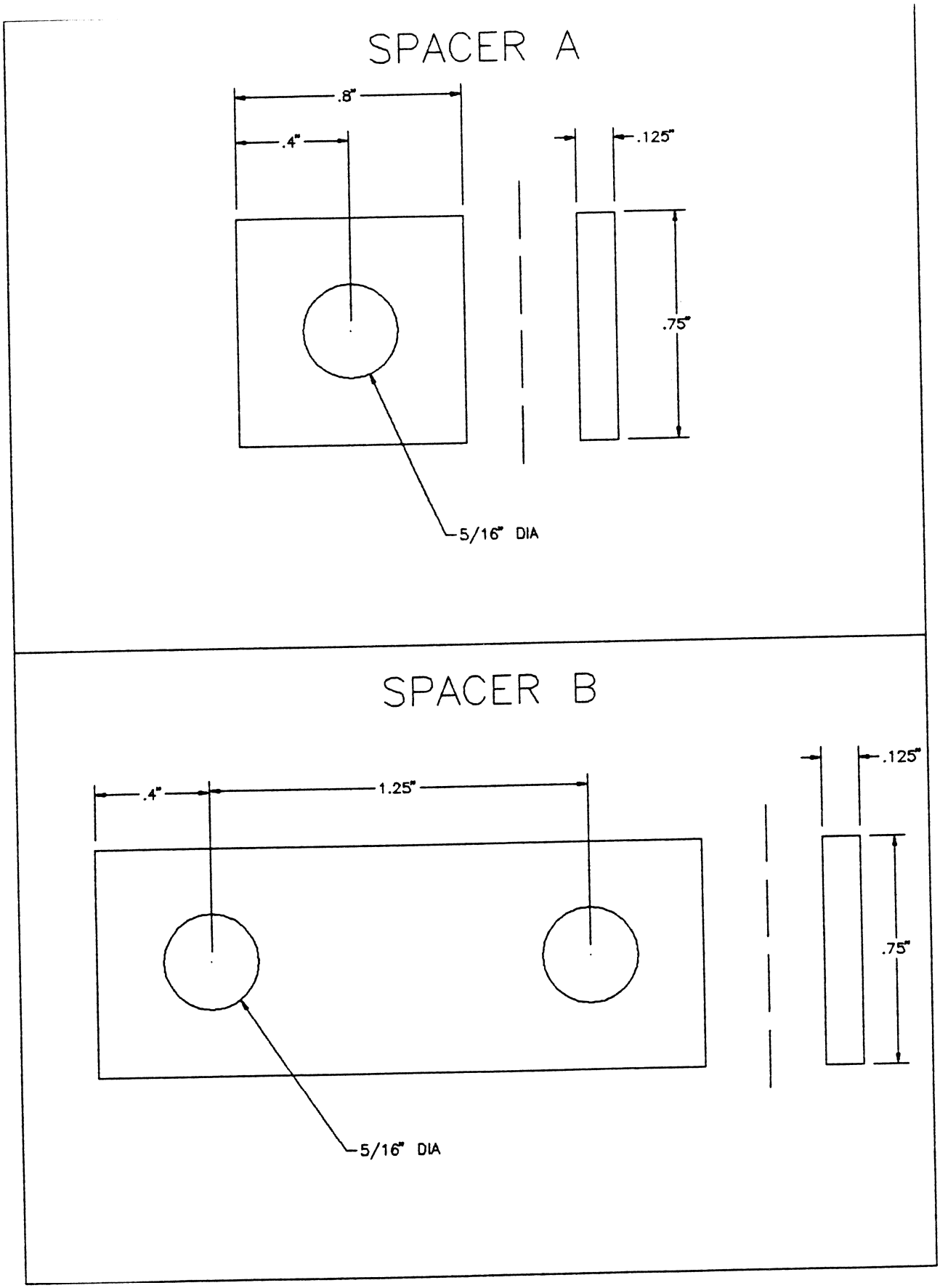


Fig. A-9 Spacers

APPENDIX B

TENSILE BAR AND GRIP DESIGN

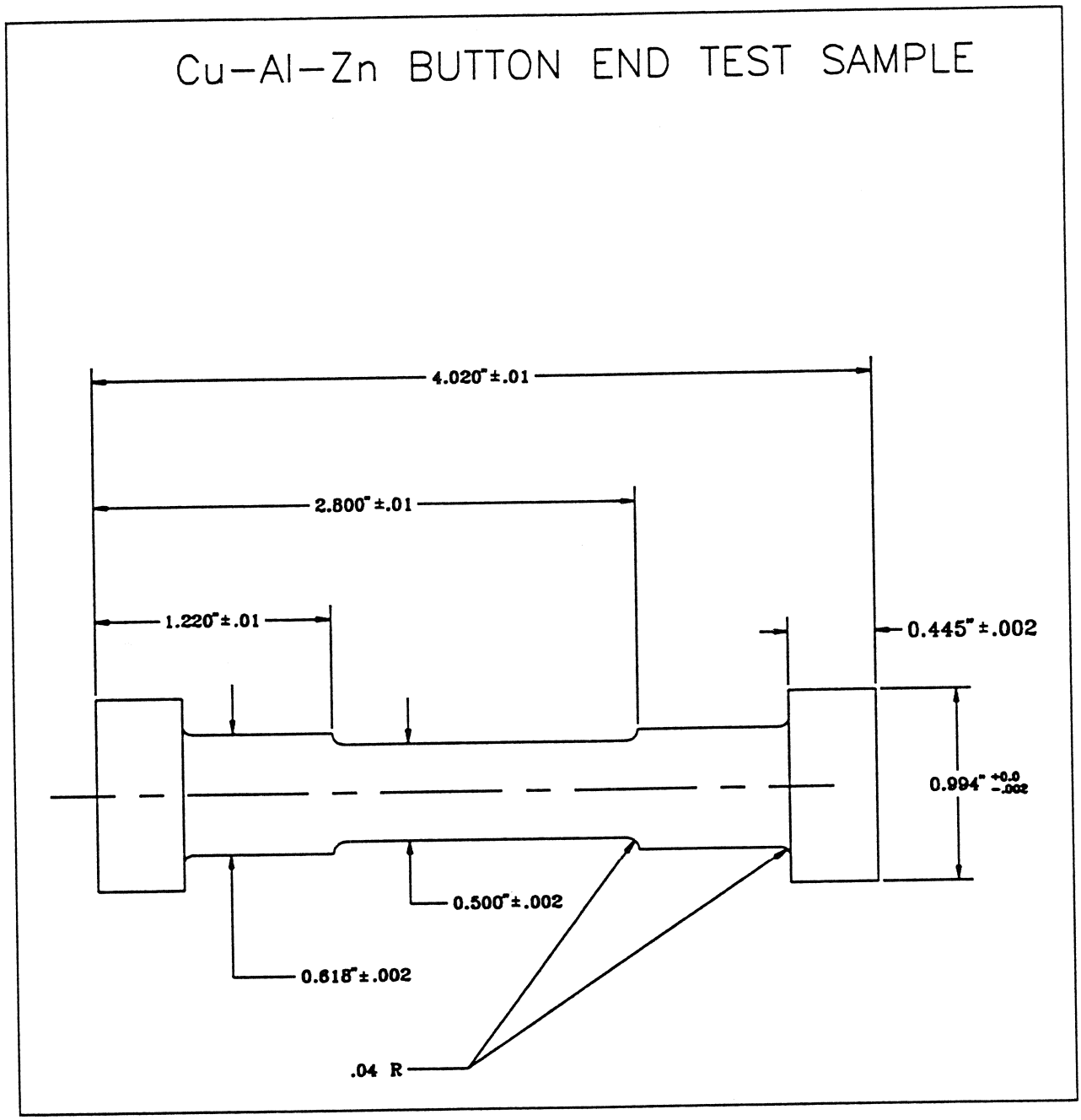


Fig B-1 Cu-Zn-Al Button-Ended Test Sample

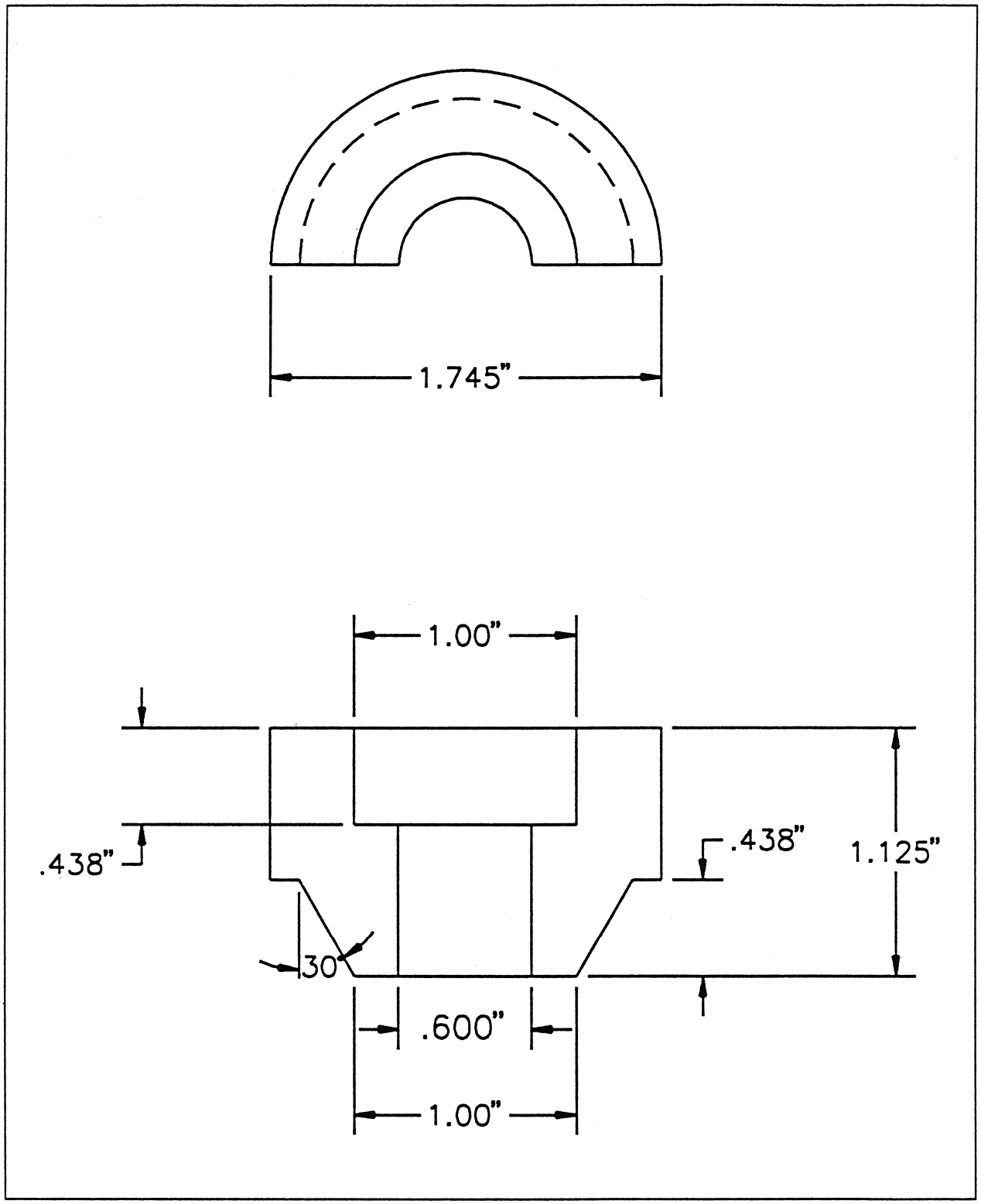


Fig B-2 Split Ring

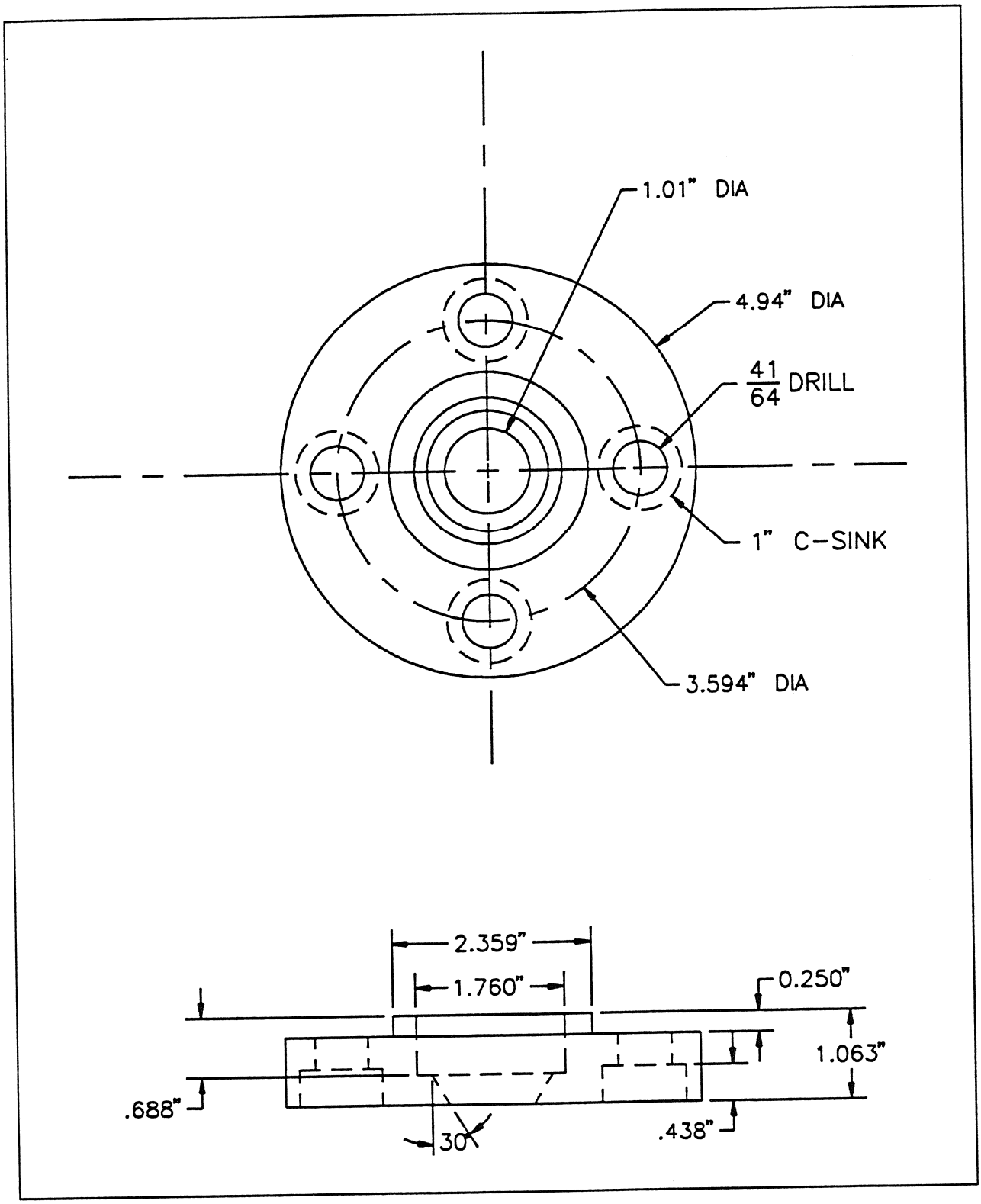


Fig B-3 Test Fixture

## NATIONAL CENTER FOR EARTHQUAKE ENGINEERING RESEARCH
## LIST OF TECHNICAL REPORTS

The National Center for Earthquake Engineering Research (NCEER) publishes technical reports on a variety of subjects related to earthquake engineering written by authors funded through NCEER. These reports are available from both NCEER's Publications Department and the National Technical Information Service (NTIS). Requests for reports should be directed to the Publications Department, National Center for Earthquake Engineering Research, State University of New York at Buffalo, Red Jacket Quadrangle, Buffalo, New York 14261. Reports can also be requested through NTIS, 5285 Port Royal Road, Springfield, Virginia 22161. NTIS accession numbers are shown in parenthesis, if available.

NCEER-87-0001 "First-Year Program in Research, Education and Technology Transfer," 3/5/87, (PB88-134275/AS).

NCEER-87-0002 "Experimental Evaluation of Instantaneous Optimal Algorithms for Structural Control," by R.C. Lin, T.T. Soong and A.M. Reinhorn, 4/20/87, (PB88-134341/AS).

NCEER-87-0003 "Experimentation Using the Earthquake Simulation Facilities at University at Buffalo," by A.M. Reinhorn and R.L. Ketter, to be published.

NCEER-87-0004 "The System Characteristics and Performance of a Shaking Table," by J.S. Hwang, K.C. Chang and G.C. Lee, 6/1/87, (PB88-134259/AS). This report is available only through NTIS (see address given above).

NCEER-87-0005 "A Finite Element Formulation for Nonlinear Viscoplastic Material Using a Q Model," by O. Gyebi and G. Dasgupta, 11/2/87, (PB88-213764/AS).

NCEER-87-0006 "Symbolic Manipulation Program (SMP) - Algebraic Codes for Two and Three Dimensional Finite Element Formulations," by X. Lee and G. Dasgupta, 11/9/87, (PB88-219522/AS).

NCEER-87-0007 "Instantaneous Optimal Control Laws for Tall Buildings Under Seismic Excitations," by J.N. Yang, A. Akbarpour and P. Ghaemmaghami, 6/10/87, (PB88-134333/AS).

NCEER-87-0008 "IDARC: Inelastic Damage Analysis of Reinforced Concrete Frame - Shear-Wall Structures," by Y.J. Park, A.M. Reinhorn and S.K. Kunnath, 7/20/87, (PB88-134325/AS).

NCEER-87-0009 "Liquefaction Potential for New York State: A Preliminary Report on Sites in Manhattan and Buffalo," by M. Budhu, V. Vijayakumar, R.F. Giese and L. Baumgras, 8/31/87, (PB88-163704/AS). This report is available only through NTIS (see address given above).

NCEER-87-0010 "Vertical and Torsional Vibration of Foundations in Inhomogeneous Media," by A.S. Veletsos and K.W. Dotson, 6/1/87, (PB88-134291/AS).

NCEER-87-0011 "Seismic Probabilistic Risk Assessment and Seismic Margins Studies for Nuclear Power Plants," by Howard H.M. Hwang, 6/15/87, (PB88-134267/AS).

NCEER-87-0012 "Parametric Studies of Frequency Response of Secondary Systems Under Ground-Acceleration Excitations," by Y. Yong and Y.K. Lin, 6/10/87, (PB88-134309/AS).

NCEER-87-0013 "Frequency Response of Secondary Systems Under Seismic Excitation," by J.A. HoLung, J. Cai and Y.K. Lin, 7/31/87, (PB88-134317/AS).

NCEER-87-0014 "Modelling Earthquake Ground Motions in Seismically Active Regions Using Parametric Time Series Methods," by G.W. Ellis and A.S. Cakmak, 8/25/87, (PB88-134283/AS).

NCEER-87-0015 "Detection and Assessment of Seismic Structural Damage," by E. DiPasquale and A.S. Cakmak, 8/25/87, (PB88-163712/AS).

NCEER-87-0016 "Pipeline Experiment at Parkfield, California," by J. Isenberg and E. Richardson, 9/15/87, (PB88-163720/AS). This report is available only through NTIS (see address given above).

NCEER-87-0017 "Digital Simulation of Seismic Ground Motion," by M. Shinozuka, G. Deodatis and T. Harada, 8/31/87, (PB88-155197/AS). This report is available only through NTIS (see address given above).

NCEER-87-0018 "Practical Considerations for Structural Control: System Uncertainty, System Time Delay and Truncation of Small Control Forces," J.N. Yang and A. Akbarpour, 8/10/87, (PB88-163738/AS).

NCEER-87-0019 "Modal Analysis of Nonclassically Damped Structural Systems Using Canonical Transformation," by J.N. Yang, S. Sarkani and F.X. Long, 9/27/87, (PB88-187851/AS).

NCEER-87-0020 "A Nonstationary Solution in Random Vibration Theory," by J.R. Red-Horse and P.D. Spanos, 11/3/87, (PB88-163746/AS).

NCEER-87-0021 "Horizontal Impedances for Radially Inhomogeneous Viscoelastic Soil Layers," by A.S. Veletsos and K.W. Dotson, 10/15/87, (PB88-150859/AS).

NCEER-87-0022 "Seismic Damage Assessment of Reinforced Concrete Members," by Y.S. Chung, C. Meyer and M. Shinozuka, 10/9/87, (PB88-150867/AS). This report is available only through NTIS (see address given above).

NCEER-87-0023 "Active Structural Control in Civil Engineering," by T.T. Soong, 11/11/87, (PB88-187778/AS).

NCEER-87-0024 "Vertical and Torsional Impedances for Radially Inhomogeneous Viscoelastic Soil Layers," by K.W. Dotson and A.S. Veletsos, 12/87, (PB88-187786/AS).

NCEER-87-0025 "Proceedings from the Symposium on Seismic Hazards, Ground Motions, Soil-Liquefaction and Engineering Practice in Eastern North America," October 20-22, 1987, edited by K.H. Jacob, 12/87, (PB88-188115/AS).

NCEER-87-0026 "Report on the Whittier-Narrows, California, Earthquake of October 1, 1987," by J. Pantelic and A. Reinhorn, 11/87, (PB88-187752/AS). This report is available only through NTIS (see address given above).

NCEER-87-0027 "Design of a Modular Program for Transient Nonlinear Analysis of Large 3-D Building Structures," by S. Srivastav and J.F. Abel, 12/30/87, (PB88-187950/AS).

NCEER-87-0028 "Second-Year Program in Research, Education and Technology Transfer," 3/8/88, (PB88-219480/AS).

NCEER-88-0001 "Workshop on Seismic Computer Analysis and Design of Buildings With Interactive Graphics," by W. McGuire, J.F. Abel and C.H. Conley, 1/18/88, (PB88-187760/AS).

NCEER-88-0002 "Optimal Control of Nonlinear Flexible Structures," by J.N. Yang, F.X. Long and D. Wong, 1/22/88, (PB88-213772/AS).

NCEER-88-0003 "Substructuring Techniques in the Time Domain for Primary-Secondary Structural Systems," by G.D. Manolis and G. Juhn, 2/10/88, (PB88-213780/AS).

NCEER-88-0004 "Iterative Seismic Analysis of Primary-Secondary Systems," by A. Singhal, L.D. Lutes and P.D. Spanos, 2/23/88, (PB88-213798/AS).

NCEER-88-0005 "Stochastic Finite Element Expansion for Random Media," by P.D. Spanos and R. Ghanem, 3/14/88, (PB88-213806/AS).

NCEER-88-0006 "Combining Structural Optimization and Structural Control," by F.Y. Cheng and C.P. Pantelides, 1/10/88, (PB88-213814/AS).

NCEER-88-0007 "Seismic Performance Assessment of Code-Designed Structures," by H.H-M. Hwang, J-W. Jaw and H-J. Shau, 3/20/88, (PB88-219423/AS).

NCEER-88-0008 "Reliability Analysis of Code-Designed Structures Under Natural Hazards," by H.H-M. Hwang, H. Ushiba and M. Shinozuka, 2/29/88, (PB88-229471/AS).

NCEER-88-0009 "Seismic Fragility Analysis of Shear Wall Structures," by J-W Jaw and H.H-M. Hwang, 4/30/88, (PB89-102867/AS).

NCEER-88-0010 "Base Isolation of a Multi-Story Building Under a Harmonic Ground Motion - A Comparison of Performances of Various Systems," by F-G Fan, G. Ahmadi and I.G. Tadjbakhsh, 5/18/88, (PB89-122238/AS).

NCEER-88-0011 "Seismic Floor Response Spectra for a Combined System by Green's Functions," by F.M. Lavelle, L.A. Bergman and P.D. Spanos, 5/1/88, (PB89-102875/AS).

NCEER-88-0012 "A New Solution Technique for Randomly Excited Hysteretic Structures," by G.Q. Cai and Y.K. Lin, 5/16/88, (PB89-102883/AS).

NCEER-88-0013 "A Study of Radiation Damping and Soil-Structure Interaction Effects in the Centrifuge," by K. Weissman, supervised by J.H. Prevost, 5/24/88, (PB89-144703/AS).

NCEER-88-0014 "Parameter Identification and Implementation of a Kinematic Plasticity Model for Frictional Soils," by J.H. Prevost and D.V. Griffiths, to be published.

NCEER-88-0015 "Two- and Three- Dimensional Dynamic Finite Element Analyses of the Long Valley Dam," by D.V. Griffiths and J.H. Prevost, 6/17/88, (PB89-144711/AS).

NCEER-88-0016 "Damage Assessment of Reinforced Concrete Structures in Eastern United States," by A.M. Reinhorn, M.J. Seidel, S.K. Kunnath and Y.J. Park, 6/15/88, (PB89-122220/AS).

NCEER-88-0017 "Dynamic Compliance of Vertically Loaded Strip Foundations in Multilayered Viscoelastic Soils," by S. Ahmad and A.S.M. Israil, 6/17/88, (PB89-102891/AS).

NCEER-88-0018 "An Experimental Study of Seismic Structural Response With Added Viscoelastic Dampers," by R.C. Lin, Z. Liang, T.T. Soong and R.H. Zhang, 6/30/88, (PB89-122212/AS). This report is available only through NTIS (see address given above).

NCEER-88-0019 "Experimental Investigation of Primary - Secondary System Interaction," by G.D. Manolis, G. Juhn and A.M. Reinhorn, 5/27/88, (PB89-122204/AS).

NCEER-88-0020 "A Response Spectrum Approach For Analysis of Nonclassically Damped Structures," by J.N. Yang, S. Sarkani and F.X. Long, 4/22/88, (PB89-102909/AS).

NCEER-88-0021 "Seismic Interaction of Structures and Soils: Stochastic Approach," by A.S. Veletsos and A.M. Prasad, 7/21/88, (PB89-122196/AS).

NCEER-88-0022 "Identification of the Serviceability Limit State and Detection of Seismic Structural Damage," by E. DiPasquale and A.S. Cakmak, 6/15/88, (PB89-122188/AS). This report is available only through NTIS (see address given above).

NCEER-88-0023 "Multi-Hazard Risk Analysis: Case of a Simple Offshore Structure," by B.K. Bhartia and E.H. Vanmarcke, 7/21/88, (PB89-145213/AS).

NCEER-88-0024 "Automated Seismic Design of Reinforced Concrete Buildings," by Y.S. Chung, C. Meyer and M. Shinozuka, 7/5/88, (PB89-122170/AS). This report is available only through NTIS (see address given above).

NCEER-88-0025 "Experimental Study of Active Control of MDOF Structures Under Seismic Excitations," by L.L. Chung, R.C. Lin, T.T. Soong and A.M. Reinhorn, 7/10/88, (PB89-122600/AS).

NCEER-88-0026 "Earthquake Simulation Tests of a Low-Rise Metal Structure," by J.S. Hwang, K.C. Chang, G.C. Lee and R.L. Ketter, 8/1/88, (PB89-102917/AS).

NCEER-88-0027 "Systems Study of Urban Response and Reconstruction Due to Catastrophic Earthquakes," by F. Kozin and H.K. Zhou, 9/22/88, (PB90-162348/AS).

NCEER-88-0028 "Seismic Fragility Analysis of Plane Frame Structures," by H.H-M. Hwang and Y.K. Low, 7/31/88, (PB89-131445/AS).

NCEER-88-0029 "Response Analysis of Stochastic Structures," by A. Kardara, C. Bucher and M. Shinozuka, 9/22/88, (PB89-174429/AS).

NCEER-88-0030 "Nonnormal Accelerations Due to Yielding in a Primary Structure," by D.C.K. Chen and L.D. Lutes, 9/19/88, (PB89-131437/AS).

NCEER-88-0031 "Design Approaches for Soil-Structure Interaction," by A.S. Veletsos, A.M. Prasad and Y. Tang, 12/30/88, (PB89-174437/AS). This report is available only through NTIS (see address given above).

NCEER-88-0032 "A Re-evaluation of Design Spectra for Seismic Damage Control," by C.J. Turkstra and A.G. Tallin, 11/7/88, (PB89-145221/AS).

NCEER-88-0033 "The Behavior and Design of Noncontact Lap Splices Subjected to Repeated Inelastic Tensile Loading," by V.E. Sagan, P. Gergely and R.N. White, 12/8/88, (PB89-163737/AS).

NCEER-88-0034 "Seismic Response of Pile Foundations," by S.M. Mamoon, P.K. Banerjee and S. Ahmad, 11/1/88, (PB89-145239/AS).

NCEER-88-0035 "Modeling of R/C Building Structures With Flexible Floor Diaphragms (IDARC2)," by A.M. Reinhorn, S.K. Kunnath and N. Panahshahi, 9/7/88, (PB89-207153/AS).

NCEER-88-0036 "Solution of the Dam-Reservoir Interaction Problem Using a Combination of FEM, BEM with Particular Integrals, Modal Analysis, and Substructuring," by C-S. Tsai, G.C. Lee and R.L. Ketter, 12/31/88, (PB89-207146/AS).

NCEER-88-0037 "Optimal Placement of Actuators for Structural Control," by F.Y. Cheng and C.P. Pantelides, 8/15/88, (PB89-162846/AS).

NCEER-88-0038 "Teflon Bearings in Aseismic Base Isolation: Experimental Studies and Mathematical Modeling," by A. Mokha, M.C. Constantinou and A.M. Reinhorn, 12/5/88, (PB89-218457/AS). This report is available only through NTIS (see address given above).

NCEER-88-0039 "Seismic Behavior of Flat Slab High-Rise Buildings in the New York City Area," by P. Weidlinger and M. Ettouney, 10/15/88, (PB90-145681/AS).

NCEER-88-0040 "Evaluation of the Earthquake Resistance of Existing Buildings in New York City," by P. Weidlinger and M. Ettouney, 10/15/88, to be published.

NCEER-88-0041 "Small-Scale Modeling Techniques for Reinforced Concrete Structures Subjected to Seismic Loads," by W. Kim, A. El-Attar and R.N. White, 11/22/88, (PB89-189625/AS).

NCEER-88-0042 "Modeling Strong Ground Motion from Multiple Event Earthquakes," by G.W. Ellis and A.S. Cakmak, 10/15/88, (PB89-174445/AS).

NCEER-88-0043 "Nonstationary Models of Seismic Ground Acceleration," by M. Grigoriu, S.E. Ruiz and E. Rosenblueth, 7/15/88, (PB89-189617/AS).

NCEER-88-0044 "SARCF User's Guide: Seismic Analysis of Reinforced Concrete Frames," by Y.S. Chung, C. Meyer and M. Shinozuka, 11/9/88, (PB89-174452/AS).

NCEER-88-0045 "First Expert Panel Meeting on Disaster Research and Planning," edited by J. Pantelic and J. Stoyle, 9/15/88, (PB89-174460/AS).

NCEER-88-0046 "Preliminary Studies of the Effect of Degrading Infill Walls on the Nonlinear Seismic Response of Steel Frames," by C.Z. Chrysostomou, P. Gergely and J.F. Abel, 12/19/88, (PB89-208383/AS).

NCEER-88-0047 "Reinforced Concrete Frame Component Testing Facility - Design, Construction, Instrumentation and Operation," by S.P. Pessiki, C. Conley, T. Bond, P. Gergely and R.N. White, 12/16/88, (PB89-174478/AS).

NCEER-89-0001 "Effects of Protective Cushion and Soil Compliancy on the Response of Equipment Within a Seismically Excited Building," by J.A. HoLung, 2/16/89, (PB89-207179/AS).

NCEER-89-0002 "Statistical Evaluation of Response Modification Factors for Reinforced Concrete Structures," by H.H-M. Hwang and J-W. Jaw, 2/17/89, (PB89-207187/AS).

NCEER-89-0003 "Hysteretic Columns Under Random Excitation," by G-Q. Cai and Y.K. Lin, 1/9/89, (PB89-196513/AS).

NCEER-89-0004 "Experimental Study of 'Elephant Foot Bulge' Instability of Thin-Walled Metal Tanks," by Z-H. Jia and R.L. Ketter, 2/22/89, (PB89-207195/AS).

NCEER-89-0005 "Experiment on Performance of Buried Pipelines Across San Andreas Fault," by J. Isenberg, E. Richardson and T.D. O'Rourke, 3/10/89, (PB89-218440/AS).

NCEER-89-0006 "A Knowledge-Based Approach to Structural Design of Earthquake-Resistant Buildings," by M. Subramani, P. Gergely, C.H. Conley, J.F. Abel and A.H. Zaghw, 1/15/89, (PB89-218465/AS).

NCEER-89-0007 "Liquefaction Hazards and Their Effects on Buried Pipelines," by T.D. O'Rourke and P.A. Lane, 2/1/89, (PB89-218481).

NCEER-89-0008 "Fundamentals of System Identification in Structural Dynamics," by H. Imai, C-B. Yun, O. Maruyama and M. Shinozuka, 1/26/89, (PB89-207211/AS).

NCEER-89-0009 "Effects of the 1985 Michoacan Earthquake on Water Systems and Other Buried Lifelines in Mexico," by A.G. Ayala and M.J. O'Rourke, 3/8/89, (PB89-207229/AS).

NCEER-89-R010 "NCEER Bibliography of Earthquake Education Materials," by K.E.K. Ross, Second Revision, 9/1/89, (PB90-125352/AS).

NCEER-89-0011 "Inelastic Three-Dimensional Response Analysis of Reinforced Concrete Building Structures (IDARC-3D), Part I - Modeling," by S.K. Kunnath and A.M. Reinhorn, 4/17/89, (PB90-114612/AS).

NCEER-89-0012 "Recommended Modifications to ATC-14," by C.D. Poland and J.O. Malley, 4/12/89, (PB90-108648/AS).

NCEER-89-0013 "Repair and Strengthening of Beam-to-Column Connections Subjected to Earthquake Loading," by M. Corazao and A.J. Durrani, 2/28/89, (PB90-109885/AS).

NCEER-89-0014 "Program EXKAL2 for Identification of Structural Dynamic Systems," by O. Maruyama, C-B. Yun, M. Hoshiya and M. Shinozuka, 5/19/89, (PB90-109877/AS).

NCEER-89-0015 "Response of Frames With Bolted Semi-Rigid Connections, Part I - Experimental Study and Analytical Predictions," by P.J. DiCorso, A.M. Reinhorn, J.R. Dickerson, J.B. Radziminski and W.L. Harper, 6/1/89, to be published.

NCEER-89-0016 "ARMA Monte Carlo Simulation in Probabilistic Structural Analysis," by P.D. Spanos and M.P. Mignolet, 7/10/89, (PB90-109893/AS).

NCEER-89-P017 "Preliminary Proceedings from the Conference on Disaster Preparedness - The Place of Earthquake Education in Our Schools," Edited by K.E.K. Ross, 6/23/89.

NCEER-89-0017 "Proceedings from the Conference on Disaster Preparedness - The Place of Earthquake Education in Our Schools," Edited by K.E.K. Ross, 12/31/89, (PB90-207895). This report is available only through NTIS (see address given above).

NCEER-89-0018 "Multidimensional Models of Hysteretic Material Behavior for Vibration Analysis of Shape Memory Energy Absorbing Devices, by E.J. Graesser and F.A. Cozzarelli, 6/7/89, (PB90-164146/AS).

NCEER-89-0019 "Nonlinear Dynamic Analysis of Three-Dimensional Base Isolated Structures (3D-BASIS)," by S. Nagarajaiah, A.M. Reinhorn and M.C. Constantinou, 8/3/89, (PB90-161936/AS). This report is available only through NTIS (see address given above).

NCEER-89-0020 "Structural Control Considering Time-Rate of Control Forces and Control Rate Constraints," by F.Y. Cheng and C.P. Pantelides, 8/3/89, (PB90-120445/AS).

NCEER-89-0021 "Subsurface Conditions of Memphis and Shelby County," by K.W. Ng, T-S. Chang and H-H.M. Hwang, 7/26/89, (PB90-120437/AS).

NCEER-89-0022 "Seismic Wave Propagation Effects on Straight Jointed Buried Pipelines," by K. Elhmadi and M.J. O'Rourke, 8/24/89, (PB90-162322/AS).

NCEER-89-0023 "Workshop on Serviceability Analysis of Water Delivery Systems," edited by M. Grigoriu, 3/6/89, (PB90-127424/AS).

NCEER-89-0024 "Shaking Table Study of a 1/5 Scale Steel Frame Composed of Tapered Members," by K.C. Chang, J.S. Hwang and G.C. Lee, 9/18/89, (PB90-160169/AS).

NCEER-89-0025 "DYNA1D: A Computer Program for Nonlinear Seismic Site Response Analysis - Technical Documentation," by Jean H. Prevost, 9/14/89, (PB90-161944/AS). This report is available only through NTIS (see address given above).

NCEER-89-0026 "1:4 Scale Model Studies of Active Tendon Systems and Active Mass Dampers for Aseismic Protection," by A.M. Reinhorn, T.T. Soong, R.C. Lin, Y.P. Yang, Y. Fukao, H. Abe and M. Nakai, 9/15/89, (PB90-173246/AS).

NCEER-89-0027 "Scattering of Waves by Inclusions in a Nonhomogeneous Elastic Half Space Solved by Boundary Element Methods," by P.K. Hadley, A. Askar and A.S. Cakmak, 6/15/89, (PB90-145699/AS).

NCEER-89-0028 "Statistical Evaluation of Deflection Amplification Factors for Reinforced Concrete Structures," by H.H.M. Hwang, J-W. Jaw and A.L. Ch'ng, 8/31/89, (PB90-164633/AS).

NCEER-89-0029 "Bedrock Accelerations in Memphis Area Due to Large New Madrid Earthquakes," by H.H.M. Hwang, C.H.S. Chen and G. Yu, 11/7/89, (PB90-162330/AS).

NCEER-89-0030 "Seismic Behavior and Response Sensitivity of Secondary Structural Systems," by Y.Q. Chen and T.T. Soong, 10/23/89, (PB90-164658/AS).

NCEER-89-0031 "Random Vibration and Reliability Analysis of Primary-Secondary Structural Systems," by Y. Ibrahim, M. Grigoriu and T.T. Soong, 11/10/89, (PB90-161951/AS).

NCEER-89-0032 "Proceedings from the Second U.S. - Japan Workshop on Liquefaction, Large Ground Deformation and Their Effects on Lifelines, September 26-29, 1989," Edited by T.D. O'Rourke and M. Hamada, 12/1/89, (PB90-209388/AS).

NCEER-89-0033 "Deterministic Model for Seismic Damage Evaluation of Reinforced Concrete Structures," by J.M. Bracci, A.M. Reinhorn, J.B. Mander and S.K. Kunnath, 9/27/89.

NCEER-89-0034 "On the Relation Between Local and Global Damage Indices," by E. DiPasquale and A.S. Cakmak, 8/15/89, (PB90-173865).

NCEER-89-0035 "Cyclic Undrained Behavior of Nonplastic and Low Plasticity Silts," by A.J. Walker and H.E. Stewart, 7/26/89, (PB90-183518/AS).

NCEER-89-0036 "Liquefaction Potential of Surficial Deposits in the City of Buffalo, New York," by M. Budhu, R. Giese and L. Baumgrass, 1/17/89, (PB90-208455/AS).

NCEER-89-0037 "A Determinstic Assessment of Effects of Ground Motion Incoherence," by A.S. Veletsos and Y. Tang, 7/15/89, (PB90-164294/AS).

NCEER-89-0038 "Workshop on Ground Motion Parameters for Seismic Hazard Mapping," July 17-18, 1989, edited by R.V. Whitman, 12/1/89, (PB90-173923/AS).

NCEER-89-0039 "Seismic Effects on Elevated Transit Lines of the New York City Transit Authority," by C.J. Costantino, C.A. Miller and E. Heymsfield, 12/26/89, (PB90-207887/AS).

NCEER-89-0040 "Centrifugal Modeling of Dynamic Soil-Structure Interaction," by K. Weissman, Supervised by J.H. Prevost, 5/10/89, (PB90-207879/AS).

NCEER-89-0041 "Linearized Identification of Buildings With Cores for Seismic Vulnerability Assessment," by I-K. Ho and A.E. Aktan, 11/1/89, (PB90-251943/AS).

NCEER-90-0001 "Geotechnical and Lifeline Aspects of the October 17, 1989 Loma Prieta Earthquake in San Francisco," by T.D. O'Rourke, H.E. Stewart, F.T. Blackburn and T.S. Dickerman, 1/90, (PB90-208596/AS).

NCEER-90-0002 "Nonnormal Secondary Response Due to Yielding in a Primary Structure," by D.C.K. Chen and L.D. Lutes, 2/28/90, (PB90-251976/AS).

NCEER-90-0003 "Earthquake Education Materials for Grades K-12," by K.E.K. Ross, 4/16/90, (PB91-113415/AS).

NCEER-90-0004 "Catalog of Strong Motion Stations in Eastern North America," by R.W. Busby, 4/3/90, (PB90-251984)/AS.

NCEER-90-0005 "NCEER Strong-Motion Data Base: A User Manuel for the GeoBase Release (Version 1.0 for the Sun3)," by P. Friberg and K. Jacob, 3/31/90 (PB90-258062/AS).

NCEER-90-0006 "Seismic Hazard Along a Crude Oil Pipeline in the Event of an 1811-1812 Type New Madrid Earthquake," by H.H.M. Hwang and C-H.S. Chen, 4/16/90(PB90-258054).

NCEER-90-0007 "Site-Specific Response Spectra for Memphis Sheahan Pumping Station," by H.H.M. Hwang and C.S. Lee, 5/15/90, (PB91-108811/AS).

NCEER-90-0008 "Pilot Study on Seismic Vulnerability of Crude Oil Transmission Systems," by T. Ariman, R. Dobry, M. Grigoriu, F. Kozin, M. O'Rourke, T. O'Rourke and M. Shinozuka, 5/25/90, (PB91-108837/AS).

NCEER-90-0009 "A Program to Generate Site Dependent Time Histories: EQGEN," by G.W. Ellis, M. Srinivasan and A.S. Cakmak, 1/30/90, (PB91-108829/AS).

NCEER-90-0010 "Active Isolation for Seismic Protection of Operating Rooms," by M.E. Talbott, Supervised by M. Shinozuka, 6/8/9, (PB91-110205/AS).

NCEER-90-0011 "Program LINEARID for Identification of Linear Structural Dynamic Systems," by C-B. Yun and M. Shinozuka, 6/25/90, (PB91-110312/AS).

NCEER-90-0012 "Two-Dimensional Two-Phase Elasto-Plastic Seismic Response of Earth Dams," by A.N. Yiagos, Supervised by J.H. Prevost, 6/20/90, (PB91-110197/AS).

NCEER-90-0013 "Secondary Systems in Base-Isolated Structures: Experimental Investigation, Stochastic Response and Stochastic Sensitivity," by G.D. Manolis, G. Juhn, M.C. Constantinou and A.M. Reinhorn, 7/1/90, (PB91-110320/AS).

NCEER-90-0014 "Seismic Behavior of Lightly-Reinforced Concrete Column and Beam-Column Joint Details," by S.P. Pessiki, C.H. Conley, P. Gergely and R.N. White, 8/22/90, (PB91-108795/AS).

NCEER-90-0015 "Two Hybrid Control Systems for Building Structures Under Strong Earthquakes," by J.N. Yang and A. Danielians, 6/29/90, (PB91-125393/AS).

NCEER-90-0016 "Instantaneous Optimal Control with Acceleration and Velocity Feedback," by J.N. Yang and Z. Li, 6/29/90, (PB91-125401/AS).

NCEER-90-0017 "Reconnaissance Report on the Northern Iran Earthquake of June 21, 1990," by M. Mehrain, 10/4/90, (PB91-125377/AS).

NCEER-90-0018 "Evaluation of Liquefaction Potential in Memphis and Shelby County," by T.S. Chang, P.S. Tang, C.S. Lee and H. Hwang, 8/10/90, (PB91-125427/AS).

NCEER-90-0019 "Experimental and Analytical Study of a Combined Sliding Disc Bearing and Helical Steel Spring Isolation System," by M.C. Constantinou, A.S. Mokha and A.M. Reinhorn, 10/4/90, (PB91-125385/AS).

NCEER-90-0020 "Experimental Study and Analytical Prediction of Earthquake Response of a Sliding Isolation System with a Spherical Surface," by A.S. Mokha, M.C. Constantinou and A.M. Reinhorn, 10/11/90, (PB91-125419/AS).

NCEER-90-0021 "Dynamic Interaction Factors for Floating Pile Groups," by G. Gazetas, K. Fan, A. Kaynia and E. Kausel, 9/10/90, (PB91-170381/AS).

NCEER-90-0022 "Evaluation of Seismic Damage Indices for Reinforced Concrete Structures," by S. Rodriguez-Gomez and A.S. Cakmak, 9/30/90, PB91-171322/AS).

NCEER-90-0023 "Study of Site Response at a Selected Memphis Site," by H. Desai, S. Ahmad, E.S. Gazetas and M.R. Oh, 10/11/90, (PB91-196857/AS).

NCEER-90-0024 "A User's Guide to Strongmo: Version 1.0 of NCEER's Strong-Motion Data Access Tool for PCs and Terminals," by P.A. Friberg and C.A.T. Susch, 11/15/90, (PB91-171272/AS).

NCEER-90-0025 "A Three-Dimensional Analytical Study of Spatial Variability of Seismic Ground Motions," by L-L. Hong and A.H.-S. Ang, 10/30/90, (PB91-170399/AS).

NCEER-90-0026 "MUMOID User's Guide - A Program for the Identification of Modal Parameters," by S. Rodriguez-Gomez and E. DiPasquale, 9/30/90, (PB91-171298/AS).

NCEER-90-0027 "SARCF-II User's Guide - Seismic Analysis of Reinforced Concrete Frames," by S. Rodriguez-Gomez, Y.S. Chung and C. Meyer, 9/30/90, (PB91-171280/AS).

NCEER-90-0028 "Viscous Dampers: Testing, Modeling and Application in Vibration and Seismic Isolation," by N. Makris and M.C. Constantinou, 12/20/90 (PB91-190561/AS).

NCEER-90-0029 "Soil Effects on Earthquake Ground Motions in the Memphis Area," by H. Hwang, C.S. Lee, K.W. Ng and T.S. Chang, 8/2/90, (PB91-190751/AS).

NCEER-91-0001 "Proceedings from the Third Japan-U.S. Workshop on Earthquake Resistant Design of Lifeline Facilities and Countermeasures for Soil Liquefaction, December 17-19, 1990," edited by T.D. O'Rourke and M. Hamada, 2/1/91, (PB91-179259/AS).

NCEER-91-0002 "Physical Space Solutions of Non-Proportionally Damped Systems," by M. Tong, Z. Liang and G.C. Lee, 1/15/91, (PB91-179242/AS).

NCEER-91-0003 "Seismic Response of Single Piles and Pile Groups," by K. Fan and G. Gazetas, 1/10/91, (PB92-174994/AS).

NCEER-91-0004 "Damping of Structures: Part 1 - Theory of Complex Damping," by Z. Liang and G. Lee, 10/10/91.

NCEER-91-0005 "3D-BASIS - Nonlinear Dynamic Analysis of Three Dimensional Base Isolated Structures: Part II," by S. Nagarajaiah, A.M. Reinhorn and M.C. Constantinou, 2/28/91, (PB91-190553/AS).

NCEER-91-0006 "A Multidimensional Hysteretic Model for Plasticity Deforming Metals in Energy Absorbing Devices," by E.J. Graesser and F.A. Cozzarelli, 4/9/91.

NCEER-91-0007 "A Framework for Customizable Knowledge-Based Expert Systems with an Application to a KBES for Evaluating the Seismic Resistance of Existing Buildings," by E.G. Ibarra-Anaya and S.J. Fenves, 4/9/91, (PB91-210930/AS).

NCEER-91-0008 "Nonlinear Analysis of Steel Frames with Semi-Rigid Connections Using the Capacity Spectrum Method," by G.G. Deierlein, S-H. Hsieh, Y-J. Shen and J.F. Abel, 7/2/91, (PB92-113828/AS).

NCEER-91-0009 "Earthquake Education Materials for Grades K-12," by K.E.K. Ross, 4/30/91, (PB91-212142/AS).

NCEER-91-0010 "Phase Wave Velocities and Displacement Phase Differences in a Harmonically Oscillating Pile," by N. Makris and G. Gazetas, 7/8/91, (PB92-108356/AS).

NCEER-91-0011 "Dynamic Characteristics of a Full-Sized Five-Story Steel Structure and a 2/5 Model," by K.C. Chang, G.C. Yao, G.C. Lee, D.S. Hao and Y.C. Yeh," to be published.

NCEER-91-0012 "Seismic Response of a 2/5 Scale Steel Structure with Added Viscoelastic Dampers," by K.C. Chang, T.T. Soong, S-T. Oh and M.L. Lai, 5/17/91 (PB92-110816/AS).

NCEER-91-0013 "Earthquake Response of Retaining Walls; Full-Scale Testing and Computational Modeling," by S. Alampalli and A-W.M. Elgamal, 6/20/91, to be published.

NCEER-91-0014 "3D-BASIS-M: Nonlinear Dynamic Analysis of Multiple Building Base Isolated Structures," by P.C. Tsopelas, S. Nagarajaiah, M.C. Constantinou and A.M. Reinhorn, 5/28/91, (PB92-113885/AS).

NCEER-91-0015 "Evaluation of SEAOC Design Requirements for Sliding Isolated Structures," by D. Theodossiou and M.C. Constantinou, 6/10/91, (PB92-114602/AS).

NCEER-91-0016 "Closed-Loop Modal Testing of a 27-Story Reinforced Concrete Flat Plate-Core Building," by H.R. Somaprasad, T. Toksoy, H. Yoshiyuki and A.E. Aktan, 7/15/91, (PB92-129980/AS).

NCEER-91-0017 "Shake Table Test of a 1/6 Scale Two-Story Lightly Reinforced Concrete Building," by A.G. El-Attar, R.N. White and P. Gergely, 2/28/91.

NCEER-91-0018 "Shake Table Test of a 1/8 Scale Three-Story Lightly Reinforced Concrete Building," by A.G. El-Attar, R.N. White and P. Gergely, 2/28/91, to be published.

NCEER-91-0019 "Transfer Functions for Rigid Rectangular Foundations," by A.S. Veletsos, A.M. Prasad and W.H. Wu, 7/31/91, to be published.

NCEER-91-0020 "Hybrid Control of Seismic-Excited Nonlinear and Inelastic Structural Systems," by J.N. Yang, Z. Li and A. Danielians, 8/1/91.

NCEER-91-0021 "The NCEER-91 Earthquake Catalog: Improved Intensity-Based Magnitudes and Recurrence Relations for U.S. Earthquakes East of New Madrid," by L. Seeber and J.G. Armbruster, 8/28/91, (PB92-176742/AS).

NCEER-91-0022 "Proceedings from the Implementation of Earthquake Planning and Education in Schools: The Need for Change - The Roles of the Changemakers," by K.E.K. Ross and F. Winslow, 7/23/91, (PB92-129998/AS).

NCEER-91-0023 "A Study of Reliability-Based Criteria for Seismic Design of Reinforced Concrete Frame Buildings," by H.H.M. Hwang and H-M. Hsu, 8/10/91.

NCEER-91-0024 "Experimental Verification of a Number of Structural System Identification Algorithms," by R.G. Ghanem, H. Gavin and M. Shinozuka, 9/18/91, (PB92-176577/AS).

NCEER-91-0025 "Probabilistic Evaluation of Liquefaction Potential," by H.H.M. Hwang and C.S. Lee," 11/25/91.

NCEER-91-0026 "Instantaneous Optimal Control for Linear, Nonlinear and Hysteretic Structures - Stable Controllers," by J.N. Yang and Z. Li, 11/15/91, (PB92-163807/AS).

NCEER-91-0027 "Experimental and Theoretical Study of a Sliding Isolation System for Bridges," by M.C. Constantinou, A. Kartoum, A.M. Reinhorn and P. Bradford, 11/15/91, (PB92-176973/AS).

NCEER-92-0001 "Case Studies of Liquefaction and Lifeline Performance During Past Earthquakes, Volume 1: Japanese Case Studies," Edited by M. Hamada and T. O'Rourke, 2/17/92.

NCEER-92-0002 "Case Studies of Liquefaction and Lifeline Performance During Past Earthquakes, Volume 2: United States Case Studies," Edited by T. O'Rourke and M. Hamada, 2/17/92.

NCEER-92-0003 "Issues in Earthquake Education," Edited by K. Ross, 2/3/92.

NCEER-92-0004 "Proceedings from the First U.S. - Japan Workshop on Earthquake Protective Systems for Bridges," 2/4/92, to be published.

NCEER-92-0005 "Seismic Ground Motion from a Haskell-Type Source in a Multiple-Layered Half-Space," A.P. Theoharis, G. Deodatis and M. Shinozuka, 1/2/92, to be published.

NCEER-92-0006 "Proceedings from the Site Effects Workshop," Edited by R. Whitman, 2/29/92.

NCEER-92-0007 "Engineering Evaluation of Permanent Ground Deformations Due to Seismically-Induced Liquefaction," by M.H. Baziar, R. Dobry and A-W.M. Elgamal, 3/24/92.

NCEER-92-0008 "A Procedure for the Seismic Evaluation of Buildings in the Central and Eastern United States," by C.D. Poland and J.O. Malley, 4/2/92.

NCEER-92-0009 "Experimental and Analytical Study of a Hybrid Isolation System Using Friction Controllable Sliding Bearings," by Q. Feng, S. Fujii and M. Shinozuka, 2/15/92, to be published.

NCEER-92-0010 "Seismic Resistance of Slab-Column Connections in Existing Non-Ductile Flat-Plate Buildings," by A.J. Durrani and Y. Du, 5/18/92.

NCEER-92-0011 "The Hysteretic and Dynamic Behavior of Brick Masonry Walls Upgraded by Ferrocement Coatings Under Cyclic Loading and Strong Simulated Ground Motion," by H. Lee and S.P. Prawel, 5/11/92, to be published.

NCEER-92-0012 "Study of Wire Rope Systems for Seismic Protection of Equipment in Buildings," by G.F. Demetriades, M.C. Constantinou and A.M. Reinhorn, 5/20/92.

NCEER-92-0013 "Shape Memory Structural Dampers: Material Properties, Design and Seismic Testing," by P.R. Witting and F.A. Cozzarelli, 5/26/92.

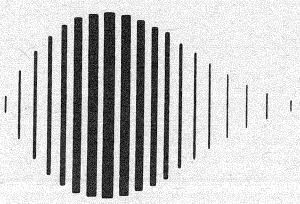

National Center for Earthquake Engineering Research
State University of New York at Buffalo